GAMMA HEATING OF GRIST-2 TEST CLUSTER PRESSURE BOUNDARIES DURING TRANSIENT TEST IN THE TREAT UPGRADE REACTOR

A Thesis

Submitted to the Graduate Faculty of the
Louisiana State University and
Agricultural and Mechanical College
in partial fulfillment of the
requirement for the degree of
Master of Science

in

The Department of Nuclear Engineering

by

Abdelaziz Ezzat Eljabri
B.Sc., Texas A&M University, 1975

May, 1979

DEDICATED TO

my family

ACKNOWLEDGMENTS

I consider myself fortunate to have had the opportunity of working under the supervision of Professor R. E. Miles. His constant assistance, invaluable guidance, useful suggestions and continual encouragements and support are gratefully acknowledged.

I am deeply indebted to the members of my examining committee (Professors J. C. Courtney, F. A. Iddings, E. N. Lambremont and R. C. McIlhenny) for providing constructive comments and helpful advice.

My special gratitude to all members of the Radiation Shielding Information Center (RSIC) at Oak Ridge National Laboratory for their invaluable help and cooperation in supplying many of the computer codes and nuclear data for this thesis.

Sincere thanks to Mrs. Priscilla Milligan and Yvonne Bourgoyne for their assistance in typing this thesis has made the final efforts go smoothly. Many thanks are also extended to the faculty, staff and students of the Nuclear Science Center at Louisiana State University for their continuous aid and encouragement during this research.

My sincere appreciation to my parents, Ezzat, Haleemah and my brothers and sisters for their spiritual, moral and financial support throughout my university career.

TABLE OF CONTENTS

TABLE OF CONTENTS (Con't)

LIST OF TABLES

LIST OF TABLES (Con't)

LIST OF TABLES (Con't)

LIST OF FIGURES

LIST OF FIGURES (Con't)

in R-Z geometry by using 90 x 30 mesh scheme. DOT utilized ANISN collapsed groups in the S_{16} P_3 approximation. As a result of this thesis, the DOT3.5 code is now operable on the LSU IBM/3033 computer system and the capability to perform one step gamma heating calculations has been established at the LSU Nuclear Science Center.

The maximum heating rate in the primary and secondary pressure boundaries calculated by DOT code are 1.96×10^{-8} and 2.00×10^{-8} watt/gm per watt of reactor power respectively assuming no contribution due to fission product-decay gammas. The calculated results were compared with previous results obtained by the point-kernel method code, QADBS-1, which included equilibrium fission product-decay gammas. The results deviate by a factor of 1.5. After subtracting the contribution of fission product-decay gammas from the point-kernel method, there still remains minor discrepancies of $\pm$ 5%. The remaining differences between the radial heating results can be traced to the inherent difference between the two methods and the difference in the two cross section sets structure.

The heating rate distribution in the axial direction is substantially different after adjusting for the inclusion of fission product-decay gammas in the point-kernel method.

In the point-kernel method the axial heating rate distributio were estimated, based on the axial buckling of the neutron flux in the TREAT reactor. While in this study the axial heating rate results were computed explicitly by the DOT3.5 computer code. Hence the axial heating rates obtained in this work are more accurate.

ABSTRACT

The Transient Reactor Test Facility (TREAT) is an irradiation test system used to supplement the fast reactor safety program. This reactor is used to study meltdown problems. In these studies the TREAT reactor is used to simulate power excursions in fast reactor cores. The quanitative data obtained from these experiments can be used to verify some of the analytical assumptions concerning the mechanism of fuel meltdown.

In order to insure that the experiments can be conducted in a safe manner without damage to the reactor core in these studies, establishment of accurate gamma heating rate in pressure boundaries is needed. The precise knowledge of the fission densities, the neutron and gamma fluxes and their respective energy spectra is essential. Determination of these functions subsequently requires sophisticated computer codes capable of performing neutron and gamma-ray transport calculations.

The ANISN code was used in this work to collapse a 58-group coupled neutron-gamma (37 groups of neutrons and 21 groups of gammas) into a 13-group coupled neutron-gamma (5 groups of neutrons and 8 groups of gammas) to be used subsequently by DOT3.5 code.

The calculation of gamma heating in the GRIST-2 test cluster pressure boundaries was performed with the use of the two-dimensional discrete ordinates computer code, DOT3.5. The reactor was modeled

CHAPTER ONE

Introduction

Nuclear reactor design is partially governed by the heat generated from nuclear interactions which arise due to the fission process. Determination of the heat generation rate in a nuclear reactor requires precise knowledge of neutron and gamma flux density and their energy spectrum as a function of space and time. The Boltzmann transport equation can be used to accurately model the processes which effect these quantities. However this equation can be salved analytically only for a very few special situations. As a result, several methods utilizing high speed computer calculations have been developed to solve the Boltzmann transport equation. These methods make use of various numerical techniques (i.e., spherical harmonic, P_ℓ expansion and discrete ordinates methods).

In the early days of reactor design, before rise of the modern digital computers, crude calculational methods were used to calculate the neutron and gamma transport. In these methods simple models and conservative approximation were used. The development of digital computers has made it practical to solve these transport problems in more detail. As the computational speed and storage capacity of computers has increased, it has become practical to use more realistic mathematical models and more complex problems.

One of the most successful numerical techniques used for solving the transport equation is the S_N method. It was first developed by Carlson[1] in 1953. One of the early applications of this method in a computer program was made by Duane[2] in 1957. The program included the inelastic and capture gamma sources in addition to the fission source. Later on, improved versions included the linear anisotropic scattering term (P_ℓ approximation for the scattering cross sections) was made available in 1959[3]. Since that time provisions have been made to include anisotropic scattering terms to any order desired. The only limitation is the order of scattering available in the cross section data. The method can be applied to both neutron and gamma-ray transport problems associated with reactor cores as well as the outside shielding layers (deep penetration) of the reactors. Typical codes based on the S_N method are DTF[4] and ANISN[5] (one-dimensional), TWOTRAN[6] and DOT[7] (two-dimensional) codes.

These codes are improved and refined as the need arises. The DOT code, for example, was first made available in 1967[8]. Then an improved version, DOT-II, followed in 1969 by adding anisotropic scattering option and by improving the convergence criteria[9]. Special features were added to the code which made it well adapted to shielding problems. Such as including albedo boundary conditions and an analytical first collision source calculation. As a result DOT-III was made available in 1973. In 1976 DOT3.5, which is an improved version of DOT-III was made

available[7]. The most significant change in DOT3.5 is a marked improvement in convergence on deep-penetration problems and the inclusion of "flexible dimensioning" in the code storage capacity.

The objective of this thesis in part was to obtain the latest and most up to date version of a two-dimensional neutron transport code and to make it operational on LSU's IBM/3033 computer. At the time this work was initiated, RSIC's DOT3.5 code was considered as the most up to date version. In addition, it was readily available and perhaps the best documented two-dimensional transport code[7]. The only other two-dimensional transport code considered was TWOTRAN, but the purpose of this work was to expand the present one-dimensional (ANISN) discrete ordinates transport calculational capabilities to two-dimensions so that "state of the art" transport calculations required in reactor design or shielding analysis can be performed.

The research for this thesis was first initiated by modifying and creating an operational load module on the LSU Computer System of DOT3.5 Code.

Gamma heating calculation of the primary and secondary pressure boundaries of TREAT upgrade reactor was chosen to demonstrate usage and analysis of the DOT3.5 code. There are two main reasons for selecting this problem:

First; a gamma heating calculation in nuclear reactor includes not only photon transport but also neutron transport calculations. Usually, this requires more than one computer code to

be utilized. However the DOT3.5 code along with a coupled neutron-gamma cross section set is capable of performing the task in a single transport calculation. This this problem was selected to build this one step gamma heating computational ability at LSU. Problems such as this not only arise in testing advanced reactor fuels in test reactors, but also in many problems where dose rates from mixed radiation fields are of interest. Such as the shielding of Cf-252 and the dose rate computations in and around a reactor core.

Second; the problem was tested previously by the traditional technique, So, the quantities of concern, namely, fluxes, fission spectra, heating rates and the eigenvalue of the system are well defined, and the results obtained by the two different techniques can be compared.

In performing the gamma heating analysis described above required a selection of suitable cross section data. The following three coupled neutron-gamma cross section sets were chosen for this work. The DLC-31/(DPL-1/FEWG1)[10] set, the DLC-47[11] (BUGLE) set, and the DLC-23[12] (CASK) set. These sets were obtained from Radiation Shielding Information Center (RSIC) at Oak Ridge National Laboratory (ORNL). They consist of 58-group (37n, 21γ), 61-group (46n, 16γ) and 40-group (22n, 18γ) respectively.

ANISN library generating routine (LIBGEN)[13] was used to convert the cross sections from ANISN format to unformulated binary data sets to be used by the ANISN and DOT3.5 codes.

Group organized macroscopic cross sections sets were created by the program TAPEMAKER[14] in order to minimize the computer storage requirements.

The sequence of steps representing this work are illustrated in (Figure 1.1) and are generally used in neutronic and photonic transport problems when one deals with ANISN, DOT and MORSE[15] codes. The work involved is documented by this thesis, computer runs, and other unpublished notes at the Nuclear Science Center at LSU to aid subsequent users of these codes.

1.1. Outline of the Present Work

The gamma heating rate in a nuclear reactor can be determined by a series of neutronic and photonic computations. In most cases, several computer codes are needed. The purpose of this work is to do the task in a single transport calculation by utilizing DOT3.5 code along with coupled neutron-gamma group cross section sets.

The remainder of this chapter discusses the heat generation in nuclear reactor (Section 1.2), methods of gamma heating calculation (Section 1.3) and previous work involving gamma heating of TREAT reactor (Section 1.4).

Chapter Two summarizes the development of the discrete ordinates theory that has lead to the development of ANISN and DOT codes. It also describes the work that has been done in this thesis on DOT code to create an operational load module on LSU's IBM/3033 computer system. In addition to the purpose of the code,

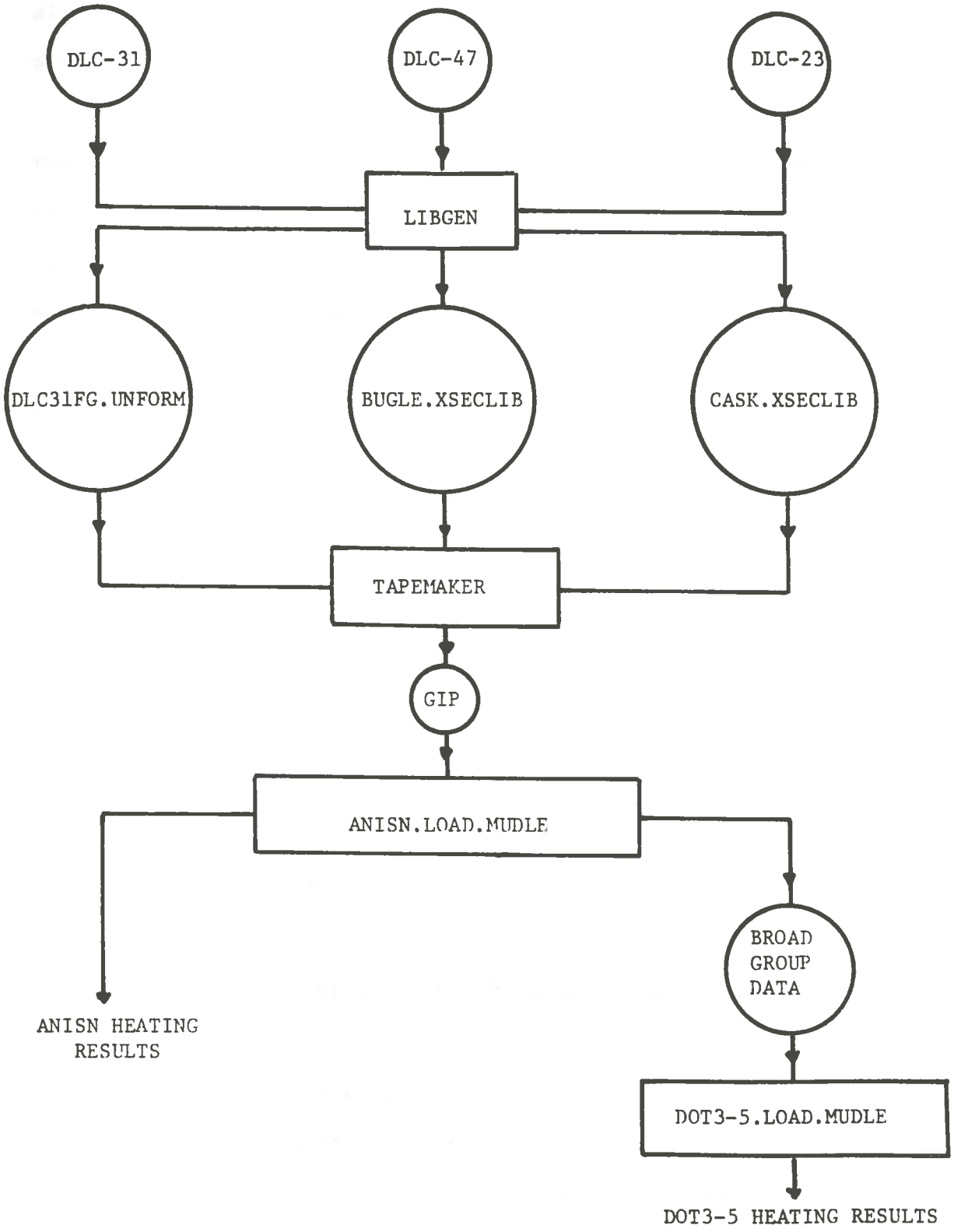

Figure 1.1. Sequence of steps used to calculate the gamma heating rate in TREAT Upgrade Reactor.

alternatives to be solved, the selection of the code, its advantages over other codes and its limitations are also discussed.

Chapter Three gives a brief description of the TREAT reactor, and discusses the modeling of the reactor into five major components which includes 27 regions and 90 x 30 mesh spacing. The various types of materials in each region and the atom density of each material are tabulated.

Chapter Four explains the mathematical equations representing the heat generation in TREAT upgrade reactor and the contribution of each of the gamma sources to the total energy deposition. It also includes a description of the calculational tools used in this work as represented by the various processing codes. Detail description of the format of the coupled neutron-gamma groups cross sections sets are also presented.

Chapter Five shows the heating rate results obtained by ANISN and DOT3.5 codes. Analysis of these results is presented and compared with those obtained by QADBS-1 code.

1.2. Heat Generation in Nuclear Reactor

To understand the gamma ray heating rate in the nuclear reactor, we need to examine the distribution of the energy released by a single fission event. This energy is distributed both in space and time, as shown in Table 1.1.

A brief description of the energy forms listed in Table 1.1 results in energy deposition[16, 17] throughout a nuclear reactor follows:

Table 1.1. Distribution of Energy Emitted in a Single Fission Event as a Function of Space and Time.

	Energy Source	Direct or Indirect	Local Deposition MeV/fission	Remote Deposition MeV/fission
1	Kinetic Energy of Fission Fragments	direct	168	negligible
2	Primary of Nuclear Fission Gammas:*			
	(a) prompt fission gammas	direct		7.64
	(b) short-lived fission products gammas	indirect		0.43
	(c) intermediate-lived fission products gammas	indirect		0.55
	(d) long-lived fission products gammas	indirect		6.65
3	Fission Products Betas	indirect	8	negligible
4	Fission Products Neutrinos	indirect		12.0**
5	Secondary or Radioactive Capture Gammas:			
	(a) prompt capture gammas	indirect		2-4
6	Recoil Nuclei from Elastic Scattering	indirect		4.0
7	Inelastic Scattering Gammas	indirect		0.69
8	Deexcitation Gammas from (n,2n), (n,p) and (n,α) reactions	indirect		negligible
9	Bremsstrahlung Gammas	indirect		0.2
10	Annihiliation Gammas	indirect		negligible
	Total		176	22.0

*prompt, $t \leq 0.05$ microsec, short-life, $0.05 < t \leq 1.0$ microsec, intermediate-life, 1.0 microsec $< t \leq 1.0$ sec, delayed, $t > 1.0$ sec.

**this energy is not recoverable since it is not deposited in the reactor.

As a result of U-235 fission event, two fission fragments are released carrying away as kinetic energy a total of 168 MeV/fission. These fission fragments lose their energy by the Wigner effect and by elastic ionization collisions. All of this energy is deposited in the fuel element essentially at the site of the fission event. More precisely, the range of the fission fragments in the TREAT reactor fuel (UO_2) is about 0.001 cm.

Because the fission fragments have an excess of neutrons, they are unstable to β^- decay. This process typically occurs several times in a given fission product decay chain before a stable isotope is reached. These beta particles which carry approximately 8 MeV/fission lose their energy primarily by inelastic collisions and Bremsstrahlung radiation. Approximately 99% of this beta energy will be deposited over a few millimeters with the remaining 1% being carried away as Bremsstrahlung radiation.

Prompt fission gammas are those emitted with the fission events. Their intensity in the reactor and their contribution to the heating rate depends on the reactor power and on the distance $|\vec{r} - \vec{r}'|$, where r is the site of fission and r' is the heating site. It also depends on the attenuation provided by the intervening material.

Since TREAT is a transient reactor, it is reasonably valid to assume the short-lived fission product decay gamma events to coincide with the prompt fission events and to neglect the long-lived fission product decay gammas.

Fission product neutrinos carry approximately 12 MeV/fission. These neutrinos have a very low probability of interaction within the reactor and can be assumed to carry their entire energy out of the reactor.

Radiative capture gammas are those emitted as a result of neutron absorption. Their contribution to the heating rate is considered significant because of their high energy. The energy emitted per fission depends on the energy and space dependent neutron flux, $\Phi(\vec{r},E)$; the microscopic capture cross sections of the various isotopes, $\alpha^{j}_{n,\gamma}(E)$; the atom densities in the various reactor regions, $N^{j}(\vec{r})$; and the capture gamma energy spectrum for each isotope, $\gamma^{j}(E)$. In terms of an equation the average total energy of capture gamma emitted per fission is:

$$\bar{E}_{n,\gamma} = \frac{\int_E \int_V \Phi(\vec{r},E) \sum_j N^{j}(\vec{r})\, \sigma^{j}_{n,\gamma}(E)\, \gamma^{j}(E)\, dE\, du}{\int_E \int_V \Phi(\vec{r},E)\, \Sigma_f(\vec{r},E)\, dE\, du} \qquad (1.2)$$

Using the above equation, the actual value of $\bar{E}_{n,\gamma}$ for TREAT upgrade reactor could be computed from a detailed neutron balance in which the fraction of fission neutron captured by each material is computed. Typical values, however, should be in the range of 1.5 to 4.0 MeV/fission. Since the TREAT reactor is graphite moderated and contains boron the principal (n,γ) reaction is due to obsorption by U-235 which releases 1.15 MeV of gamma energy/fission. Hence a value of around 2.0 MeV/fission is expected from radiative capture

reactions. Radiative capture by boron, the other principal absorber is insignificant since absorption occurs primarily by (n,γ) reactions rather than (n,γ) reactions.

Inelastic scattering processes occur when the kinetic energy of the incident neutron is larger than the energy of the first excited state of the target nucleus. In terms of an equation, this can be represented by[18]:

$$E_\ell = \frac{A + 1}{A} E_c \tag{1.3}$$

where

E_ℓ = kinetic energy of the incident neutron in the lab system,

E_c = total energy of neutron and nucleus in the center of mass system, and

A = atomic weight.

Since E_c must be greater than ε_1 (the energy of the first excited state) for inelastic scattering to occur, it follows that E_ℓ must be greater than E_t, where[18]

$$E_t = \frac{A + 1}{A} \varepsilon_1 \tag{1.4}$$

where

E_t = inelastic threshold energy.

In order for this process to occur, the incident neutron energy must be in the KeV to MeV range depending on the mass number of the target nuclei. For example, heavy nuclei such as U-238, the inelastic threshold is in the KeV range, but for light nuclei such as C-12 it is in the MeV range.

In case of inelastic scattering, part of the process energy is carried away by the scattered neutron and the other part is obsrobed by the target nucleus leaving it in excited state. Subsequently, the target nucleus looses its excitation energy by emitting one or more gammas.

The heat generation rate from neutron elastic scattering is approximately[19] $\xi\ \Sigma_s\ \Phi E$ for neutron of energy E, where

ξ = average logarithmic energy decrement per collision.

and it is defined by

$$\xi = 1 + \frac{(A-1)^2}{2A} \ln \frac{A-1}{A+1}$$

This expression can be approximated by:

$$\xi = \frac{2}{A + 2/3}$$

where

A = the mass of the target nuclei. So, the heat generation rate from neutron elastic scattering is[20]

$$\Sigma_s \Phi E \frac{2A[1 - F_1(E)]}{(A-1)^2}$$

where

F_1 = coefficient of the P_1 term in the Legendre expansion for the neutron elastic scattering cross section.

Other reactions may occur in nuclear reactors which leave the target nucleus in excited state. The scattered particles in these reactions is something other than a single neutron. Such reactions are (n,2n), (n,p) and (n,α). The excited nucleus in these reactions lose its energy of excitation by gamma emission. The energy released in most cases is about 0.5 MeV. However, these reactions are important and must be accounted for in gamma heating calculations, if the reactor contains materials with high (n,α), (n,p) or (n,2n) cross sections such as boron[21]. Otherwise, the cross sections of such reactions are low and the threshold is high. So, they may be ignored.

Bremsstrahlung radiation is caused by acceleration and deceleration of high speed beta particles in the atomic electric field. The particle loses energy by emitting Bremsstrahlung radiation. This process is important when high speed beta particles interact with material of high atomic number. Generally, the Bremsstrahlung radiation has little effect on gamma heating.

Annihiliation gammas result from the combination of electron-positron pair (arising from pair production events) that have lost their kinetic energy. Two 0.51 MeV gammas are produced for each electron-positron reaction. Since pair production process is

considered one of the forms of gamma energy deposition in nuclear reactors, annihiliation gammas must be accounted for in heating rate calculations.

1.3. Methods of Gamma Heating Calculation

In calculating gamma-ray heating in a nuclear reactor, the following steps are used:

First; the neutron flux distribution is calculated using neutron group cross sections in diffusion, Monte Carlo as transport code.

Second; the gamma source distribution, which was induced by the neutron flux at each spatial point is then calculated. This energy dependent source term is obtained from the neutron flux by utilizing gamma production cross section in an appropriate code.

Third; the gamma flux distribution, that results from the calculated gamma source is obtained by performing a fixed source gamma transport calculation using gamma interaction cross sections.

Fourth; the gamma-ray heating is determined by multiplying gamma flux by gamma energy absorption cross sections.

This step-by-step procedure is reported in earlier work[22, 23, 24, 25]. The neutronic calculations of gamma heating in a fast reactor environment[22] were accomplished with 29 neutron energy groups in the S_4P_0 approximation. The gamma transport calculations were done with 20 gamma energy groups and S_8P_3 approximations, utilizing DOT code.

The same procedures are used by Miles[23] in calculating the gamma heating in TREAT reactor. More of Miles work will be discussed in the next section.

However, the four steps technique can be combined in one step calculations, this is accomplished by utilizing the coupled neutron-gamma cross section sets along with a computer code capable of performing a single particle transport, such as, ANISN, DOT and MORSE codes. The main characteristic of the coupled neutron-gamma cross section set is that, gamma production cross sections are entered as down scattering events of the neutron groups cross sections, and gamma scattering cross sections are expanded in P_3 Legendre expansion. The various coupled neutron-gamma cross section sets which are used in the present work, their format and energy boundaries will be discussed in detail in Chapter Four.

1.4. Previous Work Involving Gamma Heating of TREAT Reactor

Miles[23] calculated the gamma heating in TREAT reactor. His work involves several computer programs. The three major programs are: SCAMP, GAMSOR and QADBS-1 along with another four programs, FDHC,MISC,SDHP and QDENS. The purpose of these programs is to prepare the input data for the three major ones.

SCAMP is an S_N neutron transport code which can be used for slab, cylinder or spherical geometry. The function of the code is to calculate the neutron flux distribution at each spatial point of the reactor. SCAMP was used to compute 33 neutron group fluxes using

a 215 mesh point model. The 33 neutron groups were then collapsed into 4 energy groups. These 4 group fluxes were used by GAMSOR to calculate the gamma source distribution at each of the 215 mesh points. The gamma source distribution along with the materials and and geometrical description of the reactor are used as input for QADBS-1 (Point-Kernel Code) which finally calculated the gamma heating rate at each spatial point.

CHAPTER TWO

Discrete Ordinate Method

2.1. Introduction

Since part of this work is devoted to modifying and creating an operational load module of DOT3.5, this chapter along with Appendix D is intended to give the reader a brief idea of discrete ordinate methods upon which the code is based and the development of the theory that support the DOT code.

The use of discrete ordinates as a technique of solving the neutron transport equation was first introduced by Wick[26] and Chandrasekhar[27]. Its early application was limited to solving simple problem involving the transport of monoenergetic neutrons isotropically scattered in a slab geometry. The basic assumption was the approximation of the integral term in Boltzmann transport equation (Appendix D, Equation D-1) by discrete ordinates quadrature, and the solid angle is divided into a number of segments and discrete directions and weights are chosen.

In the years that followed, the two-dimensional discrete ordinates (S_N) method, which is generally called the second version of the S_N method was developed by B. G. Carlson[28]. Carlson extended the previous work by including the cylindrical and spherical geometries. The implementation of the method was primarily limited to relatively easy problems, such as criticality calculation in highly enriched systems.

The S_N method became popular especially in the United States with the advancement of sophisticated digital computers. Improvements in the method were made to extend its capability to solve more complicated systems and to minimize some of its limitations. Mynatt et al.[29] have recently made such improvements. The features of their work are:

(1) Adding anisotropic scattering as an option. So, the scattering approximation can be adjusted for the specific problem. This makes the method suitable for both neutron and gamma-ray deep penetration calculation.

(2) The angular-dependent of the scattering cross section in the scattering integral of the transport equation is approximated by Legendre polynomial series (D-8).

(3) Development of analytical first collision source for monodirectional beam sources problems in which the collided and the uncollided components must be separated.

$$S(I,J,L,G) = \sum_{G'=1}^{G} \Sigma_{\ell}(G' \rightarrow G) \Phi_u(I,J,G') P_{\ell}^{m}(U) \times (2)^{1/2}$$

$$\times \left[\frac{(\ell - m)!}{(\ell + m)!}\right]^{1/2} \text{Cos } (m\psi) \qquad (2.1)$$

The parameters are defined by source, S, radial interval, I, axial interval, J, angular moment, L, group, G, Legendre coefficient of the scattering cross section from group G' to G, $\Sigma_{\ell}(G' \rightarrow G)$, the

uncollided flux, Φ_u, the direction cosine, μ, the radius vector, Cos ($m\psi$), and L corresponds to a particular pair of indices ℓ and m.

(4) Include the calculation of the flux at arbitrary point external to the system.

(5) Improve the convergence of inner iteration (Section 2.2.2).

After such improvement, the S_n method became an efficient tool of obtaining a numerical solution of the Boltzmann transport equation. The fundamental objective of the method is to evaluate the angular flux, $\Phi(\vec{r}_s,E,\vec{\Omega})\vec{\Omega},\vec{n}\ dA_s$, in a number of discrete directions. It also treats the independent variables of the time independent transport equation (D-1) such as space, $\vec{r}$, direction $\vec{\Omega}$, and energy E as discrete. So, the method actually formulate the Boltzmann transport equation into a set of finite difference equations (D-8) and (D-10), which relate the variable flux at each point to the flux at the adjacent point. This is accomplished by dividing a phase space cell into a number of discrete points, and integrating the transport equation over a finite-difference cell in space. Such algebric finite-difference equations are solvable by digital computers. The solution approaches the exact solution of the transport equation as the space, $\vec{r}$, direction, $\vec{\Omega}$, and energy, E, meshes approach differential size. This is especially true for one dimensional geometry[4]. In recent years, several computer codes based on the S_n-method have been made available. Such codes as ANISN and DTF-IV (one-dimensional), DOT and TWOTRAN (two-dimensional).

2.2. DOT3.5 Code

2.2.1. Code definition. DOT3.5 (Discrete Ordinates Transport) is the improved version of DOT-III. The main feature of the improvement lies in convergence on deep penetration problems. The code is a two-dimensional radiation transport procedure, written in FORTRAN IV. It solves the energy-dependent Boltzmann transport equation, which describes the transport of particles not under influence of an external force field in the XY, RZ and Rθ two-dimensional geometries. The transport equation is approximated by discretizing the values of each variable. In the energy variable, it is assumed that all the particles traveling with energies within given intervals interact according to cross section data averaged over those intervals.

In the variable flux, it is assumed that all the particles are traveling along one of the discrete directions. So, the flux, $\bar{\Phi}(r_i, Z_j, E_g, \Omega_d)\ \Delta E_g = \phi_{ijgd}$ is averaged in the spatial interval surrounding r_i, z_j, integrated over the energy group (g), and averaged in the solid angle segment surrounding (Ω_d).

DOT is capable of solving inhomogenous (fixed source) problems as well as homogenous (eigenvalue) problems. In the first case, the source can be either distributed throughout the system or concentrated at the system boundaries. It can also be exterior or interior to these boundaries.

In the second case, homogenous problems can be specified in which the multiplication factor is found (k calculation), in

which the equivalent logarithmic period is found (Rossi α calculation), or in which spatial dimensions or material concentration are changed to achieve a specified value of k or α (dimension and concentration searches).

The DOT user has the option of selecting the type of calculations desired. This is done by use of the input parameter (I04) from the following alternatives:

1. Fixed source problems (I04 = 0 or 5).

2. Static multiplication factor (k_{eff}), the ratio of neutron source to neutron loss in time-independent Boltzmann transport equation (I04 = 1).

3. Determination of Rossi α (inverse asymptetic reactor period) that brings the system critical when an absorber that follows the "1/v" cross section is placed in the system, (I04 = 2).

4. Determination of the fuel concentration for a given value of k, (I04 = 3).

5. Calculation the fuel zone thickness to obtain a specified value of k.

Besides these alternatives, there are some other features of the code which can be utilized. For example, the solution by the diffusion theory is available in all DOT geometries, and can be selected by groups (29$$ array). The scattering order can also be selected by group. The scaler flux output can be written on dismountable device, rather than temporary scratch storage, as the problem proceeds; if a unique logical unit is selected. This

prevents loss of data in case a problem is aborted. Angular flux, cross sections, and scalar flux output can be bypass (IB2 = 3).

Activities induced within the system can be calculated by specifying (19$$ and 20$$ arrays). Kerma factor can be inserted as activities (once it is written in ANISN format) to the cross sections input as needed.

2.2.2. Code options. (A) Boundary Conditions: Depending on the problem geometry and specifications, the user has an option of imposing a variety of boundary conditions such as vacuum, reflected, periodic, etc. Each of these boundary conditions has its own characteristic and implementation with regard to the incoming and outgoing flux. The modeling of the TREAT reactor in the problem solved in this thesis dictated use of vacuum for the right and the top boundaries (B02 = B03 = 0), and reflection for the left and the bottom boundaries (B01 = B04 = 1).

(B) Convergence: DOT has three levels of iteration:

(1) Inner iteration.

(2) Fission source iteration.

(3) Iteration for eigen value searches.

Inner iteration is necessary. It takes into account the particle down scattering (G'→G) sources

$$S_G(\text{down}) = V_{I,J}\, W_D \sum_{\ell=0}^{LMAX} A_D^{\ell,m} \sum_{G'=1}^{G-1} S_{I,J,G,G'}^{\ell,m} \times j_{I,J,G'}^{\ell,m} \qquad (2.2)$$

and within group scattering (G→G) sources

$$S_G(\text{ingroup}) = V_{I,J} W_D \sum_{\ell=0}^{LMAX} A_D^{\ell,m} S_{I,J,G,F}^{\ell,m} \times j_{I,J,G}^{\ell,m} \qquad (2\text{-}3)$$

where the parameters are defined in Equation (D-8) of Appendix D. The objective of this inner iteration is to compute the angular flux for each group and mesh point.

DOT will calculate the flux for the highest energy group first, the second highest energy group next, and so on, till it gets to the lowest energy group. The inner iteration for each energy group is continued until the scalar flux converges according to one of the following criteria[7]:

(1) If G06 = 0.0 and IZC = 0, an integral iteration test on all zones is used with EPS as the criterion. Convergence is indicated if

$$\frac{1}{V} \int \left| \frac{\phi^n(\vec{r}) - \phi^{n-1}(\vec{r})}{\phi^n(\vec{r})} \right| dr \leq \text{EPS} \qquad (2.4)$$

where the integration is over the entire system volume V.

(2) If G06 ≠ 0.0 and IZC = 0, a pointwise scalar flux criterion is used on all zones with G06 as the criterion. Convergence is indicated if

$$\text{MAX} \left| \frac{\phi^n(\vec{r}) - \phi^{n-1}(\vec{r})}{\phi^n(r)} \right| \leq \text{G06} \qquad (2.5)$$

From the calculated fluxes, the fission sources for each group are determined.

Fission source iteration and iteration for eigenvalue searches are part of outer iteration (power iteration). In a given power iteration, the fission source is determined by the flux in the previous iteration. The iteration are continued until:

$$\left| \frac{S^{n-1} - S^{n}}{S^{n-1}} \right| < EPS \tag{2.6}$$

In eigenvalue calculation S^n is given by

$$S^{n} = \frac{1}{k^{n}} \int \int \nu \Sigma_{f} \phi^{n} dE \, d\vec{r}. \tag{2.7}$$

where

k = the multiplication factor

Σ_f = macroscopic fission cross section of energy group E.

ν = number of fast neutron emitted per fission.

In the present work it is found that 20 inner iteration for each group, 20 outer iteration and specifying a pointwise scalar flux criterion (G06 $\neq$ 0) to speed the convergence are suitable.

(C) Flux: DOT provides several options for calculating the flux. Such options are: (1) Linear calculation, (2) Step-function calculation, (3) Weighted-difference, and (4) Mixed mode.

The linear option which is based on the set of the finite-difference equations (D-8) and (D-10) in which a = b = c = 0.5 is the most accurate method in solving the flux, however, the drawback

of this method is the negative fluxes that are generated, especially when the flux is decreasing rapidly between two adjacent points. For the negative flux, fix-up, the step-function in which a = b = c = 1 or the weighted difference method is used with the linear method. This is called a "mixed mode" calculation. DOT also uses the step-function or the weighted difference alone. By controlling the input parameter (MODE), the user may choose any option desired. In the present work, the mixed mode option (MODE = 0) was used and gave satisfactory results.

2.2.3. DOT3.5 subroutines. DOT3.5 computer code package was obtained from the Radiation Shielding Information Center (RSIC) at Oak Ridge National Laboratory as CCC-276[7]. The package contains the various subroutines used by DOT along with the main source program. The following is the description of these subroutines.

Subroutine	Language	Number of Logical Record	Function
WWESOL	Assembly	400	Iterative Control During Point Scaling.
GRIND	Assembly	1520	Inner Iteration Calculation.
ALOCAT	Assembly	86	Allocate Storage for DOT.
CMVBT	Assembly	37	Moves Data Array at Maximum Speed.
JOBNUM	Assembly	34	Return the Job Name to the User.
ITIME	Assembly	72	Print the Day and the Time of Day.
ICLOCK	Assembly	65	Gives Elapsed Time.
IAND,IOR	Assembly	38	Not Needed on the IBM Equipment.
Source	Fortran	6445	Performs all other calculations.

Beside these subroutines, a fortran version of GRIND, ALOCAT, CMVBT, JOBNUM, ITIME and ICLOCK were included in the package, but they were not used for the load module.

2.2.4. Load Module of DOT3.5. DOT3.5 consists of several subroutines as indicated in the previous section, In creating a load module of the code, two steps are followed: (a) each subroutine was separately compiled by the appropriate language compiler to create an object module[30, 31, 32], (b) the set of the object modules were processed by the linkage editor to form an operational "Load Module".

Creating the assembler object modules caused no difficulty. The difficulty arose in creating an object module of the Fortran source program. When the source was compiled by (H) Compiler, a diagnostic of high severity was generated in subroutine INP. The compilation failed, the reason is the argument table exceeded. The diagnostic can be avoided by rewriting the subroutine, and that may cause a change in its characteristic and effect the output. The same type of diagnostics were generated when the source was compiled by (H.Extended) Compiler, a new version of (H) Compiler, it was added to LSU computer system at the end of July 1978. Fortunately, no diagnostics were generated, at this time by subroutine (INP). Since the source program can't be compiled entirely by any of the two compilers alone, two of them should be used. That was accomplished by breaking the source program into three separate

parts. The first part consists of the first four subroutines (MAIN, MESAGE, LOCO and DOT) as one unit under a new data set name, DSN = 'MAIN.LOCO.DOT', and was compiled by (H) Compiler. The second part consists of subroutine (INP), which comes in order after the first part. It was assigned a data set name, DSN = 'INP', and was compiled by (H-Extended) Compiler. The third part consists of the rest of the source program, which was assigned a date set name, DSN = 'DOT3-5', and was compiled by (H) compiler.

The detailed procedures of creating an operational load module of DOT3.5 code along with the necessary JCL are included in (Appendix A). The JCL for executing the "Load Module", and a typical sample problem input are shown in (Appendix B and C) respectively. The "Load Module" now resides on a permanent disk (USER02) of the LSU Computer System under a cataloged partioned data set name 'NSMILE.DOT3-5.LOADS'.

2.2.5. Code limitation. 1. Problem size: one of the improvement features of DOT3.5 from its previous version DOT-III is that no limitation on the problem size, DOT3.5 can handle small problems, ranging from 64,000 words (256k) to a problem as large as the installation permits. The reason is that DOT uses a technique called "flexible dimensioning"[7]. The code takes all the available space specified by the user and assigned it dynamically via the subroutine (ALOCAT) to fit the problem requirement. For any given problem, the code prints a message specifying the required amount of storage for that problem and the storage available. If the available

storage is not enough, an error message will be printed. For evaluating the amount of space required for a specific problem, the user is referred to Reference 7.

2. Running Time: the machine time required for DOT3.5 runs is given by the following formula[7]:

$$\text{Flux work} = FW = A04 * IM * JM * \Sigma II(LC)$$

$$\text{Running time} = RT = [A + \frac{FW}{FR}] * \frac{150}{SF}$$

where:

A04, IM, and JM are input parameters,

II(LC) = the total number of inner iteration for the LCth. outer iteration, all groups,

FR = flux rate,

SR = speed factor, and

A = overhead quantity, range from 0.5-5 minutes.

CHAPTER THREE

Modeling of the TREAT Upgrade Reactor

3.1. Introduction

The TREAT reactor is considered an irradiation test system supplementary to the fast reactor safety program in which the reactor meltdown problem can be studied in-pile. The reactor is capable of subjecting a large sample volume to conditions simulating various types of the transient nuclear excursions. The purpose of the TREAT is to provide quantitative data and to verify some of the analytical assumptions concerning the mechanism of melting down of the fast reactor fuel elements by nuclear heating analogous to a power excursion in the fast reactor core.

The TREAT reactor is designed to generate a large transient thermal flux in test elements to be located in a test hole with a great margin of safety and without doing any damage to the reactor itself. The graphite moderator serves as a heat sink in the testing process, absorbing the heat generated in a short period of time and more rapidly than the coolant could carry it away. Furthermore, on heating, the graphite would also raise the energy of the thermal neutrons and increases the probability of neutron leakage. This would cause the reactor to have a large negative temperature coefficient.

The reactor could be operated safely with fuel temperatures up to 600°C, producing an energy release of 2500 Mw-sec, with a

reactor period as short as 23 miniseconds. It is capable of generating power bursts up to 18,000 Mw. Several types of safety and fuel development tests may be conducted. Safety tests such as: fuel dynamics, coolant interaction and coolant expulsion and re-entry. Fuel development tests such as: FTR fuel performance tests, demonstration plant fuel performance tests and advanced fuel performance tests.

3.1.1. Description of the TREAT reactor. TREAT (Transient Reactor Test Facility) is a homogenous, graphite moderated, graphite reflected reactor[33, 34, 35, 36, 37]. The reactor cavity is designed to accommodate a core size of 6 feet 4 inches square by 4 feet high, or a total of 361 fuel elements, with a minimum graphite reflector thickness of 2 feet. Figure 3.1 is a perspective view of the reactor showing it loaded with a viewing slot into the center. Figure 3.2 is a plain view of the reactor.

The fuel assembly, Figure 3.3, consists of an upper and lower graphite reflector sections, and a central uranium oxide (UO_2)-bearing graphite fuel section. The fuel section (4 ft. long) contains six 8-inch fuel blocks canned in Zircaloy-3 (25 mil thick). The upper and the lower graphite reflector sections (each 2 ft. long) are contained in aluminum cans (50 mil thick). The 1/4 inch ribbed Zirconium spacer above and below the fuel section has the function of delaying the heat transfer from the fuel to the reflector and thus protecting the aluminum cans during severe transient. Figure 3.4 shows the TREAT core support and alignment. The reactor is

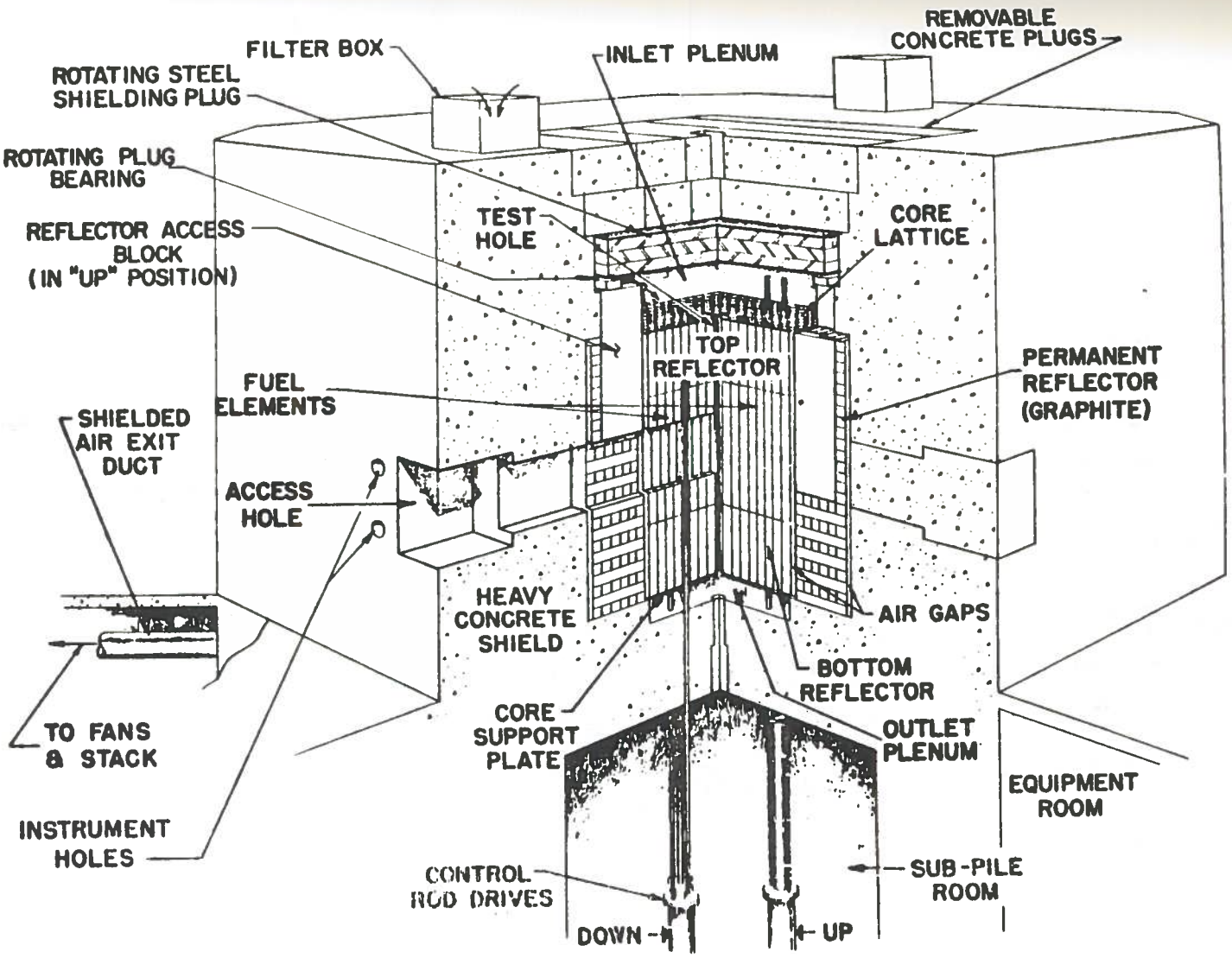

Figure 3.1. TREAT Reactor Perspective

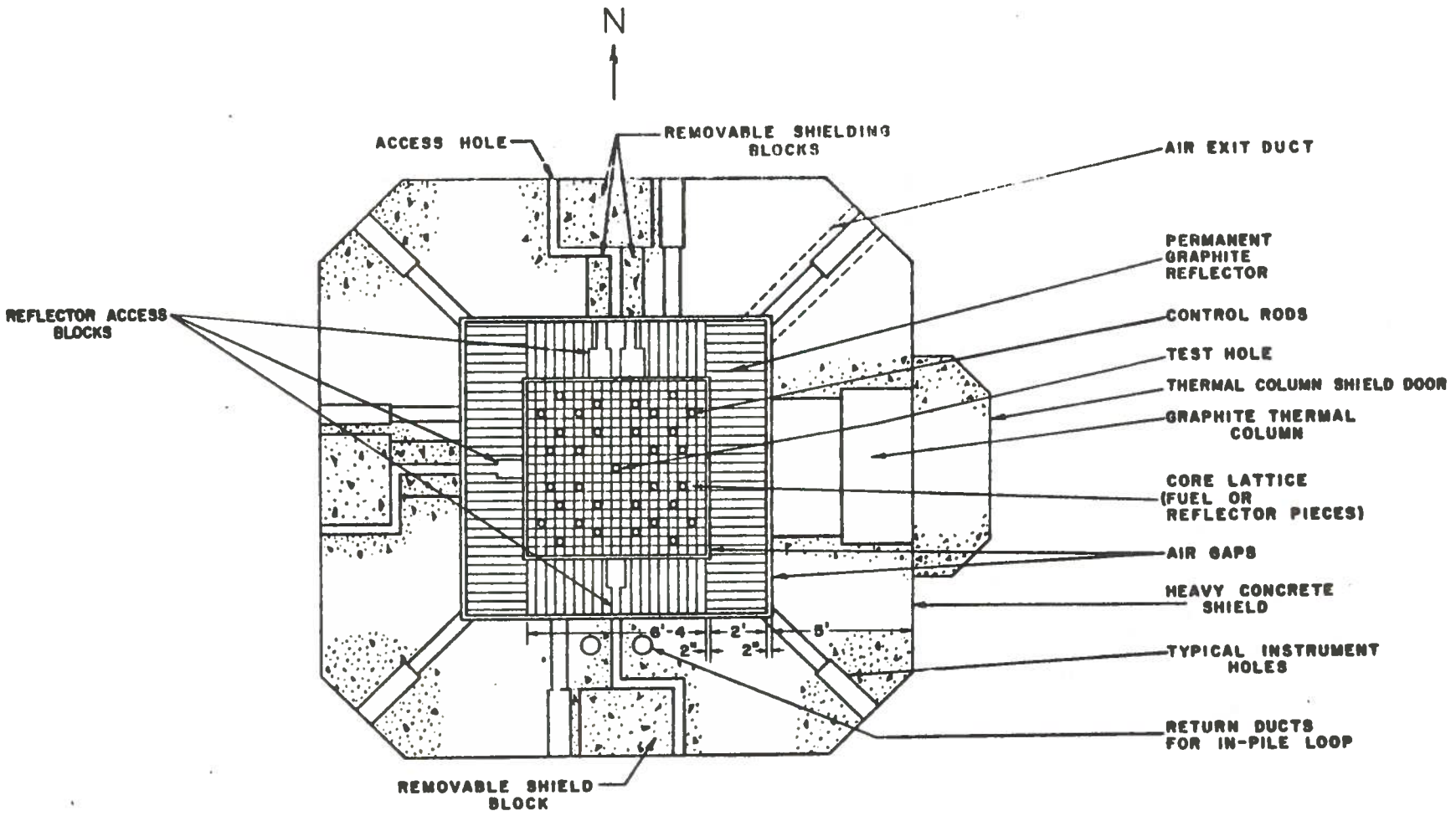

Figure 3.2. TREAT Plain View

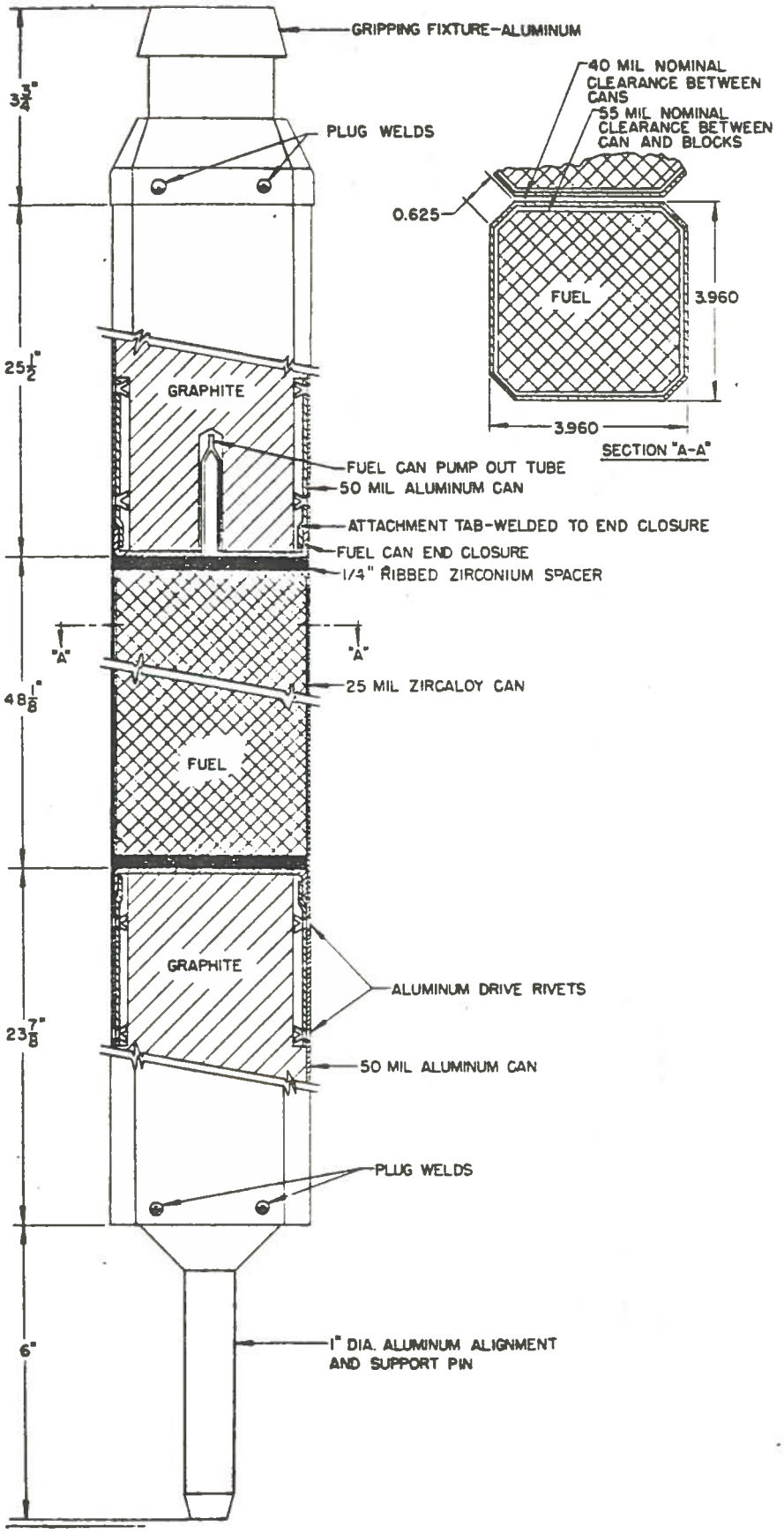

Figure 3.3. Standard TREAT Fuel Assembly

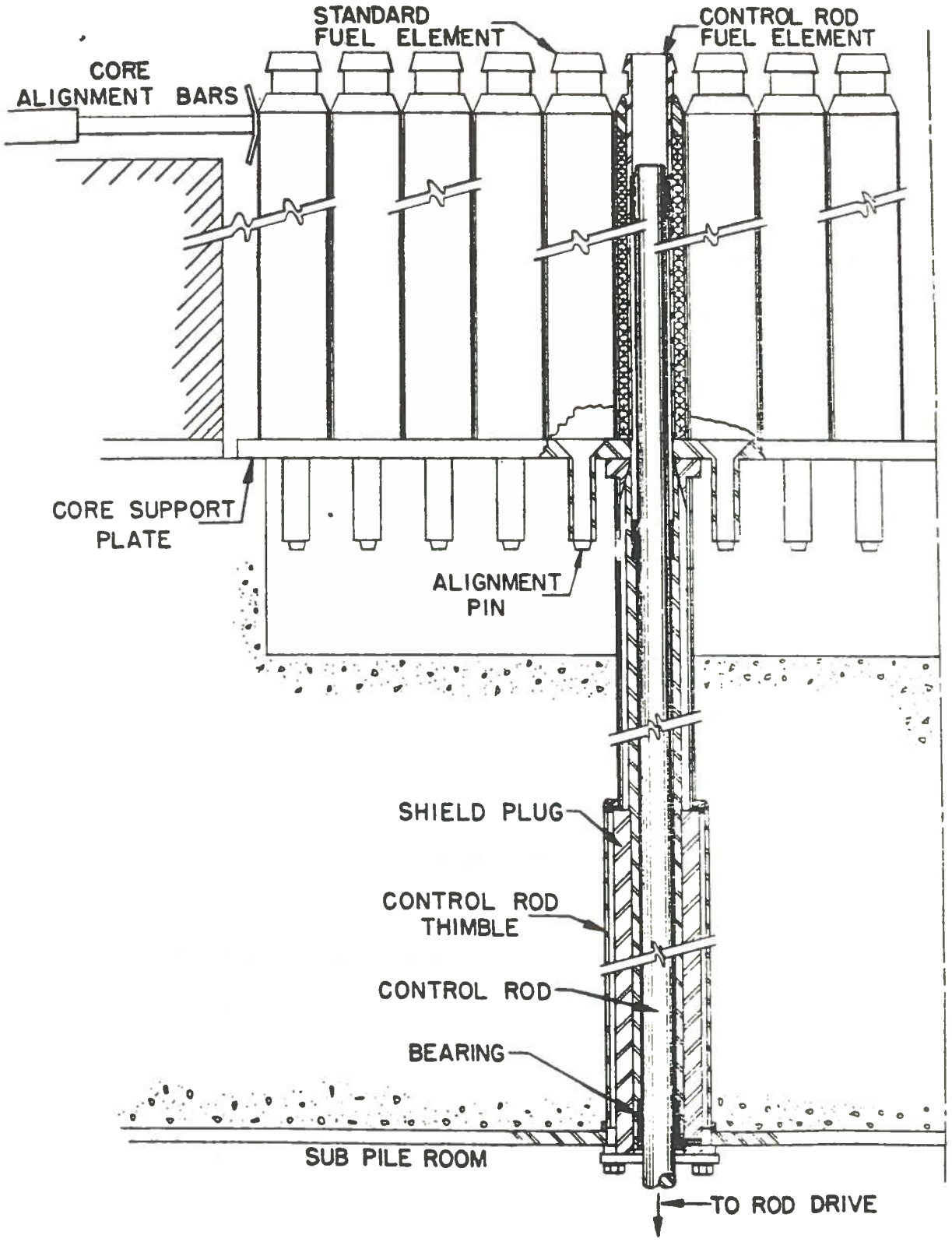

Figure 3.4. TREAT Core Support and Alignment.

shielded, Figure 3.5, with 15 ft. high and 5 ft. thick heavy concrete (density 220 lb/ft^3). The bottom 3 ft shield forms the ceiling of the sub-pile room. The upper 3 ft consists of removable heavy concrete blocks.

The TREAT upgrade reactor is similar to the TREAT reactor in most details, except for the graded fuel concentration of the convert or region. The fuel concentration decreases with increasing radial distance away from the test hole in order to produce a hard neutron spectrum in the test hole.

The GRIST-2 test cluster included in the modeling in this thesis is just one of the many test clusters. The testing of this test cluster in the TREAT reactor will be performed to support the (Gas Cooled Fast Reactor) experimental program in identifying inherent reactor shutdown mechanism and reactivity insertion rates associated with hypothetical "Unprotected Loss of Cooling and Transient Overpower Events".

In TREAT modeling, the reactor is divided into five major components:

(1) GRIST-2 test cluster.

(2) Test capsule.

(3) Convertor regions.

(4) Driver fuel.

(5) Reflector.

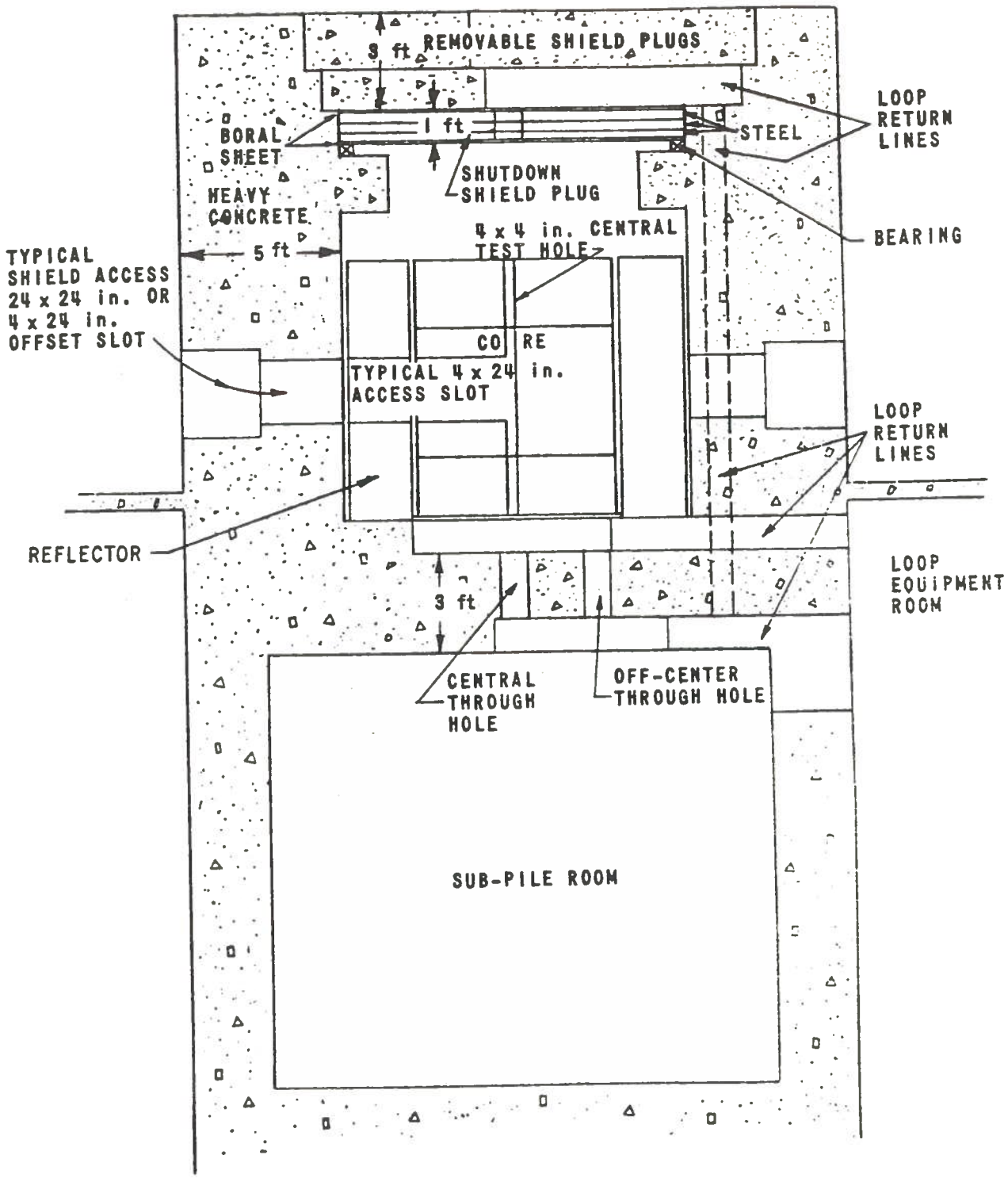

Figure 3.5. TREAT Shielding and Experimental Facilities.

3.2. GRIST-2 Test Cluster

The GRIST-2 test cluster, which forms the center section of the reactor, composed of 37 uranium oxide (UO_2) fuel pins each with 0.315 cm radius and 1.09 cm pitch arranged in hexagonal array Figure 3.6. The pins density is 9.83 gm/cm^3, and the uranium enrichment varies throughout the cluster in order to achieve a flat radial-power distribution. The cladding consists of stainless steel (SS-316) with ID of 0.644 cm and OD of 0.725 cm. The fuel pins are contained in a stainless steel hexagonal can. The atom densities for the various pins, the cladding and the hexagonal can are included in Table 3.1.

The hexagonal geometry of GRIST-2 has to be cylindricallized in order to be modeled by SCAMP[23], ANISN and DOT3.5 codes. This is accomplished by using a cylindrical model of the hexagonal can with the same cross sectional area as shown in Figure 3.7. For the hexagonal fuel pins array case, the array was divided into four cylindrical regions. Each region represents one of the four hexagonal ring of Figure 3.7 and contains a certain number of pins. The cross sectional area of each region is set proportional to the number of pins it contains, with a total cross sectional area of the four rings [$(3.608)^2\pi = 40.8961\ cm^2$]. The number of pins, the cross sectional area and the radii of each region are given in Table 3.2. The cylindrical model of the four regions are shown in Figure 3.8.

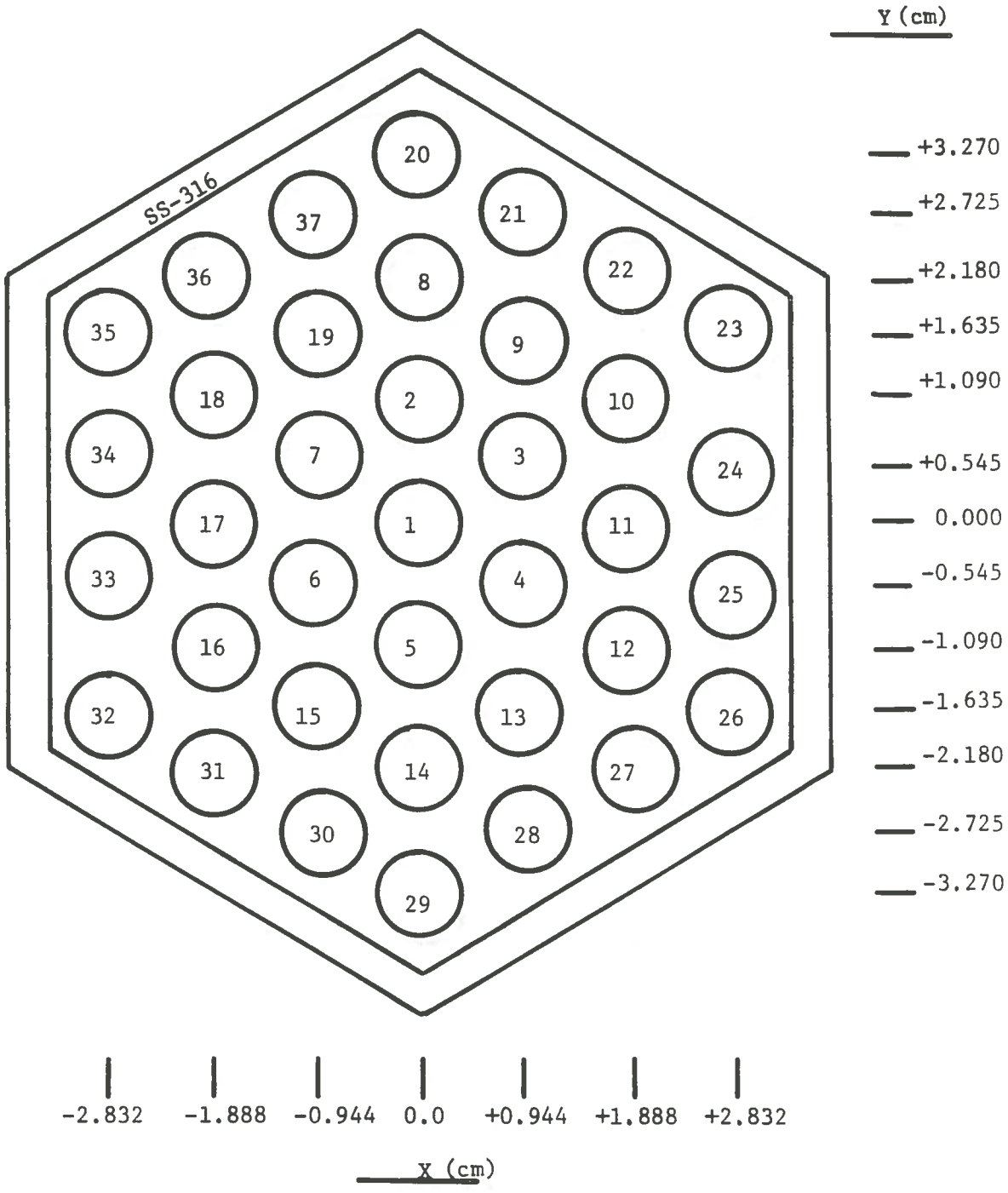

Figure 3.6. Representation of GRIST-2 Test Cluster

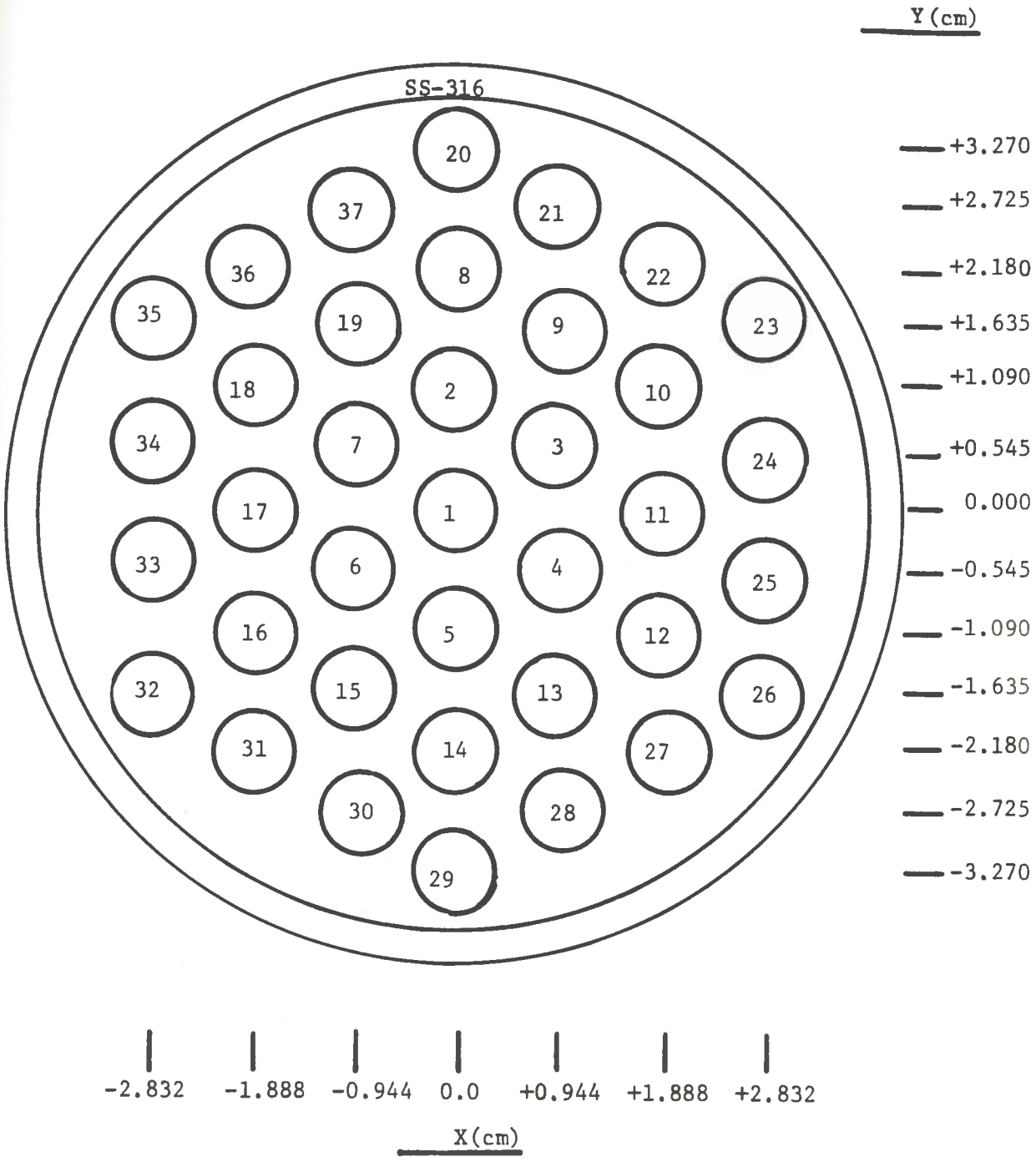

Figure 3.7. Cylindrical Model of the (SS-316) Hexagonal Can

The atom densities of the materials in each region are determined by multiplying the atom densities in Table 3.1 by the ratio, R, where

$$R = \frac{\text{total fuel pin (or cladding) cross sectional area in region i}}{\text{cross sectional area of region i}}$$

The radius of each fuel pin is 0.315 cm, that gives it a cross sectional area of 0.3117 cm^2. The cladding has an inside diameter of 0.644 cm and outside diameter of 0.725 cm, giving it a cross sectional area of 0.0871 cm^2. The cross sectional area of each region is given in Table 3.2. So, R, for the fuel pin is 0.2820, and for the cladding is 0.0788, and they are the same for all the regions. The atom densities for the materials in each of the cylindricallized four regions are given in Table 3.3.

3.3. Test Capsule

The test capsule of TREAT consists of concentric cylindrical annulli composed of 4 stainless steel, 2 Zircar,1 cadmium filter, and 4 void regions. The thickness and the relative positron of each region are shown in Figure 3.9. The atom concentration of each material is given in Table 3.4.

3.4. Converter Regions

The TREAT upgrade reactor consists of 19 converter regions. The cylindricallized modeling and the thickness of these regions are shown in Figure 3.10. The atom concentrations are given in

Table 3.1. GRIST-2 Atom Concentration (atom/barn-cm).

Isotope	Center Pin	Ring 1	Ring 2	Ring 3	SS-316	Zircaloy-3	Filter
U-235	2.0621-2*	1.9956-2	1.8185-2	1.6191			
U-238	1.5325-3	2.1894-3	3.9413-3	5.9128-3			
O	4.4307-2	4.4292-2	4.4250-2	4.4205-2		3.0676-3	1.0000-2
C					4.0300-4		
Cr					1.5810-2		
Mn					1.5000-3		
Fe					5.7230-2		
Ni					9.8820-3		
Mo					1.2600-3		
Zr						1.4385-3	
Cs-113							5.0000-3

* Read as 2.0621×10^{-2}

Table 3.2. Cross-Sectional Area and Radii of 4 Region Cylindrical Modeling of GRIST-2 Test Cluster.

Region Number	Number of Pins in the Region	Cross-Sectional Area (cm^2)	Radius (cm)
1	1	1.1053	0.5932
2	6	6.6318	1.5693
3	12	13.2636	2.5855
4	18	19.8954	3.6080
	37	40.8961	

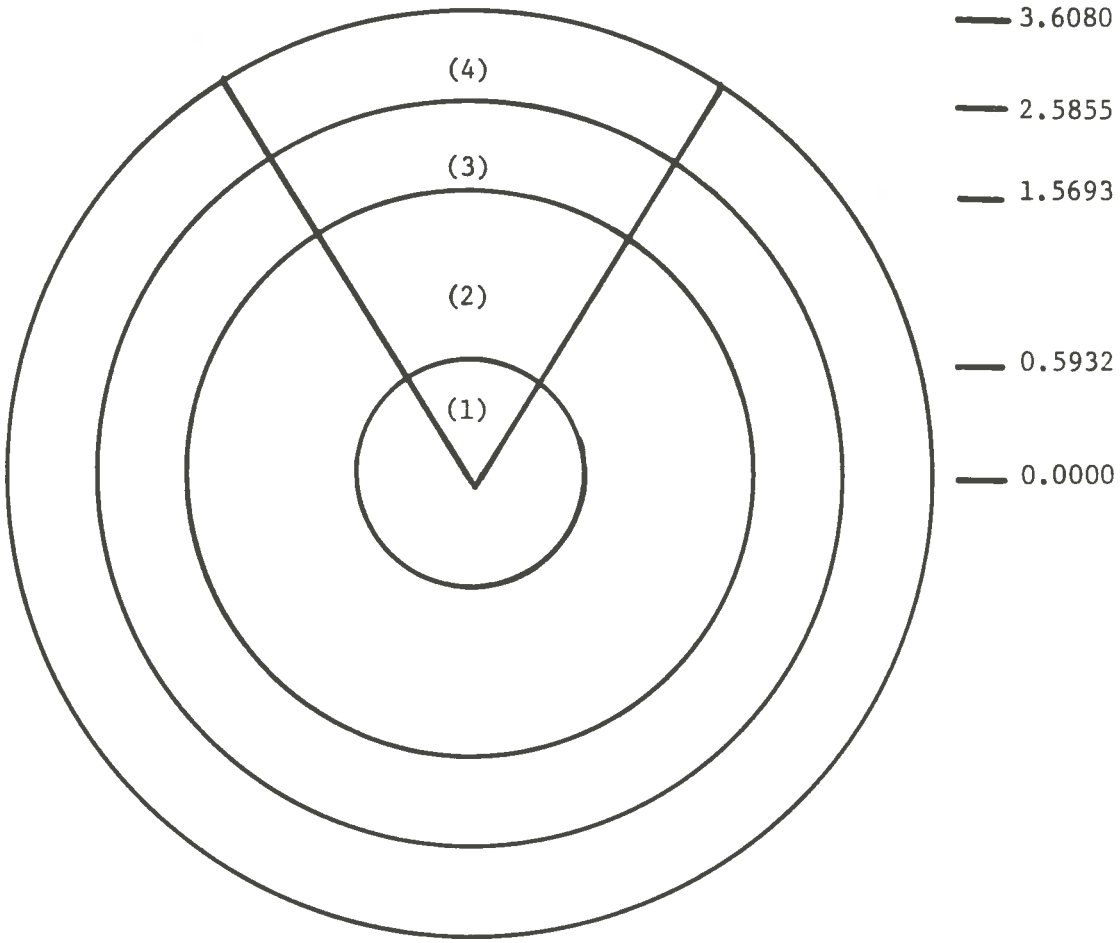

Figure 3.8. Cylindrical Model of GRIST-2 Test Cluster. Dimensions are in cm.

Table 3.3. Smeared Atom Densities (atom/barn-cm) in the Four Regions Cylindrical Modeling of the GRIST-2 Test Cluster.

Isotope	Region (1)	Region (2)	Region (3)	Region (4)
C	3.1760-5*	→	→	→
O	1.2500-2	1.2490-2	1.248-2	1.2470-2
Cr	1.2460-3	→	→	→
Mn	1.1820-4	→	→	→
Fe	4.5110-3	→	→	→
Ni	7.7880-4	→	→	→
Mo	9.9310-5	→	→	→
U-235	5.8170-3	5.6280-3	5.1282-3	4.5660-3
U-238	4.3230-4	6.1740-4	1.1110-3	1.6670-3

* Read as 3.1760×10^{-5}

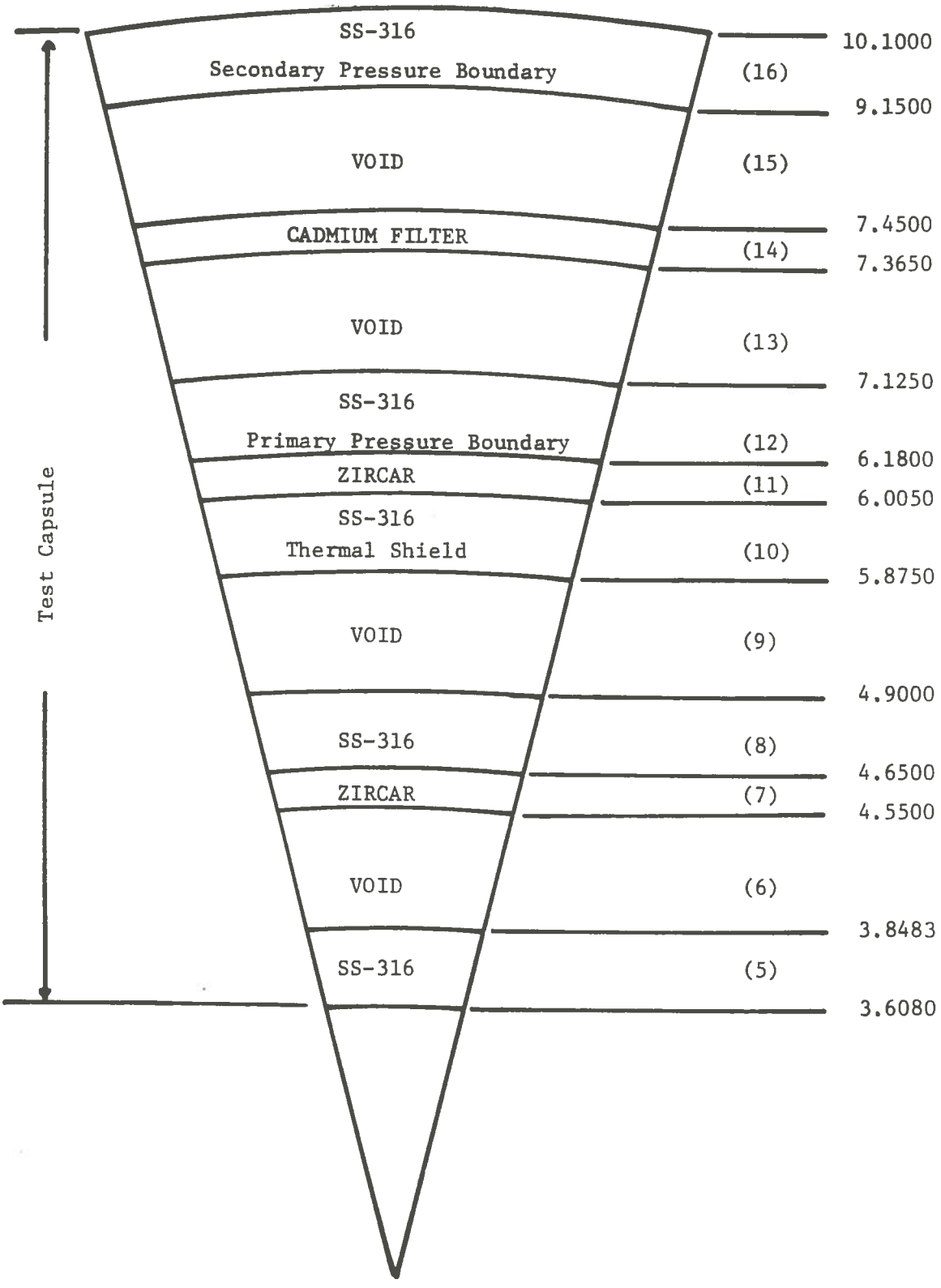

Figure 3.9. Cylindrical Model of the Test Capsule. Dimensions are in cm .

Table 3.4. Atom Concentration (atom/barn-cm) by Region in DOT3.5 Modeling of the Test Capsule of TREAT Upgrade Reactor.

Isotope	Region (5)	Region (6)	Region (7)	Region (8)	Region (9)	Region (10)
Cd						
C	4.0300-4*			4.0300-4		4.0300-4
O		2.500-10	3.0676-3		2.500-10	
Zr			1.4385-3			
Cr	1.5810-2			1.5810-2		1.5810-2
Mn	1.5000-3			1.5000-3		1.5000-3
Fe	5.7230-2			5.7230-2		5.7230-2
Ni	9.8820-3			9.8820-3		9.8820-3
Mo	1.2600-3			1.2600-3		1.2600-3

* Read 4.0300×10^{-4}

Table 3.4. Continued.

Isotope	Region (11)	Region (12)	Region (13)	Region (14)	Region (15)	Region (16)
Cd				5.0000-3		
C		4.0300-4				4.0300-4
O	3.0676-3		2.500-10	1.0000-2	2.500-10	
Zr	1.4385-3					
Cr		1.5810-2				1.5810-2
Mn		1.5000-3				1.5000-3
Fe		5.7230-2				5.7230-2
Ni		9.8820-3				9.8820-3
Mo		1.2600-3				1.2600-3

Table 3.5. Atom Concentration (atom/barn-cm) by Region for TREAT Upgrade Reactor.

Isotope	Conv. 1	Conv. 2	Conv. 3	Conv. 4	Conv. 5	Conv. 6
C	6.8584-2*	6.8665-2	6.8716-2		7.3022-2	7.3042-2
O	2.2815-4	1.8914-4	1.6394-4		1.4322-4	1.3354-4
Cr	5.1579-4	→	→	→	4.2201-4	→
Mn	1.3566-5	→	→	→	1.1100-5	→
Fe	2.0820-3	→	→	→	1.7034-3	→
Al	1.1052-4	→	→	→	9.0423-5	→
Ni	1.2692-5	→	→	→	1.0384-5	→
U-235	1.0666-4	8.8420-5	7.6645-5	→	6.6958-5	6.2429-5
U-238	7.4149-6	6.1469-6	5.3283-6	→	4.6548-6	4.3400-6
V	1.2448-5	→	→	→	1.0184-5	→

Isotope	Conv. 7	Conv. 8	Conv. 9	Conv. 10	Conv. 11
C	7.3058-2	7.3074-2	7.3089-2	7.3103-2	7.3118-2
O	1.2523-4	1.1763-4	1.1035-4	1.0326-4	9.6208-5
Cr	→	→	→	→	→
Mn	→	→	→	→	→
Fe	→	→	→	→	→
Al	→	→	→	→	→
Ni	→	→	→	→	→
U-235	5.8546-5	5.4993-5	5.1588-5	4.8274-5	4.4979-5
U-238	4.0700-6	3.8230-6	3.5863-6	3.3550-6	3.1269-6
V	→	→	→	→	→

* Read 6.8584×10^{-2}

Table 3.5. Continued

Isotope	Conv. 12	Conv. 13	Conv. 14	Conv. 15	Conv. 16
C	7.3133-2	7.3147-2	7.3163-2	7.3214-2	7.3223-2
O	8.9062-5	8.1694-5	7.4262-5	4.9102-5	4.4895-5
B	0.0	→	→	→	→
Cr	4.2201-4	→	→	→	→
Mn	1.1100-5	→	→	→	→
Fe	1.7034-3	→	→	→	→
Al	9.0423-5	→	→	→	→
Ni	1.0384-5	→	→	→	→
Zr	0.0	→	→	→	→
Cd	0.0	→	→	→	→
U-235	4.1636-5	3.8192-5	3.4717-5	2.2955-5	2.0988-5
U-238	2.8945-6	2.6551-6	2.4135-6	1.5958-6	1.4591-6
V	1.0184-5	→	→	→	→
Sn	0.0	→	→	→	→

Table 3.5. Continued

Isotope	Conv. 17	Conv. 18	Conv. 19	Driver	Reflector
C	7.3231-2	7.3239-2	7.3245-2	7.6210-2	8.366-2
O	4.1076-5	3.7465-5	3.4025-5	1.6460-5	0.0
B	→	→	→	6.4710-7	1.860-7
Cr	→	→	→	5.2200-8	0.0
Mn	→	→	→	0.0	0.0
Fe	→	→	→	1.4450-5	1.801-5
Al	→	→	→	0.0	0.0
Ni	→	→	→	7.7050-9	0.0
Zr	→	→	→	9.8600-4	0.0
Cd	→	→	→	1.6100-10	0.0
U-235	1.9203-5	1.7515-5	1.5907-5	7.6761-6	0.0
U-238	2.6551-6	2.4135-6	1.4591-6	5.5653-7	0.0
V	→	→	→	0.0	0.0
Sn	→	→	→	2.1340-6	0.0

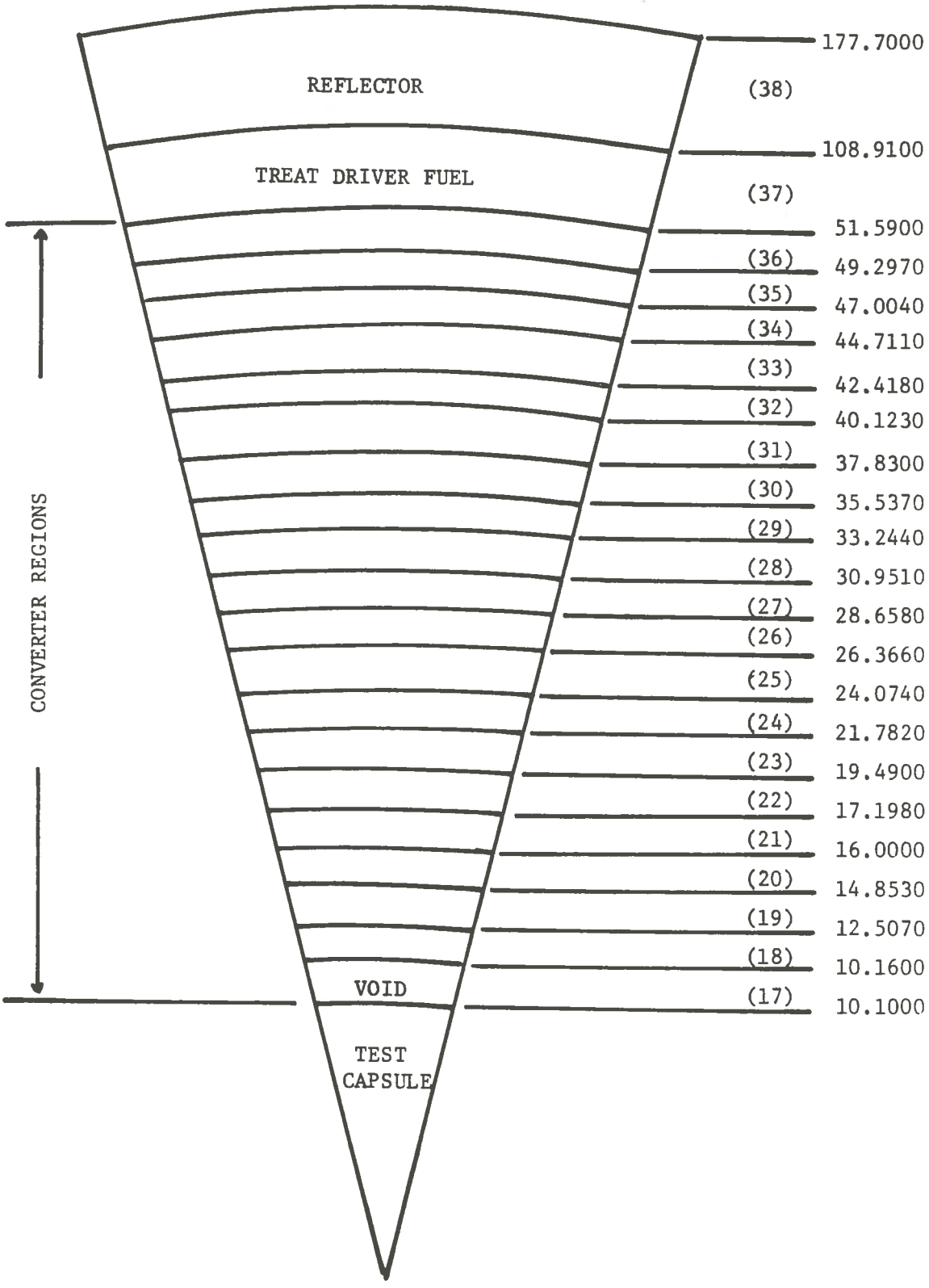

Figure 3.10. Cylindrical Model of TREAT Upgrade Reactor
Dimensions are in cm .

Table 3.5. For the purpose of reducing the problem size, some of the regions are combined, and eight regions are formed from the original 19 regions. The region number, inner and outer boundaries for each region formed are given in Table 3.6. The modeling of the eight regions along with the driver fuel and the reflector regions are shown in Figure 3.11.

The atom densities for the regions formed are computed by using the following formula.

$$P_{j,k} = \frac{\sum_i A_i P_{i,j}}{A_k}$$

where

$P_{j,k}$ = the atom density for the j-th isotope in the k-th formed region (atom/b-cm),

A_i = cross sectional area of the i-th converter region (cm^2),

$P_{i,j}$ = the atom density for the j-th isotope, in the i-th converter region (atom/b-cm), and

A_k = cross sectional area of the k-th formed region (cm^2).

The atom densities for the materials in each region including the driver fuel and the reflector regions are given in Table 3.7.

Table 3.6. Region Numbers and Boundaries Used in DOT3.5 Modeling of the TREAT Upgrade Reactor.

DOT3.5 Region Number	Inner Boundary (cm)	Outer Boundary (cm)	TREAT Regions Combined to form Regions for DOT3.5 Model
17	10.100	10.160	Void
18	10.160	12.507	Converter 1
19	12.507	14.853	Converter 2
20	14.853	17.198	Converter 3, 4
21	17.198	19.490	Converter 5
22	19.490	26.366	Converter 6, 7, 8
23	26.366	33.244	Converter 9, 10, 11
24	33.244	40.123	Converter 12, 13, 14
25	40.123	51.590	Converter 15, 16, 17, 18, 19
26	51.590	108.910	TREAT Driver
27	108.910	177.700	Reflector

Table 3.7. Atom Concentration (atom/barn-cm) by Region in DOT3.5 Modeling of TREAT Upgrade Reactor.

Isotope	Region (17)	Region (18)	Region (19)	Region (20)	Region (21)	Region (22)
C		6.8584-2	6.8665-2	6.8716-2	7.3022-2	7.3060-2
O	2.500-10*	2.2815-4	1.8914-4	1.6394-4	1.4322-4	1.2490-4
Al		1.1052-4	1.1052-4	1.1052-4	9.0423-5	9.0423-5
V		1.2448-5	1.2448-5	1.2448-5	1.0184-5	1.0184-5
Cr		5.1579-4	5.1579-4	5.1579-4	4.2201-4	5.2201-4
Mn		1.3566-5	1.3566-5	1.3566-5	1.1100-5	1.1100-5
Fe		2.0820-3	2.0820-3	2.0820-3	1.7034-3	1.7034-3
Ni		1.2692-5	1.2692-5	1.2692-5	1.0384-5	1.0384-5
U-235		1.0666-4	8.8420-5	7.6645-5	6.6958-5	5.8410-5
U-238		7.4149-6	6.1469-6	5.3283-6	4.6548-6	4.0600-6

* Read 2.500×10^{-10}

Table 3.7. Continued.

Isotope	Region (23)	Region (24)	Region (25)	Region (26)	Region (27)
B-10				1.2823-7*	3.6828-8
B-11				5.1939-7	1.4917-7
Cd				1.6100-10	0.0
C	7.3100-2	7.3150-2	7.3230-2	7.6210-2	8.3660-2
O	1.0290-4	8.1360-5	4.0940-5	1.6460-5	0.0
Zr				9.8600-4	0.0
Al	9.0423-5	9.0423-5	9.0423-5	0.0	0.0
V	1.0184-5	1.0184-5	1.0184-5	0.0	0.0
Cr	4.2201-4	4.2201-4	4.2201-4	5.2200-8	0.0
Mn	1.110-5	1.1100-5	1.1100-5	0.0	0.0
Fe	1.7034-3	1.7034-3	1.7034-3	1.4450-5	1.8010-5
Ni	1.0384-5	1.0384-5	1.0384-5	7.7050-9	0.0
U-235	4.8110-5	3.8040-5	1.9140-5	7.6761-6	0.0
U-238	3.3450-6	2.6440-6	1.3300-6	5.5653-7	0.0

* Read 1.2823×10^{-7}

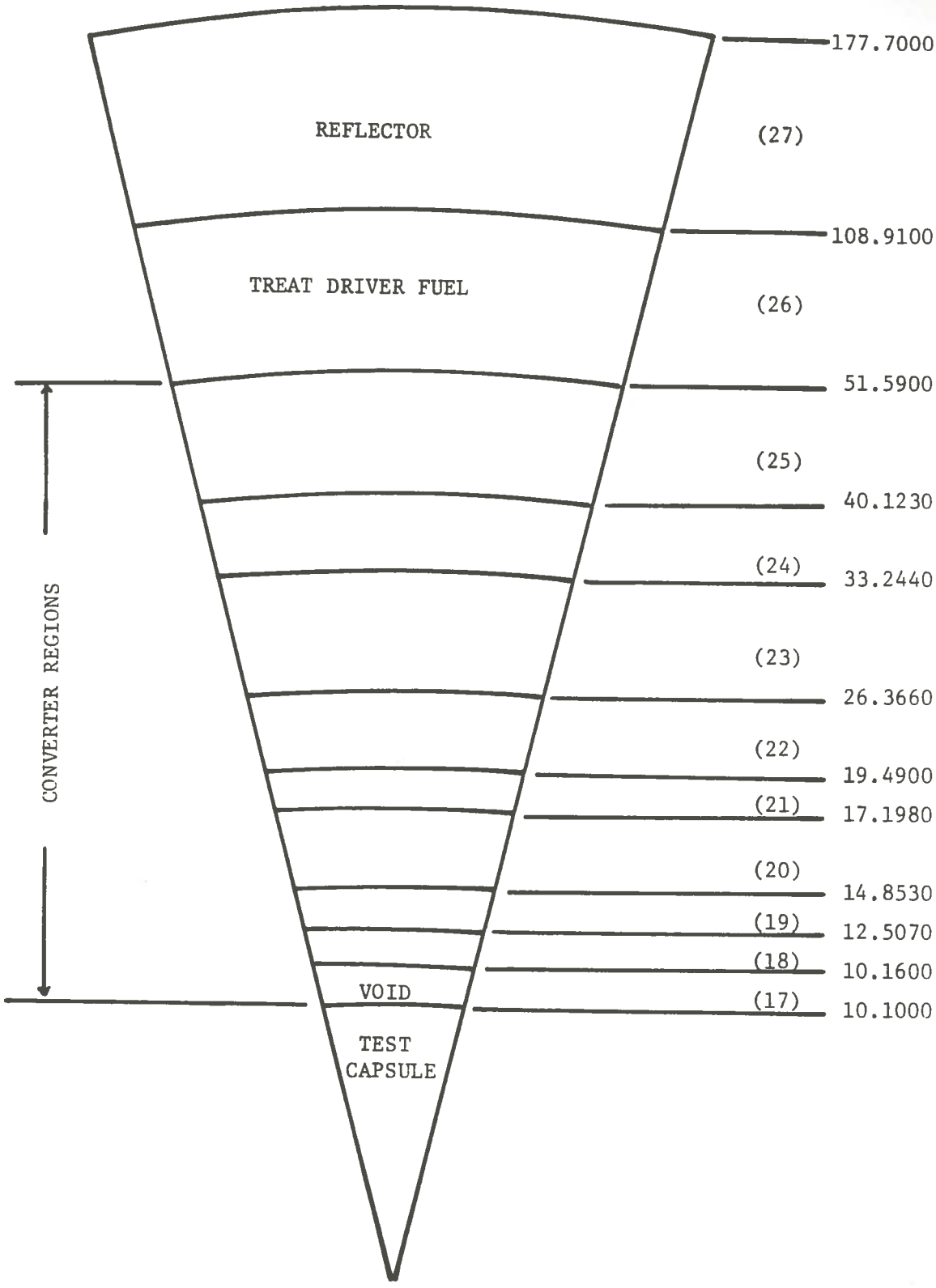

Figure 3.11. Cylindrical Model in DOT3-5 Modeling of TREAT Upgrade Reactor. Dimensions are in cm.

CHAPTER FOUR

Gamma Heating Calculations

The heat generation in the fuel region of the reactor is mainly caused by the dissipation of the kinetic energy of the fission fragments. In reactor components and the structural materials, the heat generation is partially caused by gamma radiation emerging from the reactor fuel region, and partially associated with the recoil nuclei which are produced by the neutron capture and gamma-ray interaction with the reactor materials. The neutron capture results in more gamma production which are transported to other reactor locations before depositing their energy. Investigation of gamma production and its interaction with reactor materials that lead to energy deposition is referred to as gamma heating.

4.1. Gamma Energy Deposition Reactions

In a nuclear reactor, three types of gamma-ray interaction[38] with matter are considered:

(1) Pair Production.

(2) Compton Scattering.

(3) Photoelectric Effect.

In all of these interactions there is a transfer of energy from the gamma-ray to the matter with which it interacts. This transfer of energy gives rise to gamma heating rate.

In pair production a gamma-ray is annihiliated and an electron-positron pair is created. It may occur when the photon energy is greater than 1.02 MeV, which is the minimum amount of energy needed to create an electron-positron pair. Excess energy of the reaction goes into kinetic energy of the particle formed.

Compton scattering is an elastic collision between a photon and "free" electron. It results in creation of recoil electron and scattered photon of lower energy than the incident photon. The energy difference between the incident and scattered photon is transferred to the free electron. The amount of energy transferred in any collision can be calculated by applying the laws of conservation of energy and momentum.

Photoelectric effect is the process in which a photon gives up all its energy to an electron, which subsequently dissipates its energy in the medium mainly by excitation of orbital electron and by ionization.

Gamma heating rate at any spatial point in a reactor may be expressed by a general formula[39]:

$$H_\gamma(\vec{r}) = \sum_i N_i(\vec{r}) \sum_j \int_E \sigma_{ji}(E)\varepsilon_{ji}(E)\Phi(\vec{r},E)dE \qquad (4.1)$$

where

$H_\gamma(\vec{r})$ = gamma heating rate at the spatial point r (MeV/cm^3).

$N_i(\vec{r})$ = number density of element i at point r ($atom/cm^3$).

$\sigma_{ji}(E)$ = microscopic cross section of element i for reaction j at gamma energy E ($cm^2/atom$).

$\varepsilon_{ji}(E)$ = energy deposition per reaction j in element i (MeV).

$\Phi(\vec{r},E)$ = gamma flux at the spatial point r and energy E (gamma/cm^2-sec).

define[40] k_{ji}:

$$k_{ji}(E) = \sigma_{ji}(E)\ \varepsilon_{ji}(E) \tag{4.2}$$

and

$$k_i(E) = \sum_j k_{ji}(E) \tag{4.3}$$

where

$k_{ji}(E)$ = microscopic kerma factor for reaction j in element i at energy E.

$k_i(E)$ = kerma factor for all materials in the system at energy E. (Kerma is an acronym for Kinetic Energy Released in the Materials).

The gamma-ray kerma factor can now be defined in terms of the three fundamental gamma-ray interaction (i.e., photoelectric effect, Compton scattering, and pair production).

$$\sum_j k_{ji} = k_\gamma^i = \sigma_{Pe}^i E + \sigma_{pp}^i (E-1.02) + \sigma_{Ca}^i E \tag{4.4}$$

where

k_γ^i = gamma kerma factor for element i (MeV cm^2/atom).

E_i = gamma energy (MeV).

σ^i_{Pe} = photoelectric effect microscopic cross section for element i (barn/atom).

σ^i_{pp} = pair production microscopic cross section for element i (barn/atom).

σ^i_{Ca} = Compton microscopic absorption cross section for element i (barn/atom).

From Equation 4.1 and 4.3, the gamma heating rate at spatial point r in a reactor for element i is

$$H_\gamma(\vec{r}) = \sum_i N_i(\vec{r}) \int_E \Phi(\vec{r},E)\, k_i(E)\, dE \tag{4.5}$$

To visualize the gamma-ray heating in a nuclear reactor, we need to examine the distribution of gamma energy released by a single fission event. This energy is distributed both in space and time, as shown in Table 4.1.

The volumetric thermal source strength in a reactor is normally computed by use of the equation

$$q'''(\vec{r}) = \gamma N(\vec{r}) \sigma_f(E) \Phi(\vec{r},E) \tag{4.6}$$

where γ is taken as the energy released per fission. This equation assumes that all recoverable energy released either directly or indirectly as a result of fission is deposited at the site of the fission event. In reality this is not so, since gammas and neutrons released in fission may be transported to a significant distance

Table 4.1. Distribution of Gamma Energy Sources per Fission in TREAT Upgrade Reactor as a Function of Space and Time.

	Gamma Energy Source	Direct or Indirect	Remote Disposition (MeV/fission) DLC-31 (FEWG)	Remote Disposition (MeV/fission) DLC-23 (CASK)
1	Primary or Nuclear Fission Gammas:			
	(a) Prompt fission gammas.	Indirect	7.64	7.64
	(b) Short-lived fission product-decay gamma.	"		0.43
	(c) Intermediate-lived fission product gamma.	"		0.55
	(d) Long-lived fission product-decay gamma.	"		6.65
2	Secondary or Radiative Capture Gammas:			
	(a) Prompt capture gamma.	Indirect	4.0	4.0
3	Inelastic Scattering Gammas:	Indirect	0.69	0.69
4	Gammas from (n,2n), (n,p) and (n,) Reactions:	Indirect	negligible	negligible
5	Bremsstrahlung Gammas:	Indirect	negligible	negligible
6	Annihiliation Gammas:	Indirect	accounted* for	accounted* for
	Total		12.33	19.96

*The contribution of annihiliation gammas is taken care of in the coupled neutron-gamma cross section sets by expanding the gamma scattering cross sections in a P_3 Legendre expansion (Equation 4.7).

before interacting with reactor materials, and thereby liberate their energy. This point is especially critical in assessing the heat generation in nonfuel regions. Therefore, in order to assess the heat generation throughout the reactor it is important to know the energy liberated directly and indirectly as a result of fission. Furthermore, it is important to assess whether this energy is liberated locally (i.e., near the site of fission event) or whether it is transported to a new location before it is liberated.

Table 4.1 lists the contributions of the various energy sources which are transported away from the site of a fission event that are included in the various cross section sets used in this thesis. This information is needed in comparing the results obtained from using the various cross section sets, and in estimating the heating due to those processes that were omitted.

However, annihiliation gammas and their contribution to the total heating rate which was not specified in Table 4.1 needs to be discussed further.

The contribution of annihiliation gammas is taken care of in the coupled neutron-gamma cross section sets by expanding[41] the gamma scattering cross sections in a P_3 Legendre expansion using the Klein-Nishina[38] equation. It is accounted for in the zeroth moments gamma scattering cross section which is modified for the pair production events as follow[42]:

$$\sigma_s^m(E \to E') = \sigma_{so}(E \to E') + \sigma_{pp}(E) \cdot 2\delta(E-0.5) \qquad (4.7)$$

where

$\sigma_s^m(E \rightarrow E')$ = the modified zeroth moment gamma scattering cross section.

E = energy of the incident gamma (MeV).

E' = energy of the scattered gamma (MeV).

$\sigma_{so}(E \rightarrow E')$ = the zeroth moment gamma scattering cross section.

$\sigma_{pp}(E)$ = pair production cross section.

δ = the krouecker delta.

4.2. Mechanics of Gamma Heating Calculations

In performing gamma heating calculations in TREAT upgrade reactor, the following tools are utilized.

4.2.1. Cross sections libraries. Gamma heating rate determination can be accomplished by performing a series of neutron and photon calculations. A single transport calculation can be used if miltigroup coupled neutron-gamma cross section sets are available. Such sets contain all essential information needed to perform the task when they are used with a computer code such as ANISN, DOT or MORSE. It is of particular advantage to utilize such sets.

Table 4.2 shows the general format and ordering of data in coupled neutron-gamma cross section table. Table 4.3 gives a format for one of the coupled neutron-gamma cross section libraries utilized in this thesis. The library contains 58 groups (37n, 21γ) and forms a matrix of 61 in the vertical direction by 58 in the horizontal direction. The first column lists the ANISN format for

Table 4.2. Coupled Neutron-Gamma Group Cross Sections Table.

Position	Cross Section Type	
1	Activity	
.	Activity	
.	Activity	
.	Activity	
IHT-2	Absorption	
IHT-1	nu x Fission	
IHT	Total	
IHT+1	$\sigma g+NUS \rightarrow g$	Upscatter transfers thermal neutron groups are only nonzero entries
.		
.		
.		
IHS-1	$\sigma g+1 \rightarrow g$	
IHS	$\sigma g \rightarrow g$	
IHS+1	$\sigma g-1 \rightarrow g$	Neutron gamma downscatter transfers or gamma group secondary gamma ray interaction transfers
.		
.		
.		
IHS+MDSG		
IHS+MDSG+1	$\sigma g-(MDSG+1) \rightarrow g$	Gamma group gamma ray production cross sections
.		
.		
.		
IHM	$\sigma g-TDS \rightarrow g$	

IHT = Position of total cross section.
IHS = Position of self scatter cross section.
NUS = Number of groups of upscatter.
NDS = Number of neutron downscatter groups.
GDS = Number of gamma downscatter groups.
MDSG = Larger of neutron downscatter groups or secondary gamma ray transfer groups.
TDS = Total number of downscatter groups, NDS+GDS.

The notations GDS, MDSG, and TDS are not listed in ANISN cross section table, they are introduced in this table for the purpose of illustration.

Table 4.3. Format of DLC-31/(DPL-1/FEWG1) Coupled Neutron-Gamma Cross Sections Library.

Cross Section	Neutron Groups						Gamma Groups			
	1	2	--	--	--	37	38	--	57	58
σ_a			σ_a					σ_a		
$\nu\sigma_f$								$\nu\sigma$ (gammas) = 0		
σ_t										
σ_{gg}	$\sigma_{1\to1}$	Neutron Within Group Scatter Cross Sections					$\sigma_{38\to38}$	Gamma Within Group Scatter Cross Sections		
$\sigma_{g-1\ g}$	0	$\sigma_{1\to2}$					$\sigma_{37\to38}$			
⋮	0	0								
$\sigma_{g-25\to g}$	0	0	0						$\sigma_{37\to57}$	$\sigma_{38\to58}$
⋮	0	0	0	0			Gamma Production			
$\sigma_{g-36\to g}$	0	0	0	0	0	$\sigma_{1\to37}$		Cross Sections		
$\sigma_{g-37\to g}$	0	0	0	0	0	0	$\sigma_{1\to38}$			
⋮	0	0	0	0	0	0	0			
$\sigma_{g-56\to g}$	0	0	0	0	0	0	0	0	$\sigma_{1\to57}$	
$\sigma_{g-57\to g}$	0	0	0	0	0	0	0	0	0	$\sigma_{1\to58}$

the various cross sections that are included. The absorption cross section, σ_a, which is given by

$$\sigma_a(E) = \sigma_{Pe}(E) + \sigma_{Ca}(E) + \sigma_{pp}(E) \tag{4.8}$$

is entered in position 1. Position 2 which is for σ_f is entered as zero in the absence of photofission.

The total cross section which is given by

$$\sigma_t(E) = \sigma_a(E) + \sigma_s(E) \tag{4.9}$$

is entered in position 3, where σ_s include gamma rays produced due to Compton scattering and the annihiliation gammas due to pair production interactions.

The ingroup gamma-ray scattering cross section is in position 4 and is given by Equation 4.7, where E' is interpreted to lie within the same group as energy E. The down scattering cross sections for this illustration is in position 5. Gamma production cross sections includes the production cross sections for all gamma-producing neutron reactions, i.e.,

$$\sigma_{gg'} = \sigma_{gg'}(\text{fission}) + \sigma_{gg'}(n,2n) + \sigma_{gg'}(n,\gamma) + \sigma_{gg'}(n,n')\gamma + \ldots \text{etc.} \tag{4.10}$$

(where g represents neutron group, and g' represents gamma group) were generated by using POPOP4[43] code, and entered as down scattering events from the 37 neutron groups to 21 gamma groups.

Secondary gamma-ray interaction cross sections are expanded in P_3 Legendre expansion using Klein-Nishina expression to include anisotropic scattering. The zeroth moment transfer cross sections are modified (Equation 4.7) to account for pair production and annihiliation interactions.

Three coupled neutron-gamma cross section sets are utilized in this work. They were obtained from the Radiation Shielding Information Center (RSIC) at ORNL. The DLC-31/(DPL-1 FEWG1) library contains 58 coupled neutron-gamma group (37n, 21γ), and includes cross sections for 35 nuclides. The DLC-47 library which consists of G1 coupled neutron-gamma groups (45n, 16γ), and includes cross sections for 66 nuclides. The DLC-23 library contains 40 coupled neutron-gamma groups (22n, 18γ), and includes cross sections for 26 nuclides.

The libraries energy group structure are listed in Tables 4.4, 4.5, and 4.6, respectively. For more information regarding the libraries, the reader is referred to References 10, 11, and 12.

4.2.2. Processing codes.

1. TAPEMAKER

ANISN and DOT have the options of reading the cross sections input from cards or from external devices (i.e., tapes or disks). They have the capability of performing cross section mixing for the various materials and mixtures involved in the problem of concern. However, when dealing with problems containing many

Table 4.4. Neutron and Gamma-Ray Energy Boundaries for the DLC-31/(DPL-1/FEWG1) (37n, 21 gamma) Coupled Cross Section Library.

Neutron Groups		Gamma-ray Groups	
Group No.	Upper Energy (MeV)	Group No.	Upper Energy (MeV)
1	1.960+1**	1	1.400+1
2	1.690+1	2	1.000+1
3	1.490+1	3	8.000+0
4	1.420+1	4	7.000+0
5	1.380+1	5	6.000+0
6	1.280+1	6	5.000+0
7	1.220+1	7	4.000+0
8	1.110+1	8	3.000+0
9	1.000+1	9	2.500+0
10	9,050+0	10	2.000+0
11	8.190+0	11	1.500+0
12	7.410+0	12	1.000+0
13	6.380+0	13	7.000-1
14	4.970+0	14	4.500-1
15	4.720+0	15	3.000-1
16	4.070+0	16	3.000-1
17	3.010+0	17	1.500-1
18	2.390+0	18	7.000-2
19	2.310+0	19	4.500-2
20	1.830+0	20	3.000-2
21	1.110+0	21	2.000-2
22	5.500-1		(1.000-2)
23	1.580-1		
24	1.110-1		
25	5.250-2		
26	2.480-2		
27	2.190-2		
28	1.030-2		
29	3.350-3		
30	1.230-3		
31	5.830-4		
32	1.010-4		
33	2.900-5		
34	1.070-5		
35	3.060-6		
36	1.130-6		
37	4.140-7		
	(1.000-11)		

** Read as $1.960 \times 10^{+1}$

Table 4.5. Neutron and Gamma-Ray Energy Group Boundaries for the DLC-47 (45n, 16 gamma) Coupled Cross Section Library.

Neutron Groups		Gamma-ray Groups	
Group No.	Upper Energy (MeV)	Group No.	Upper Energy (MeV)
1	1.733+1*	1	1.400+1
2	1.402+1	2	1.000+1
3	1.419+1	3	8.000+0
4	1.350+1	4	7.000+0
5	1.000+1	5	6.000+0
6	7.408+0	6	5.000+0
7	6.065+0	7	4.000+0
8	4.966+0	8	3.000+0
9	4.066+0	9	2.500+0
10	3.679+0	10	2.000+0
11	2.725+0	11	1.500+0
12	2.365+0	12	1.000+0
13	2.307+0	13	7.000-1
14	2.231+0	14	4.500-1
15	1.653+0	15	3.000-1
16	1.353+0	16	1.000-1
17	8.629-1		(1.000-2)
18	8.209-1		
19	7.427-1		
20	6.081-1		
21	4.979-1		
22	3.688-1		
23	2.985-1		
24	2.972-1		
25	1.832-1		
26	1.111-1		
27	6.738-2		
28	4.087-2		
29	2.479-2		
30	2.358-2		
31	1.503-2		
32	9.119-3		
33	5.531-3		

* Read as $1.733 \times 10^{+1}$

Table 4.5. Continued.

Neutron Groups	
Group No.	Upper Energy (MeV)
34	3.355-3
35	2.035-3
36	1.234-3
37	7.485-4
38	4.540-4
39	2.754-4
40	1.670-4
41	1.013-4
42	6.144-5
43	3.727-5
44	1.068-5
45	4.140-7
	(1.000-11)

Table 4.6. Neutron and Gamma-ray Energy Groups Boundaries for the DLC-23 (22n, 18 gamma) Coupled Cross Section Library.

Neutron Groups		Gamma-ray Groups	
Group No.	Upper Energy (MeV)	Group No.	Upper Energy (MeV)
1	1.492+1**	1	1.000+1
2	1.220+1	2	8.000+0
3	1.000+1	3	6.500+0
4	8.180+0	4	5.000+0
5	6.360+0	5	4.000+0
6	4.960+0	6	3.000+0
7	4.060+0	7	2.500+0
8	3.010+0	8	2.000+0
9	2.460+0	9	1.660+0
10	2.350+0	10	1.330+0
11	1.830+0	11	1.000+0
12	1.110+0	12	8.000-1
13	5.500-1	13	6.000-1
14	1.110-1	14	4.000-1
15	3.350-3	15	3.000-1
16	5.830-4	16	2.000-1
17	1.010-4	17	1.000-1
18	2.900-5	18	5.000-2
19	1.010-5		(1.000-2)
20	3.060-6		
21	1.120-7		
22	4.140-7		
	(1.000-8)		

** Read as $1.492 \times 10^{+1}$

elements and mixtures, the required core storage far exceeds the allowable storage at the installation. The problem can be overcome by using an auxilary program called TAPEMAKER or Group Independent Program (GIP).

TAPEMAKER uses a sorting technique. It retrieves the cross sections of the element or materials needed for the problem from the entire matrix of the cross sections library and performs the cross section mixing required for each material or zone. It then arranges the cross sections according to the group, material number and cross section position (Table 4.2). This allows ANISN and DOT to store the cross sections of a single group in the memory while performing the calculations of that group. Then, the next group data replaces the first and so on.

Since TAPEMAKER takes care of the mixing tables, the input arrays concerning these tables in ANISN and DOT should be omitted as long as TAPEMAKER is used. These arrays are (10$, 11$, 12* and 13$) in both codes.

TAPEMAKER was operational on the IBM 360/65 computer system which uses both high speed core and low speed core. The following changes were made in the work done on this thesis to make it operational on the new system IBM/3033.

(1) HIARCHY 1,AAA card is omitted. HIARCHY subparameter specifies the core hierarchy in which the buffers will be assigned. The default value (0) represents the high speed core.

(2) REGION.GO=(hK,ℓK) parameter was changed to REGION.GO= hK,

where

h = the number of contiguous 1024-byte (1K) areas of high speed core.

ℓ = the number of contiguous 1024-byte (1K) areas of low speed core.

(3) Omitting (AAA) from the COMMON block of each subroutine where it appears.

(4) Increase the program storage capacity from 75,000 locations to 150,000 locations by replacing DUMMY(75000) to DUMMY (150000) on the COMMON card of each subroutine.

A sample input data of the program is given in Appendix E. A point of particular importance should be mentioned, when TAPEMAKER is used with DOT, the following four input parameters must be given:

MCR = MTP = 0,

NCR1 = logical unit number for GIP data set,

MT = the value of MT in the GIP problem, and

MO1 = 0.

2. ANISN

ANISN is a discrete ordinates transport code with an isotropic scattering. The general purpose of the code is to solve the energy-dependent Boltzmann transport equation in one-dimensional geometry for fixed source, reaction rates, eigenvalue and critical dimensions calculations. The basic form of the solution is the

flux, $\bar{\Phi}(r_i,E_g,\Omega_d)\Delta E_g = \phi_{igd}$, averaged in the spatial interval surrounding r_i, integrated over the energy group, g, and averaged in the solid segment surrounding direction Ω_d.

Another purpose of the code is to collapse fine groups cross sections set into weighted broader structure. The fine group weighting function is the scalar flux divided by a macroscopic total cross section (i.e., $W_f = \phi_o^g/\Sigma_t^g$). Reference 5 provides more information concerning ANISN.

A second load module was made of ANISN in this work so that larger problems could be handled, and so that the increased computing capability of the new IBM/3033 could be more fully utilized.

The specific modifications made in creating the second load module are:

(1) Increase the code memory storage capacity from 40,000 locations to 200,000 locations to fit the size of the problem at hand.

(2) Include ITIME subroutine with the load module instead of compiling it separately along with each ANISN run.

The modified ANISN load module now resides on a permanent disk (USER02) of the LSU Computer System under data set name 'NSMILE.ANISN.LOADS'. The old load module still resides on the same disk under data set name 'NSMILE.LOADS'.

ANISN was used, in this work, to perform two types of calculations. The first; calculation used a one-dimensional model to compute the gamma heating rate deposited in primary and

secondary pressure boundaries of TREAT upgrade reactor. The second; collapsing the DLC-31/(DPL-1/FEWG1), 58 coupled neutron-gamma fine groups cross sections into 13 (5n, 8γ) coarse groups set to be used later by the DOT code. The coarse groups structure is given in Table 4.7.

Calculating gamma heating rate in the two pressure boundaries was obtained by utilizing three coupled neutron-gamma cross sections libraries, DLC-31/(DPL-1/FEWG1), DLC-47 and DLC-23. The groups energy structure of the libraries are listed in Tables 4.4, 4.5, and 4.6 respectively.

In the three cases, the TREAT reactor was modeled into (214) mesh spacing. The primary and the secondary pressure boundaries were divided into 12 and 10 mesh spacing respectively. The mesh spacing of the two pressure boundaries are given in Table 4.8.

The DLC-31/(DPL-1/FEWG1) library has the advantage over the other two by having the kerma factor included along with the cross section under a separate material number (material number 1). This kerma factor is treated as an activity in ANISN input. So, the code calculated the heating rate directly, the only thing the results needed was just manipulation of the units.

Since the unit of the elemental kerma factor is given by (Rads/atom)/(gamma/(cm^2 gm)), the results were multiplied by the quantity N/A, where

Table 4.7. Neutron and Gamma-Ray Energy Boundaries for Fine and Coarse DLC-31/(DPL-1/FEWG1) Coupled Cross Section Libraries.

Neutron Groups			Gamma Groups		
Fine Group No.	Coarse Group No.	Upper Energy (MeV)	Fine Group No.	Coarse Group No.	Upper Energy (MeV)
1		1.960+1*	1		1.400+1
2		1.690+1	2		1.000+1
3		1.490+1	3	1	8.000+0
4		1.420+1	4		7.000+0
5		1.380+1	5		6.000+0
6		1.280+1	6		5.000+0
7		1.220+1	7	2	4.000+0
8		1.110+1	8		3.000+0
9		1.000+1	9	3	2.500+0
10		9.050+0	10	4	2.000+0
11	1	8.190+0	11		1.500+0
12		7.710+0	12	5	1.000+0
13		6.380+0	13	6	7.000-1
14		4.970+0	14	7	4.500-1
15		4.720+0	15		3.000-1
16		4.070+0	16		1.500-1
17		3.010+0	17		1.000-1
18		2.390+0	18	8	7.000-2
19		2.310+0	19		4.500-2
20		1.830+0	20		3.000-2
21		1.110+0	21		2.000-2
					(1.000-2)

* Read as $1.960 \times 10^{+1}$

Table 4.7. Continued.

Neutron Groups		
Fine Group No.	Coarse Group No.	Upper Energy (MeV)
22		5.500-1
23		1.580-1
24		1.110-1
25		5.250-2
26		2.480-2
27	2	2.190-2
28		1.030-2
29		3.350-3
30		1.230-3
31		5.830-4
32	3	1.010-4
33		2.900-5
34		1.070-5
35		3.060-6
36	4	1.130-6
37		4.140-7
	5	(1.000-11)

Table 4.8. ANISN Modeling of Primary and Secondary Pressure Boundaries.

Bound No.	Primary Bound (cm)	Secondary Bound (cm)
1	6.18000E+00	9.15000E+00
2	6.25875E+00	9.24500E+00
3	6.33750E+00	9.34000E+00
4	6.41625E+00	9.43500E+00
5	6.49500E+00	9.53000E+00
6	6.57375E+00	9.62500E+00
7	6.65250E+00	9.72000E+00
8	6.73125E+00	9.81500E+00
9	6.81000E+00	9.91000E+00
10	6.88875E+00	1.00050E+01
11	6.96750E+00	1.01000E+01
12	7.04625E+00	
13	7.12500E+00	

N = Avogadro's number (.602 x 10^{24} atom/gm-mole)

A = material atomic weight (gms/gm-mole)

to give calculated unit of (Rads/cm^2)/gamma.

To obtain the desired unit of heating rate in (watt/gm) per watt of reactor power, the calculated unit (Rad-cm^2)/gamma was multiplied by (10^{-5} watt-sec/gm-Rads) x FNORM.

wheree

FNORM = unitless normalization factor which depends on the reactor power.

FNORM can be explained as follows: In multigroup diffusion or transport codes the source term is usually normalized to 1.0 neutron/sec for the entire reactor. This implies

$$\int_0^\infty \int_v S(\vec{r},E)\, dv\, dE = \int_0^\infty \int_v \nu\Sigma_f(\vec{r})\phi(\vec{r},E)\, dv\, dE = 1.0 \qquad (4.11)$$

where the corresponding multigroup equations are represented as:

$$M\phi_g(\vec{r}) = \frac{1}{k}\, \nu\Sigma_{f,g}\phi_g(\vec{r}) \qquad (4.12)$$

where

k = the system eigenvalue.

M = an appropriate transport or diffusion theory operator

Therefore in normalizing the computer output to a given power, P, we must scale the results as follow:

$$\text{FNORM} = (3.121 \times 10^{10} \frac{\text{fission}}{\text{watt-sec}})\ (\nu \frac{\text{neutron}}{\text{fission}})\ (\text{P watt})/(1.0\ \text{n/sec})$$

$$= 3.121 \times 10^{10}\ \nu P \qquad (4.13)$$

Equation 4.12 indicates a final correction of 1/k must be applied to the results. So,

$$FNORM = 3.121 \times 10^{10} \nu P \frac{1}{\lambda} \tag{4.14}$$

where

ν = number of fast neutron emitted per fission

P = reactor power in watts

λ = the system eigenvalue = k

In the present problem ν, was assigned a value of 2.43 neutron and P = 1.

However, the gamma kerma factor is not included in the other two cross section libraries, (DLC-47 and DLC-23). The heating rate using these cross section sets was determined by the following procedure:

The energy deposition rate per gram in material, i, from a gamma group, g, having energy, E_g, as a result of gamma flux, Φ_g, is given by

$$\text{Energy deposition} = \Phi_g \bar{E}_g (\mu_k/p)^i \text{ MeV/gm-sec.} \tag{4.15}$$

where

$(\mu_k)^i$ = energy-transfer coefficient of material i for gamma group, g, if μ_k is determined per unit mass (i.e., μ_k/p) is called kerma[39].

In terms of Rad/sec,

$$\text{Energy deposition} = 1.602 \times 10^{-8} \Phi_g \bar{E}_g (\mu_k/p)^i \text{ Rad/sec} \tag{4.16}$$

The heating rate (watt/gm) results from the energy deposition can be expressed as

$$\text{Heating rate} = 1.602 \times 10^{-13} \Phi_g \bar{E}_g (\mu_k/p)^i \text{ watt/gm} \qquad (4.17)$$

The total heating rate of n, gamma groups in material, i, is

$$\text{Total heating rate} = 1.602 \times 10^{-13} \sum_{g=1}^{n} \Phi_g \bar{E}_g (\mu_k/p)_g^i \text{ watt/gm} \qquad (4.18)$$

All the terms in Equation 4.18 are known except (μ_k/p). The gamma fluxes, Φ_g, at each spatial point of the two pressure boundaries are obtained by ANISN using the two cross sections libraries. $\bar{E}_g$ is the average of the upper and lower energy limits of gamma group, g, simply $\bar{E}_g = (E_g + E_g - 1)/2$. The values of the energy transfer coefficients for iron at each gamma energy group are obtained by extrapolation tabulated values given by Hubbel and Berger[44]. The obtained values as a function of gamma energy are listed in Table 4.9. So, the gamma heating rate was determined from Equation 4.18.

The calculated values of gamma heating rate and analysis of the results will be given and discussed in Chapter Five. ANISN sample problem input data is given in Appendix F.

3. DOT3.5

Calculation of the gamma heating rate deposited in the two pressure boundaries of the TREAT upgrade reactor by the use of DOT is the main purpose of this thesis. The calculations were made in

Table 4.9. Energy Transfer Coefficient of Ion as a Function of Gamma Energy.

DLC-47 Library		DLC-23 Library	
Gamma Energy $\bar{E}g$ (MeV)	(μ_k/p) gm/cm^2	Gamma Energy $\bar{E}g$ (MeV)	(μ_k/p) gm/cm^2
12.00	0.0246	9.00	0.0229
9.00	0.0229	7.25	0.0215
7.50	0.0219	5.75	0.0211
6.50	0.0214	4.50	0.0209
5.50	0.0211	3.50	0.0209
4.50	0.0209	2.75	0.0213
3.50	0.0209	2.25	0.0219
2.75	0.0213	1.83	0.0222
2.25	0.0219	1.50	0.0243
1.75	0.0231	1.17	0.0251
1.25	0.0250	1.90	0.0263
0.85	0.271	0.70	0.0275
0.575	0.0288	0.50	0.0299
0.375	0.0315	0.35	0.0315
0.200	0.0450	0.25	0.0655
0.055	1.0711	0.15	0.0985
		0.075	0.3505
		0.030	10.5000

R-Z geometry by using 90 x 30 mesh scheme. The primary and secondary pressure boundaries were divided into 6 and 5 mesh spacing respectively. The mesh spacing of the two pressure boundaries are listed in Table 4.10.

DOT utilized ANISN collapsed 13 (5n, 8γ) groups cross sections set (along with the associated kerma factor) in the $S_{16}P_3$ approximation. Before utilizing the collapsed groups cross sections set, two ANISN runs were performed for the same modeling of the TREAT reactor using the fine groups and the collapsed groups cross sections. The two eigenvalues were compared. The collapsed groups set eigenvalue deviated by a factor of 0.1% from the corresponding fine groups set eigenvalue. The deviation is negligible. This gives us a good indication of the accuracy of the results obtained in utilizing the collapsed groups set instead of the fine groups set.

The 13 collapsed groups kerma factor were determined by weighting the 58 fine groups kerma factor with ANISN flux. The weighting was accomplished by using the formula:

$$k_i = \frac{\sum_{j=1}^{J} \Phi_j \, k_j}{\sum_{j=1}^{J} \Phi_j} \qquad (4.19)$$

where

k_i = kerma factor for the ith collapsed group.

Φ_j = flux of the jth fine group.

Table 4.10. DOT3.5 Modeling of Primary and Secondary Pressure Boundaries.

Bound No.	Primary Bound (cm)	Secondary Bound (cm)
1	6.1800E+00	9.1500E+00
2	6.3375E+00	9.3400E+00
3	6.4950E+00	9.5300E+00
4	6.6525E+00	9.7200E+00
5	6.8100E+00	9.9100E+00
6	6.9675E+00	1.0100E+01
7	7.1250E+00	

k_j = kerma factor for jth fine group.

J = number of fine groups for each collapsed group.

The collapsed groups kerma factor is given in Table 4.11.

As we mentioned early in this section, Equation 4.8 indicates a final correction of 1/k must also be applied to the results. This factor could be included with the equation for FNORM (Equation 4.14), but for some application such as gamma calculations where kerma scale factors are applied in transport calculation before the eigenvalue is known (i.e., DOT calculations) it is preferable to use the two step procedure and simply scale the final results by 1/k.

So, the kerma factors that are given in Table 4.11 were multiplied by the appropriate units of Equation 4.13. The results were then punched on cards in ANISN format and inserted as an additional materials activity cross section along with the 13 groups cross sections. A DOT run was made and the results were scaled by the eigenvalue to give the desired heating rate units of (watt/gm per watt of reactor power).

The computed heating rate results will be given and analyzed in Chapter Five.

Table 4.11. Kerma Factor in (rads/atom)/(gamma/(cm^2 gm)) for the Gamma Coarse Groups in the Primary and Secondary Pressure Boundaries.

Primary Pressure Boundaries		Secondary Pressure Boundaries	
Group No.	Kerma Factor	Group No.	Kerma Factor
1	2.3369E-07	1	2.3441E-07
2	1.1947E-07	2	1.1987E-07
3	8.6945E-08	3	8.6945E-08
4	6.5414E-08	4	6.5400E-08
5	4.6466E-08	5	4.6466E-08
6	3.4206E-08	6	3.4206E-08
7	2.4602E-08	7	2.4602E-08
8	1.7555E-08	8	1.7815E-08

CHAPTER FIVE

Results and Conclusions

The gamma heating rate in primary and secondary pressure boundaries of TREAT upgrade reactor are obtained by the use of ANISN and DOT3.5 codes. Since both regions are unfueled, the only gamma produced within these regions are those emitted as a result of neutron capture and inelastic scattering. However, gamma produced in other reactor regions from prompt fission, fission product-decay, capture and inelastic scattering enter the primary and secondary pressure boundaries from exterior regions. As these gammas interact with the pressure boundary, they also liberate energy within this region.

These terms are difficult to separate out since each region has a contribution to each of these external gamma sources. However, we can analyze the gamma sources which originate within the two pressure boundaries and use this analysis to check our cross section sets.

The investigation of the neutron capture and inelastic scattering reactions contribution to the heating rate will be discussed in Sections 5.1 and 5.2. The heating rates calculated by ANISN utilizing different groups cross sections sets will be investigated in Section 5.3. DOT3.5 calculations will be discussed in Section 5.4. The remainder of the chapter will be left to the conclusion.

5.1. Inelastic Scattering Gamma Energy

The energy produced from neutron inelastic scattering can be represented[40] in the following general form:

$$\bar{E}_r = E_n - \bar{E}_{n'} - \bar{\varepsilon} \tag{5.1}$$

where

$\bar{E}_r$ = average recoil energy.

E_n = incident neutron energy.

$\bar{E}_{n'}$ = average kinetic energy of the secondary neutron emitted in the laboratory system.

$\bar{\varepsilon}$ = average excitation of the residual nucleus.

The parameter, $\bar{\varepsilon}$, is defined by the following equation

$$\bar{\varepsilon} = \frac{A^2+1}{A(A+1)} E_n - \frac{A+1}{A} \bar{E}_{n'}, \tag{5.2}$$

where

A = atomic mass number of the isotope.

As the excited residual nucleus returns back to its ground state, a total gamma energy E is emitted. So, the total gamma energy released as a result of neutron inelastic scattering is given by

$$E_\gamma^{in} = \frac{A^2+1}{A(A+1)} E_n - \frac{A+1}{A} \bar{E}_{n'}, \tag{5.3}$$

When one deals with isotope of heavy mass number, Equation 5.3 can be approximated by

$$E_{\gamma}^{in} = \frac{A}{A+1} E_n - \frac{A+1}{A} \bar{E}_{n'} \tag{5.4}$$

Once the inelastic scattering cross sections are entered as part of the neutron group cross sections, the inelastic gamma energy yield is given by

$$E_{\gamma}^{in},\ g \to g' = \frac{A}{A+1} E_g - \frac{A+1}{A} E_{g'} \tag{5.5}$$

where

$E_{\gamma}^{in},g\to g'$ = gamma energy produced per inelastic collision from neutron g to g'.

E_g = average neutron energies in group g.

$E_{g'}$ = average neutron energies in group g'.

A = atomic mass number.

Assume $\sigma_{g\to g'}^{in}$ is the corresponding inelastic scattering cross section. Thus, in a coupled neutron-gamma cross section library containing G neutron groups, the total inelastic scattering gamma-energy-production cross section for neutron group g is given by[15]

$$\overline{E\sigma}_g^{in} = \sum_{g'}^{G} E_{\gamma,g\to g'}^{in} \cdot \sigma_{g\to g'}^{in},\ \text{MeV-barn} \tag{5.6}$$

The gamma energy source produced by inelastic scattering gamma-energy-production cross section from neutron group g in material i is

$$E_{\gamma}^{in} = \overline{E\sigma}_g^{in} \cdot N_i \cdot \Phi_g \tag{5.7}$$

where

E_γ^{in} = gamma energy source produced by inelastic scattering gamma-energy-production cross section (MeV/cm^3-sec).

$\overline{E\sigma}_g^{in}$ = as defined in Equation 5.6.

N_i = atom density of material i (atom/b-cm).

Φ_g = neutron group g flux (n/cm^2-sec).

So, the gamma energy source at any spatial point $(\vec{r})$ in the two pressure boundaries produced from G neutron groups is

$$E_\gamma^{in}(\vec{r}) = \sum_i \sum_g \overline{E\sigma}_g^{in,i} \cdot N_i \cdot \Phi_g(\vec{r}) \text{ MeV/cm}^3\text{-sec} \qquad (5.8)$$

5.2. Gamma Energy Yield From (n,γ) Reaction

The concept of gamma energy produced by neutron capture was first introduced in a simple form in Chapter One. In this section, we will discuss in more details and in specific terms this energy yield and its contribution to the total heating rate.

For the purpose of illustration, let us consider the DLC-31 coupled neutron-gamma group cross section library. The library contains 37 neutron groups and 21 gamma groups. The neutron capture cross section for iron in neutron group, 23, is (6.93×10^{-4} cm^{-1}). We assume N_i is the atom density in (atom/barn-cm) of iron, say, in primary pressure boundary, and Φ_{23} is the total neutron flux in (n/cm^2-sec) for that group in the same region.

Thus the number of capture in iron in group, 23, is represented by

$$C_{23} = \sigma_a^{23} \cdot N_i \cdot \Phi_{23} \tag{5.9}$$

For each neutron capture, a line spectrum of gammas is produced. If we assume a gamma group, g, with energy, E_g, in (MeV), and the corresponding production cross section from neutron group, 23, is $\sigma_{23\to g}$ (barn). Then the gamma-energy yield in group, g, per neutron capture in neutron group, 23, is given by

$$E_\gamma^{23\to g} = E_g \cdot \sigma_{23\to g} \cdot N_i \cdot \Phi_{23} \text{ MeV/cm}^3\text{-sec} \tag{5.10}$$

where all the terms are defined previously.

Thus, the gamma energy produced per neutron capture in group, 23, in the primary pressure boundary is given by

$$E_\gamma^{23} = \frac{\sum_{g=38}^{58} E_g \cdot \sigma_{23\to g} \cdot N_i \cdot \Phi_{23}}{\sigma_{a,23}\, N_i \cdot \Phi_{23}} \text{ MeV/capture} \tag{5.11}$$

The values of $(\sigma_{23\to g} \cdot N_i)$ and E_g for the 21 gamma groups are listed in Table 5.1. After cancelling N_i and Φ_{23} from Equation 5.11, we obtain

$$E_\gamma^{23} = \frac{\sum_{g=38}^{58} E_g \cdot \sigma_{23\to g}}{\sigma_{a,23}} \tag{5.12}$$

Equation 5.12 can be presented in the following general form

$$E_{\gamma,g} = \frac{\sum_{g'} E_{g'} \cdot \sigma_{g\to g'}}{\sigma_{a,g}} \tag{5.13}$$

Table 5.1. Gamma Production Cross Sections for Iron From Neutron Group, 23, in DLC-31 Coupled Neutron-Gamma Cross Section Library.

Gamma Group g	Gamma Energy Eg (MeV)	(n,γ) $\sigma_{23\rightarrow g} \cdot N_i$ (cm^{-1})
38	14.0	0.0
39	10.0	1.027-4*
40	8.0	1.837-4
41	7.0	8.560-5
42	6.0	7.800-5
43	5.0	1.441-4
44	4.0	2.431-4
45	3.0	1.750-4
46	2.5	2.133-4
47	2.0	2.508-4
48	1.0	2.755-4
49	0.7	1.880-4
50	0.45	1.426-4
51	0.30	1.273-4
52	0.15	5.043-5
53	0.10	2.690-4
54	0.07	2.940-6
55	0.045	2.280-5
56	0.030	6.397-5
57	0.020	4.248-5
58	0.010	4.230-5

* Read as 1.027×10^{-4}

The gamma energy produced as a result of neutron group, 23, capture computed using Equation 5.12 is 9.92 MeV/capture. This value is reasonably close to that obtained by computing the mass defect (7.64 MeV/capture) for (n,γ) reaction for iron the principle nuclide in the primary pressure boundary. If the mass defect for the other nuclides were computed and properly weighted and account was taken for the energy of group, 23, neutrons, a value very close to 9.92 MeV/capture would be expected. This was not done since information to compute the mass defects of all isotopes required is not available.

5.3. ANISN Results

The gamma heating rates in the primary and secondary pressure boundaries were obtained by use of the ANISN code. The calculations are based on a S_4P_3 approximation one-dimensional model, and uses three different coupled neutron-gamma cross section sets, DLC-31, DLC-47 and DLC-23.

The results of these runs are presented in Table 5.2, but they don't provide good gamma heating results because the model does not present the gamma-ray attenuation distances correctly. Nevertheless, they are discussed below for the purpose of evaluating the cross section sets used.

Figures 5.1 and 5.2 show the calculated heating rates at various points on the two pressure boundaries. A comparison of these results reveals some differences. These differences are attributed to the following factors:

Table 5.2. ANISN Gamma Heating Rates in Primary and Secondary Pressure Boundaries.

Heating Rate x 10^6 (watt/gm per watt of reactor power)

Boundary No.	Boundary (cm)	DLC31-FG LIB. 37n-21 gamma	DLC-47 LIB. 45n-16 gamma	DLC-23 LIB. 22n-18 gamma
		Primary Pressure Boundaries		
1	6.18000E+00	1.0619	1.1949	1.5593
2	6.25875E+00	1.0581	1.1853	1.5460
3	6.33750E+00	1.0557	1.1771	1.5357
4	6.41625E+00	1.0548	1.1702	1.5270
5	6.49500E+00	1.0553	1.1646	1.5213
6	6.57375E+00	1.0572	1.1602	1.5184
7	6.65250E+00	1.0605	1.1571	1.5181
8	6.73125E+00	1.0654	1.1551	1.5207
9	6.81000E+00	1.0719	1.1544	1.5263
10	6.88875E+00	1.0801	1.1549	1.5349
11	6.96750E+00	1.0900	1.1567	1.5468
12	7.04625E+00	1.1018	1.1599	1.5624
13	7.12500E+00	1.1116		
		Secondary Pressure Boundaries		
1	9.15000E+00	1.0875	1.1545	1.5361
2	9.24500E+00	1.0846	1.1569	1.5388
3	9.34000E+00	1.0838	1.1605	1.5461
4	9.43500E+00	1.0849	1.1658	1.5580
5	9.53000E+00	1.0879	1.1725	1.5744
6	9.62500E+00	1.0928	1.1807	1.5958
7	9.72000E+00	1.0999	1.1903	1.6224
8	9.81500E+00	1.1093	1.2015	1.6548
9	9.91000E+00	1.1221	1.2144	1.6950
10	1.00050E+01	1.1438	1.2291	1.7544
11	1.01000E+01	1.1587		

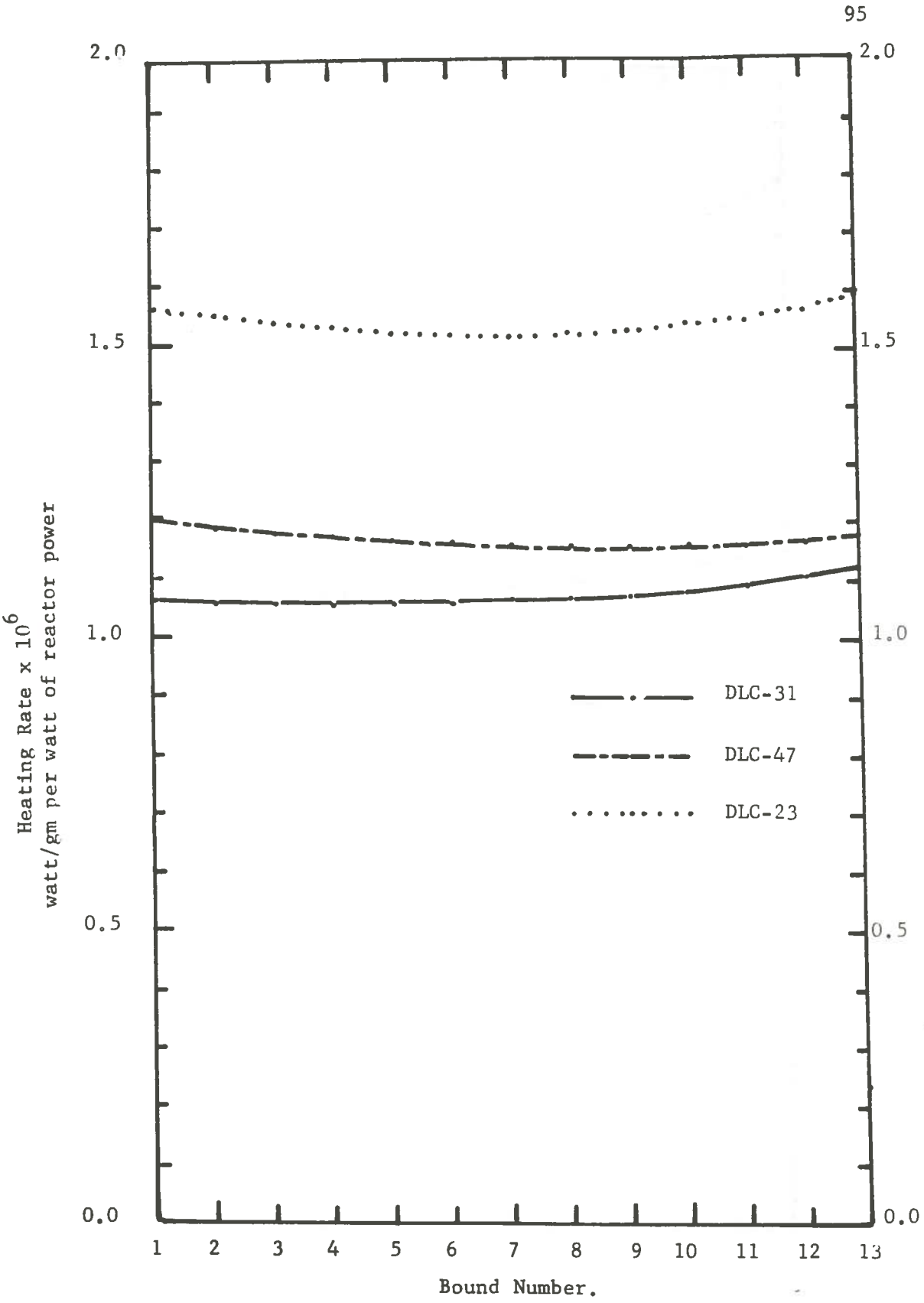

Figure 5.1. ANISN Results of Gamma Heating Rate at Various Points of Primary Pressure Boundary of TREAT Upgrade Reactor.

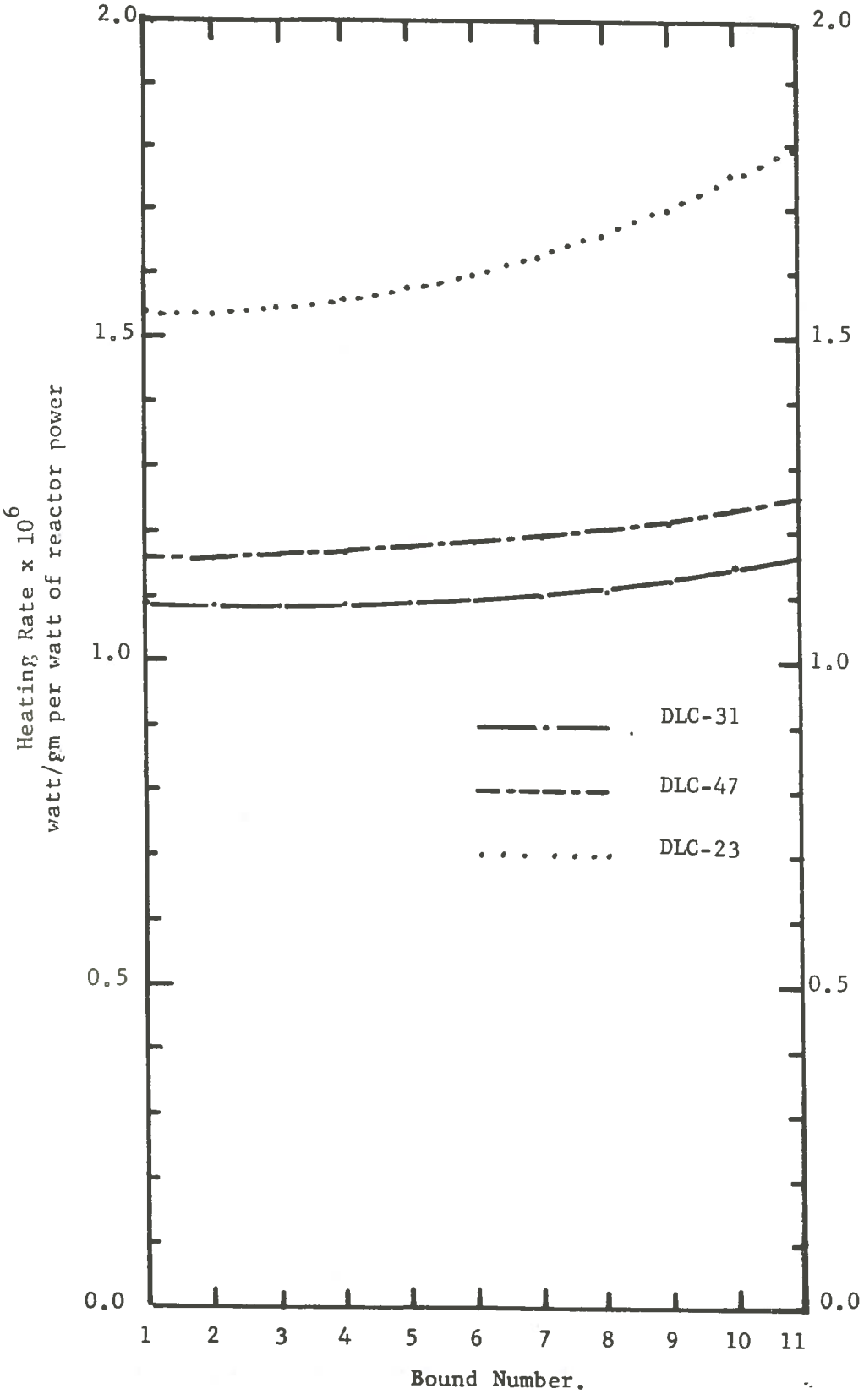

Figure 5.2. ANISN Results of Gamma Heating Rate at Various Points of Secondary Pressure Boundary of TREAT Upgrade Reactor.

(1) Gamma source: The type of gamma sources included in a cross section library sometimes depends on the purpose for which the library was designed as well as the neutron and gamma ray interaction processes.

The DLC-23 cross section library was designed for use in designing depleted fuel shipping cask. Therefore in this library a gamma source due to fission product gammas of 7.63 MeV/fission was included. This source is equivalent to equilibrium fission product gamma-ray emission rates. On the other hand in the DLC-31 cross section library which was designed for light water reactor shielding applications, this gamma source was omitted.

Prompt fission gammas that contribute 7.538 MeV/fission are included in DLC-31 and DLC-23 libraries. However, we are not certain what contribution prompt fission supplies in the DLC-47 library. Neutron capture and inelastic scattering gamma-ray contributions for any cross section set depend on the neutronic system. For the TREAT reactor, this contribution can be estimated from the ratio of the DLC-23/DLC-31 ANISN results. This ratio is approximately 1.42, hence the contribution from neutron capture and inelastic scattering is given approximately as x in the following equation

$$\frac{7.63 + 7.538 + x}{7.63 + 7.538} = 1.42$$

solving for x, we obtain, x = 6.37 MeV/fission due to gammas produced from neutron capture and enelastic scattering interactions.

(2) Group structure: After normalizing the results obtained using DLC-23, and DLC-47 cross section sets to the mid plane of DLC-31 cross section set pressure boundary results, there still remains minor discrepancies of $\pm$ 5% as shown in Figures 4.3 and 5.4. This discrepancy is caused by variation in the group structure.

Tables 5.3, 5.4, and 5.5 list the normalized relative gamma groups fluxes for the three cross sections libraries in the two regions of concern. These values are plotted as a function of gamma energy group as shown in Figures 5.5 and 5.6. By looking at the gamma spectra, one can see the variations in the gamma flux distribution between the three libraries. Such variations cause some of the differences in the heating results.

5.4. DOT3.5 Results

The neutron and gamma fluxes calculated by DOT code using the DLC-31 cross section library collapsed to 5 neutron groups and 8 gamma groups are printed out by energy group block and by mesh spacing. The heating rates are printed out by mesh blocks.

Table 5.6 lists the normalized gamma groups flux densities ($\sum_{i=1}^{g} \Phi_i = 1.0$) in the primary and secondary pressure boundaries. The gamma spectra in the two regions are shown in Figures 5.7 and 5.8. Gamma spectra indicates that the eighth gamma group is the largest contributer to the flux density in both regions. Its contribution is about 45% of the total gamma groups fluxes. This

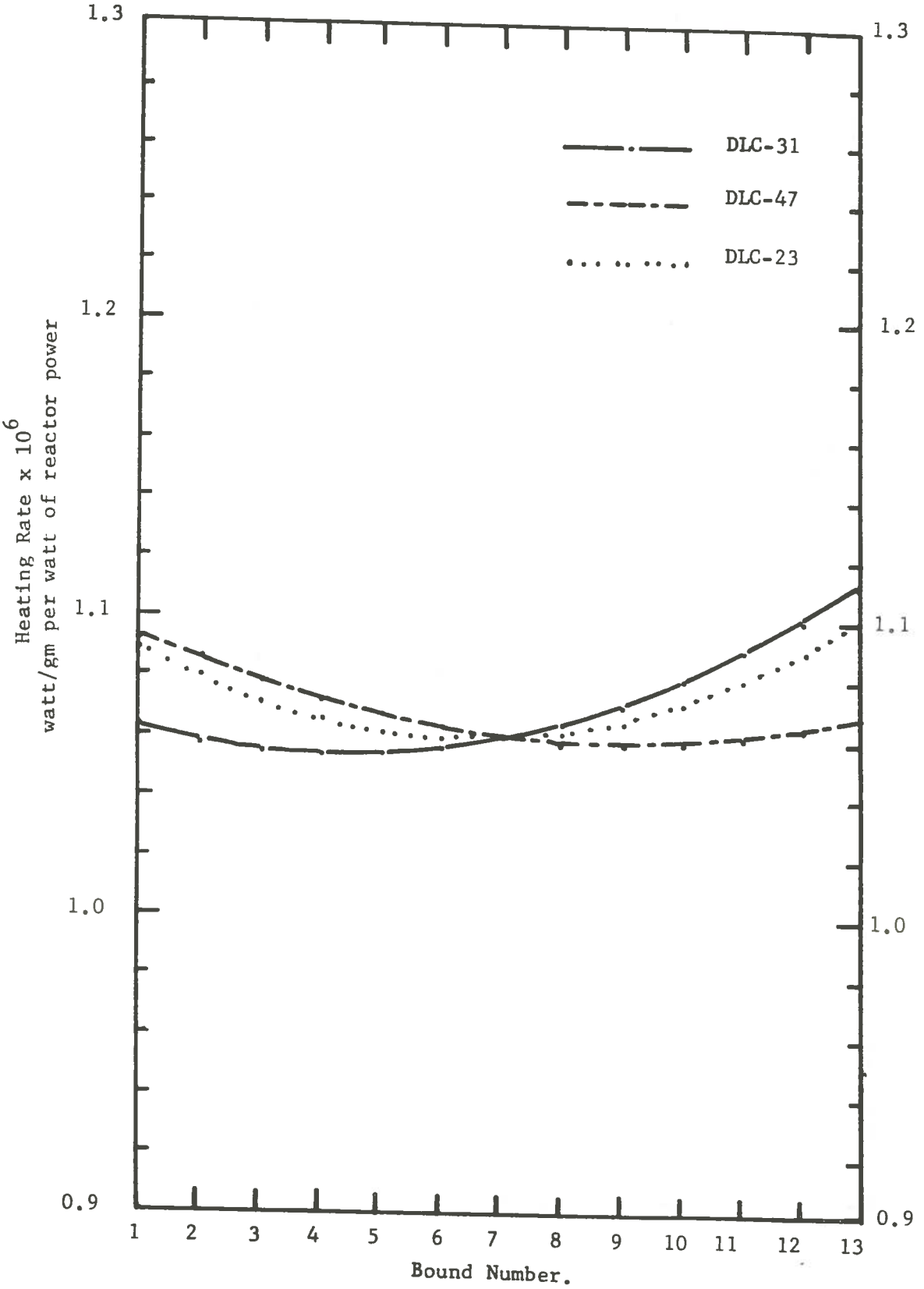

Figure 5.3. ANISN Results of Gamma Heating Rate at Various Points of Primary Pressure Boundary of TREAT Upgrade Reactor Normalized to DLC-31 Cross Section Set Results at Mid-plane.

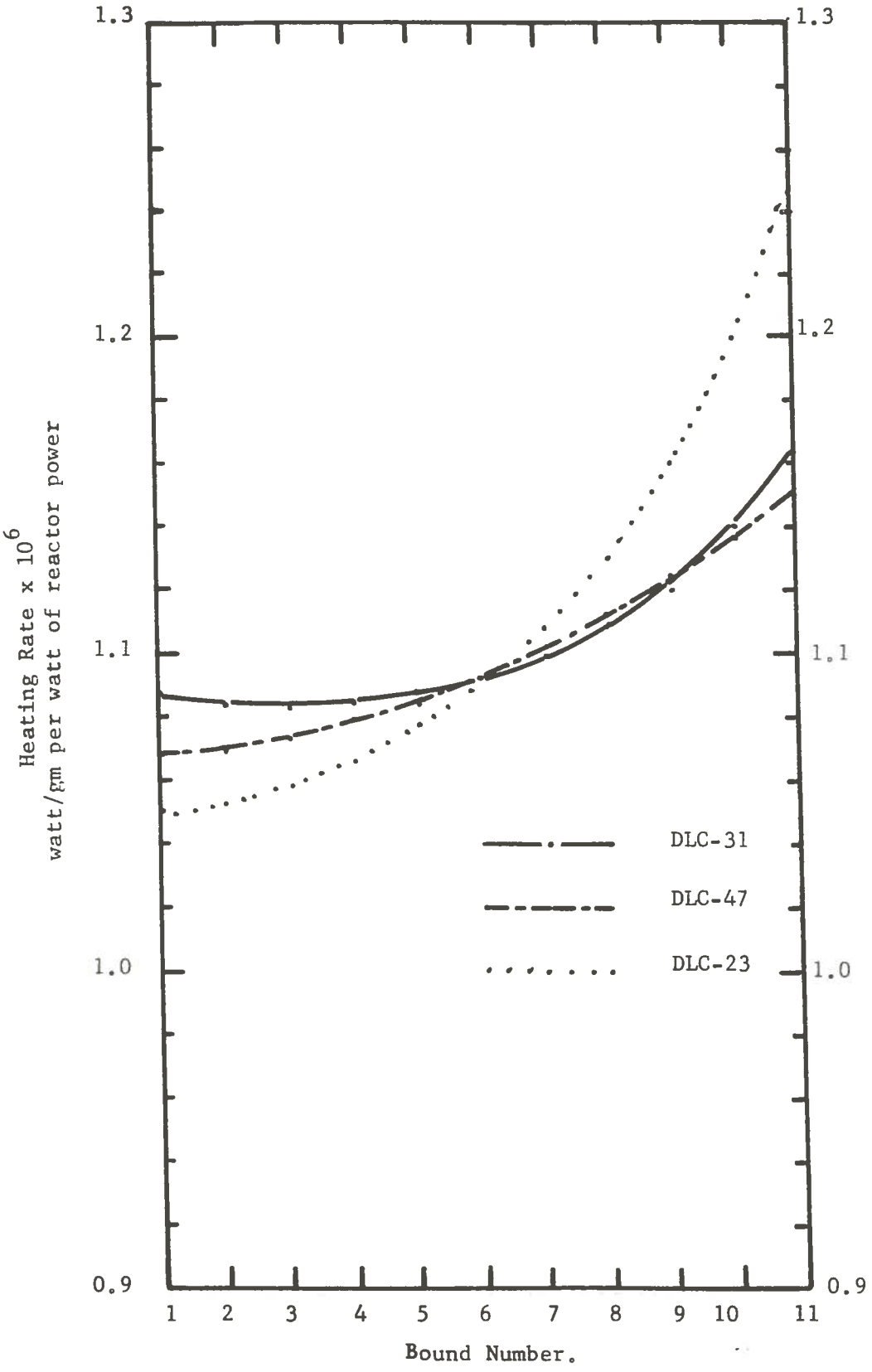

Figure 5.4. ANISN Results of Gamma Heating Rate at Various Points of Secondary Pressure Boundary of TREAT Upgrade Reactor Normalized to DLC-31 Cross Section Set Results at Mid-plane.

Table 5.3. ANISN Flux Spectra in the Primary and Secondary Pressure Boundaries.

(DLC-31/(DPL-1/FEWG1 Library))

Gamma Energy (MeV)		Normalized Relative Group Flux	
Lower limit	Upper limit	Primary	Secondary
0.010	0.020	0.000	0.000
0.020	0.030	0.000	0.000
0.030	0.045	0.000	0.000
0.045	0.070	0.000	0.000
0.070	0.100	0.009	0.012
0.100	0.150	0.061	0.069
0.150	0.300	0.246	0.257
0.300	0.450	0.134	0.134
0.450	0.700	0.198	0.177
0.700	1.000	0.104	0.096
1.000	1.500	0.087	0.082
1.500	2.000	0.053	0.049
2.000	2.500	0.035	0.032
2.500	3.000	0.023	0.022
3.000	4.000	0.024	0.023
4.000	5.000	0.013	0.013
5.000	6.000	0.006	0.006
6.000	7.000	0.005	0.005
7.000	8.000	0.015	0.015
8.000	10.000	0.006	0.006
10.000	14.000	0.000	0.000

Table 5.4. ANISN Flux Spectra in the Primary and Secondary Pressure Boundaries.

(DLC-47 Library)

Gamma Energy (MeV)		Normalized Relative Group Flux	
Lower limit	Upper limit	Primary	Secondary
0.01	0.10	0.000	0.000
0.10	0.30	0.270	0.308
0.30	0.45	0.145	0.139
0.45	0.70	0.161	0.153
0.70	1.00	0.123	0.112
1.00	1.50	0.100	0.092
1.50	2.00	0.059	0.054
2.00	2.50	0.039	0.035
2.50	3.00	0.026	0.024
3.00	4.00	0.030	0.028
4.00	5.00	0.015	0.015
5.00	6.00	0.009	0.009
6.00	7.00	0.006	0.006
7.00	8.00	0.014	0.015
8.00	10.00	0.007	0.007
10.00	14.00	0.000	0.000

Table 5.5. ANISN Flux Spectra in the Primary and Secondary Pressure Boundaries.

(DLC-23 Library)

Gamma Energy (MeV)		Normalized Relative Group Flux	
Lower limit	Upper limit	Primary	Secondary
0.01	0.05	0.000	0.000
0.05	0.10	0.007	0.010
0.10	0.20	0.148	0.175
0.20	0.30	0.163	0.171
0.30	0.40	0.106	0.107
0.40	0.60	0.169	0.160
0.60	0.80	0.083	0.078
0.80	1.00	0.060	0.055
1.00	1.33	0.075	0.067
1.33	1.66	0.045	0.041
1.66	2.00	0.035	0.032
2.00	2.50	0.034	0.030
2.50	3.00	0.021	0.019
3.00	4.00	0.022	0.020
4.00	5.00	0.010	0.010
5.00	6.50	0.007	0.007
6.50	8.00	0.011	0.011
8.00	10.00	0.004	0.004

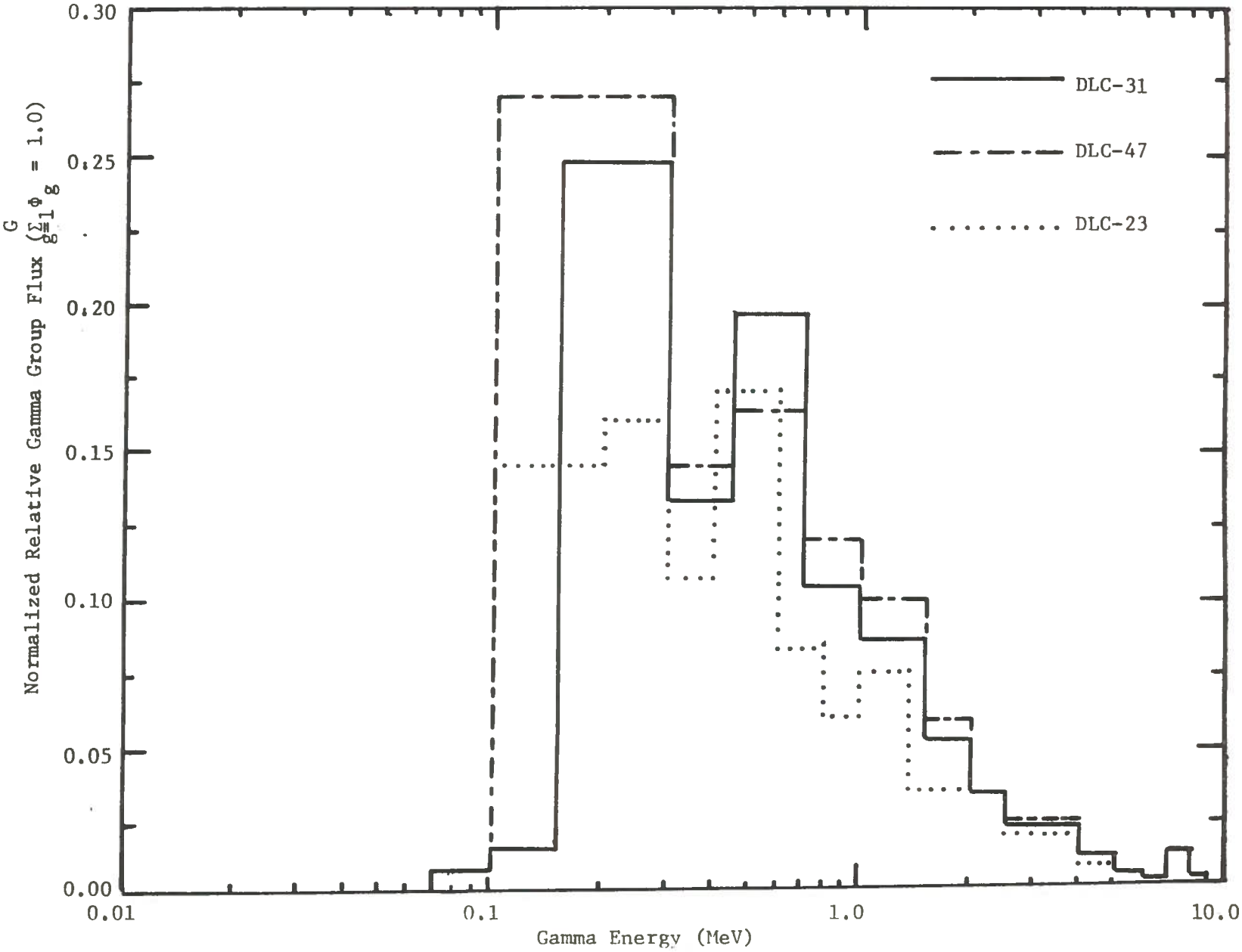

Figure 5.5. ANISN Results of Gamma Spectra in Primary Pressure Boundary

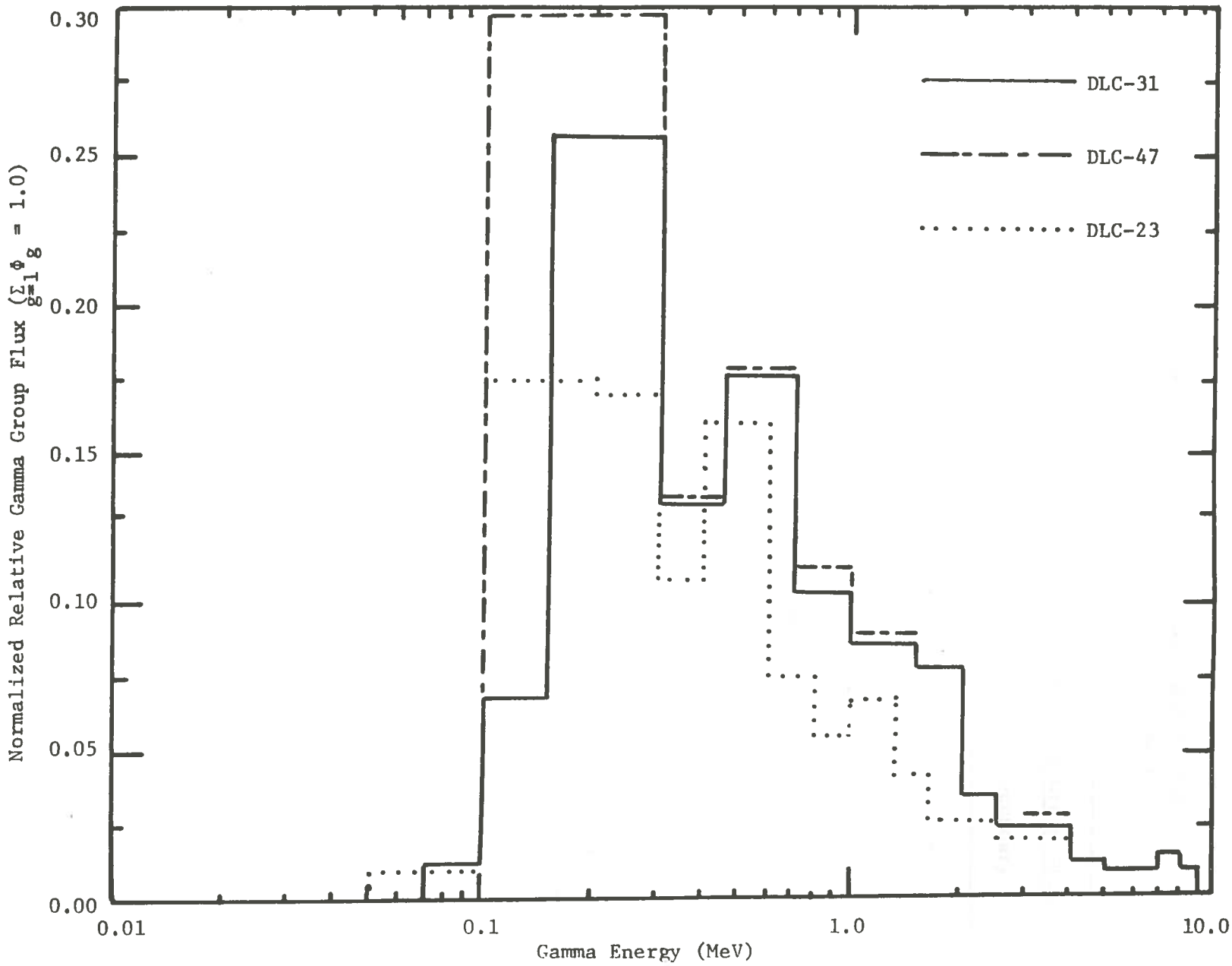

Figure 5.6. ANISN Results of Gamma Spectra in Secondary Pressure Boundary.

Table 5.6. DOT3.5 Flux Spectra in the Primary and Secondary Pressure Boundaries of TREAT Upgrade Reactor.

Gamma Energy (MeV)		Normalized Relative Group Flux	
Lower limit	Upper limit	Primary	Secondary
0.01	0.30	0.440	0.474
0.30	0.45	0.194	0.177
0.45	0.70	0.102	0.096
0.70	1.00	0.086	0.082
1.00	2.00	0.087	0.081
2.00	2.50	0.022	0.021
2.50	4.00	0.036	0.036
4.00	14.00	0.031	0.033

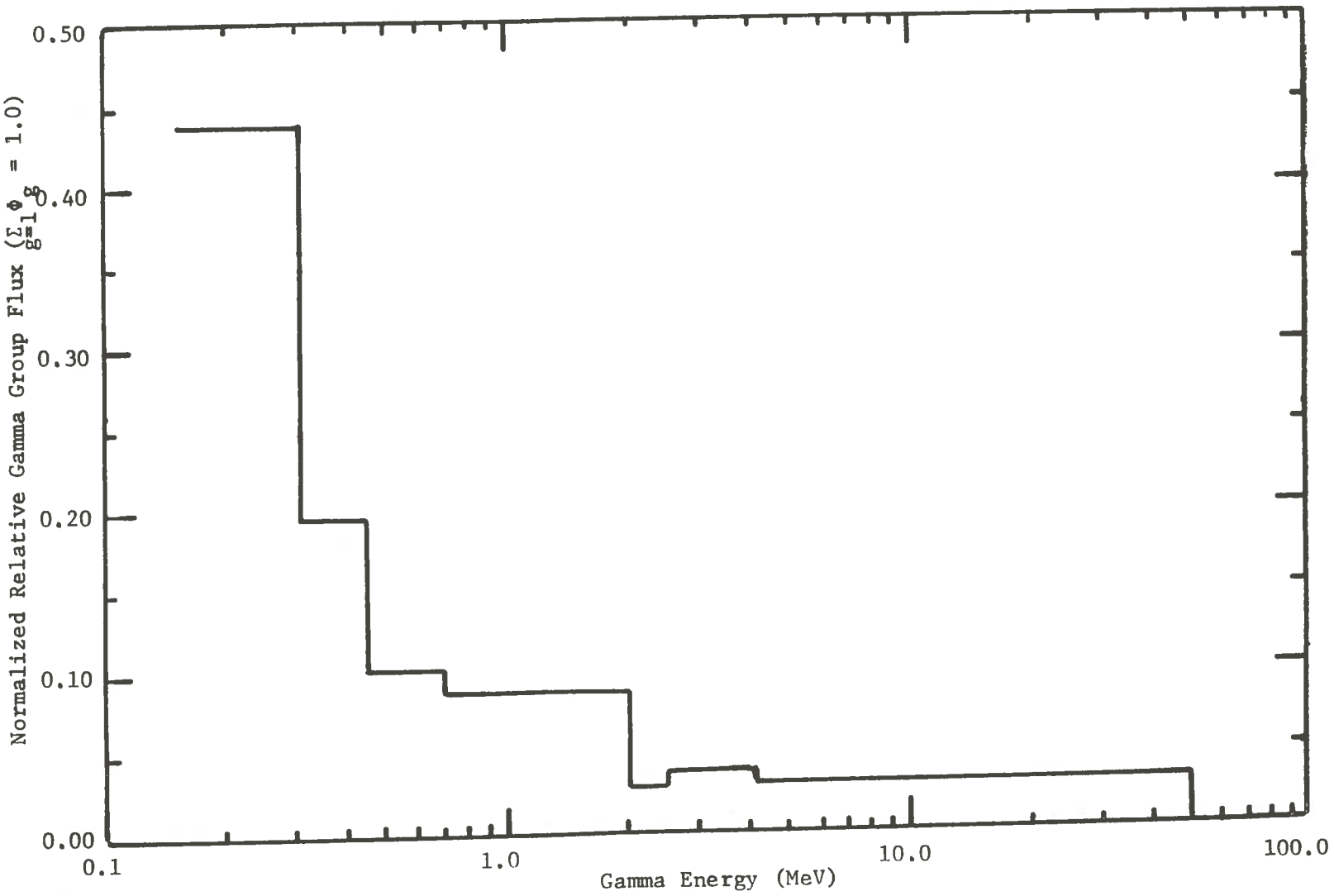

Figure 5.7. DOT3.5 Results of Gamma Spectra in Primary Pressure Boundary.

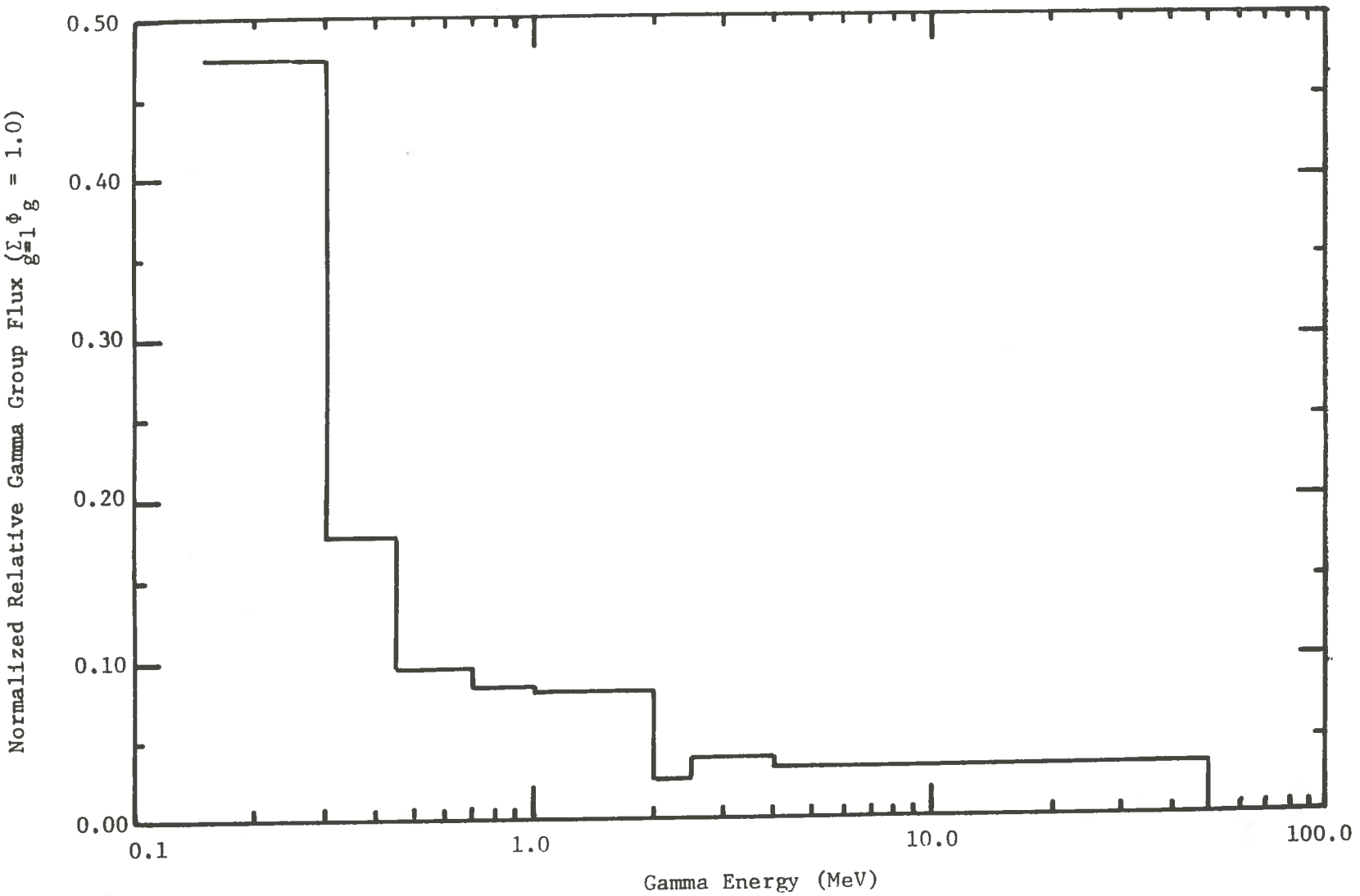

Figure 5.8. DOT3.5 Results of Gamma Spectra in Secondary Pressure Boundary.

is due mainly to the wide range of energies it covers (0.01-0.3) MeV, and because the photoelectric effect, which deposit all gamma energy upon interacting with matter, is the dominant process in this energy range.

The gamma heating rates calculated by DOT and QAD at various points in the two regions of concern are listed in Tables 5.7, 5.8, and 5.9. The values are plotted in Figures 5.9 and 5.10. DOT heating rate results are lower than QAD heating rate results by a factor of 1.5. The reason is due to the following factors:

(1) Gamma source: As mentioned in Section 3.4, the DLC-31 coupled neutron-gamma cross section library does not include fission product decay gammas while in the QAD calculation fission product decay gammas contributed 7.1 MeV/fission out of a total of 19.74 MeV/fission from all gamma source. Hence, fission product decay gammas contribute 36% of the total heating rate in the QAD calculation. If this factor is subtracted from the QAD results then the results agree within $\pm$ 5% as shown in Figure 5.11 and 5.12.

The discrepancies in Figures 5.11 and 5.12 are due to variations in group structure, differences in the model used, unaccounted for differences in cross section sets, and to inherent differences between the discrete ordinates and the point-kernel method. The point-kernel method takes into account the multiple buildup factors, and the discrete ordinates explicitly takes into account the effect of scattering.

Table 5.7. Gamma Heating Rates in the Primary and Secondary Pressure Boundaries (Along the Axial Mid Plane, Z = 0.0).

Heating Rate x 10^8 (watt/gm per watt of reactor power)

Primary Pressure Boundaries			Secondary Pressure Boundaries		
Boundary No.	Bound (cm)	Heating Rate	Boundary No.	Bound (cm)	Heating Rate
1	6.1800	1.87732	1	9.1500	1.91593
2	6.3375	1.86722	2	0.3400	1.91240
3	6.4950	1.86758	3	9.5300	1.92336
4	6.6525	1.87837	4	9.7200	1.94824
5	6.8100	1.90000	5	9.9100	1.98757
6	6.9675	1.93373	6	10.1000	2.01217
7	7.125	1.96516			

Table 5.8. DOT3.5 Gamma Heating Rates in the Primary Pressure Boundaries (Along the Axial Mid Plane, Z = 0.0).

Heating Rates x 10^8 (watt/gm per watt of reactor power)

Boundary No.	Bound (cm)	DOT3.5 Results	QADBS-1 Results
1	6.1800	1.87732	2.7420
2	6.3375	1.86722	
3	6.4950	1.86758	2.6400
4	6.6525	1.87835	
5	6.8100	1.90000	2.4740
6	6.9675	1.93373	
7	7.1250	1.96516	2.4970

Table 5.9. DOT3.5 Gamma Heating Rates in the Secondary Pressure Boundaries (Along the Axial Mid Plane, Z = 0.0).

Heating Rate x 10^8 (watt/gm per watt of reactor power)

Boundary No.	Bound (cm)	DOT3.5 Results	QADBS-1 Results
1	9.1500	1.91593	2.7120
2	9.3400	1.91240	
3	9.5300	1.92336	2.6220
4	9.7200	1.94824	
5	9.9100	1.98757	2.5370
6	10.1000	2.01217	2.5860

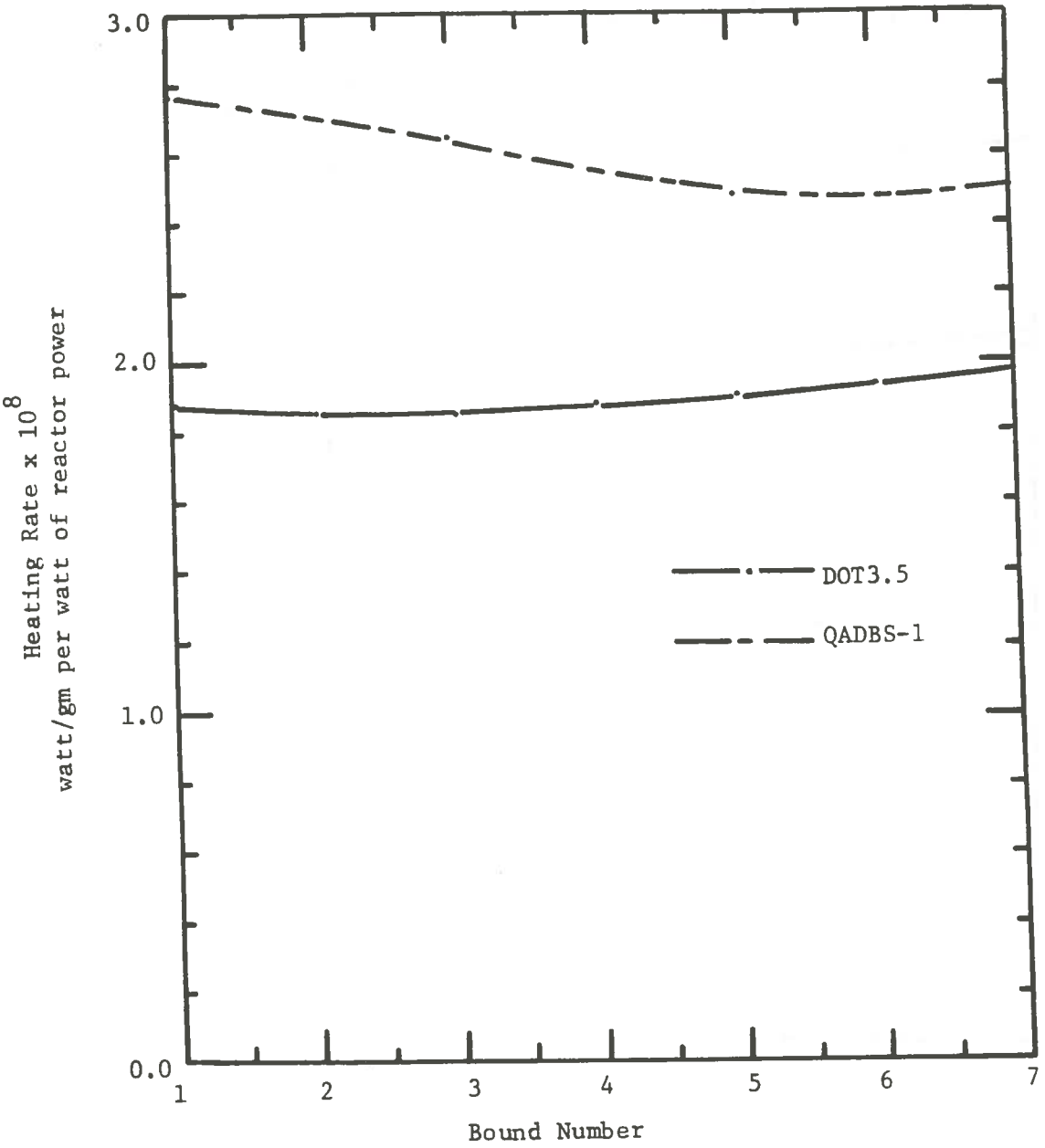

Figure 5.9. Heating Rate at Various Points of Primary Pressure Boundary of TREAT Upgrade Reactor.

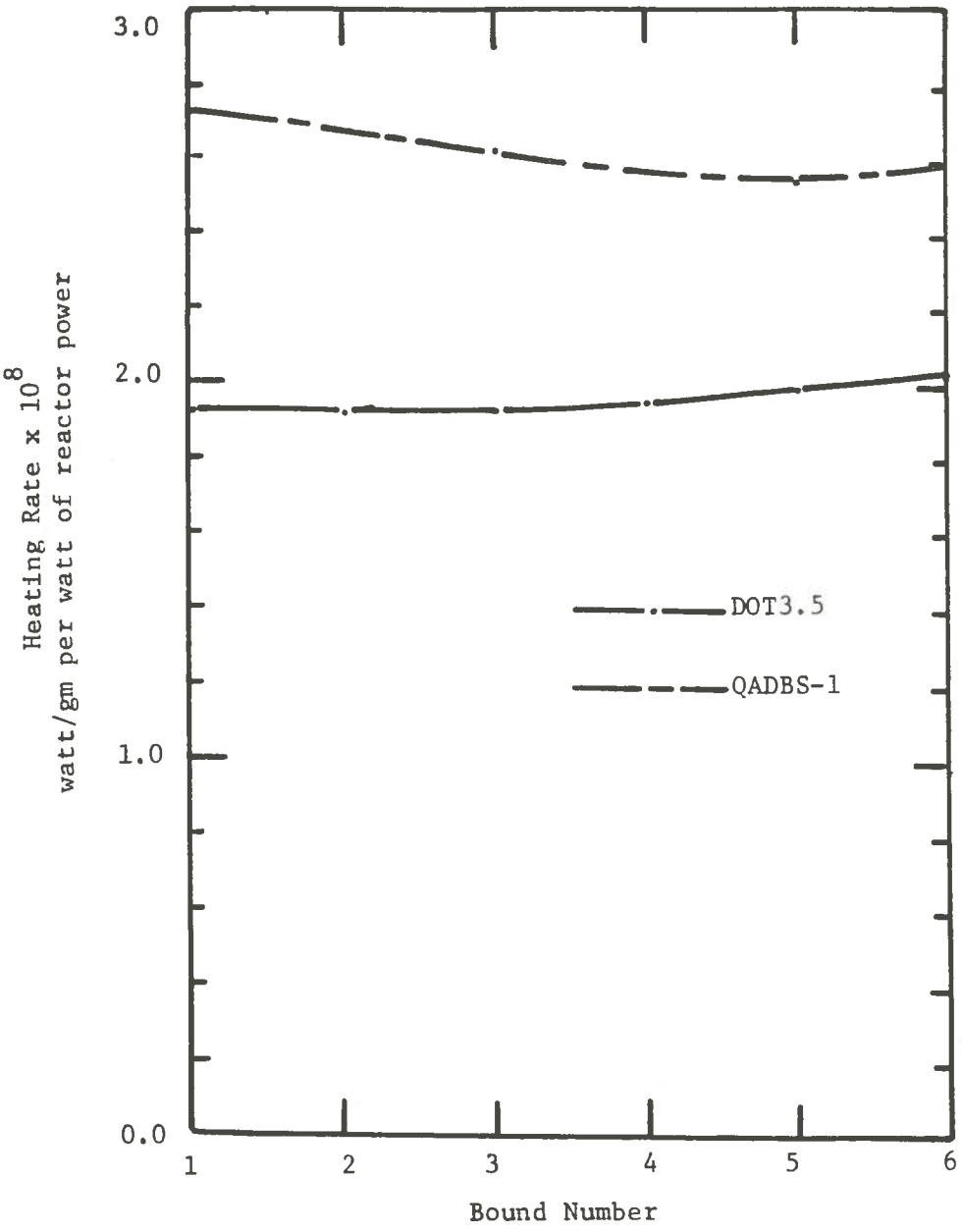

Figure 5.10. Heating Rate at Various Points of Secondary Pressure Boundary of TREAT Upgrade Reactor.

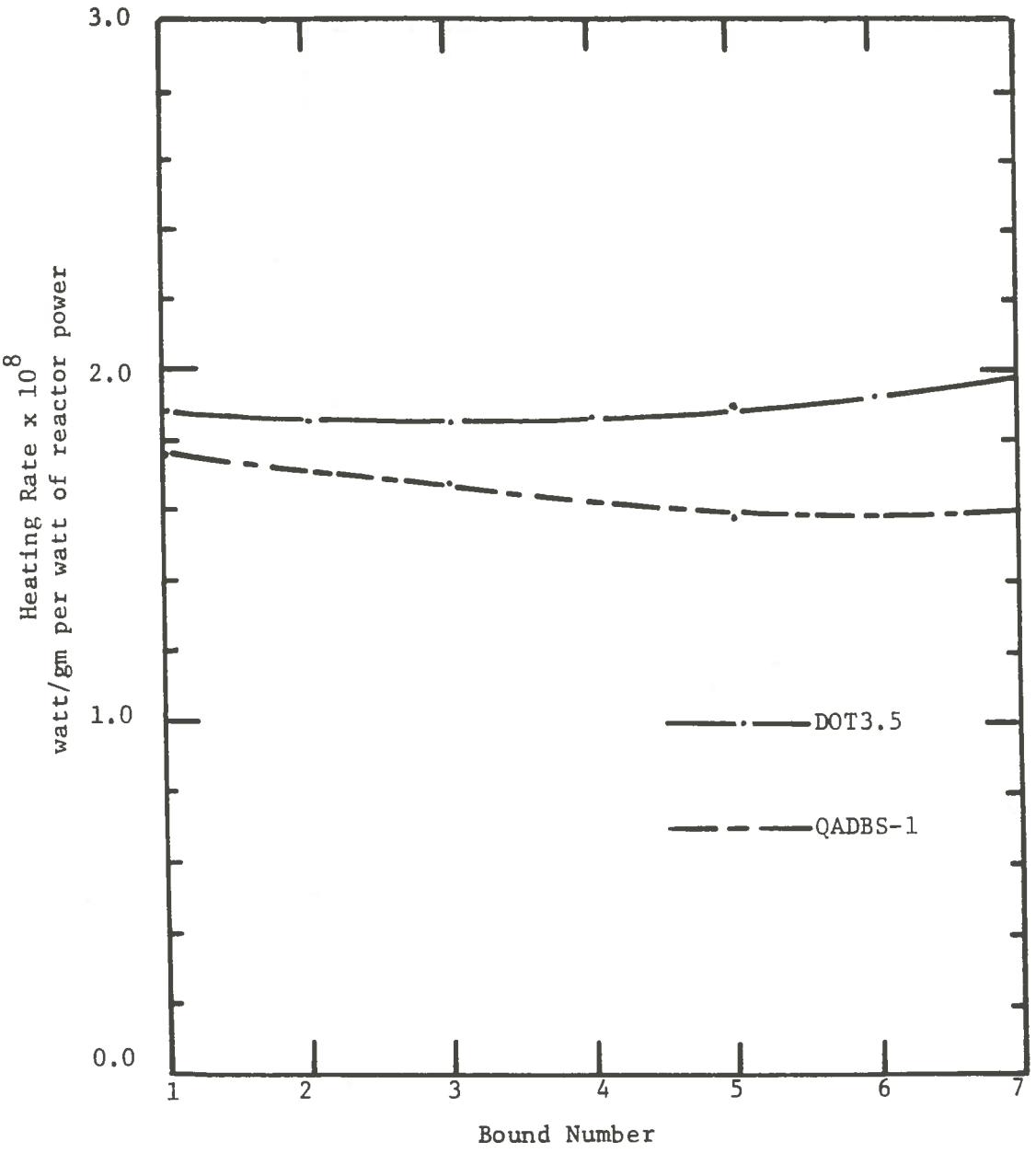

Figure 5.11. Heating Rate at Various Points of Primary Pressure Boundary of TREAT Upgrade Reactor with Modified QADBS-1 Results to correct for Fission Product Decay Gammas.

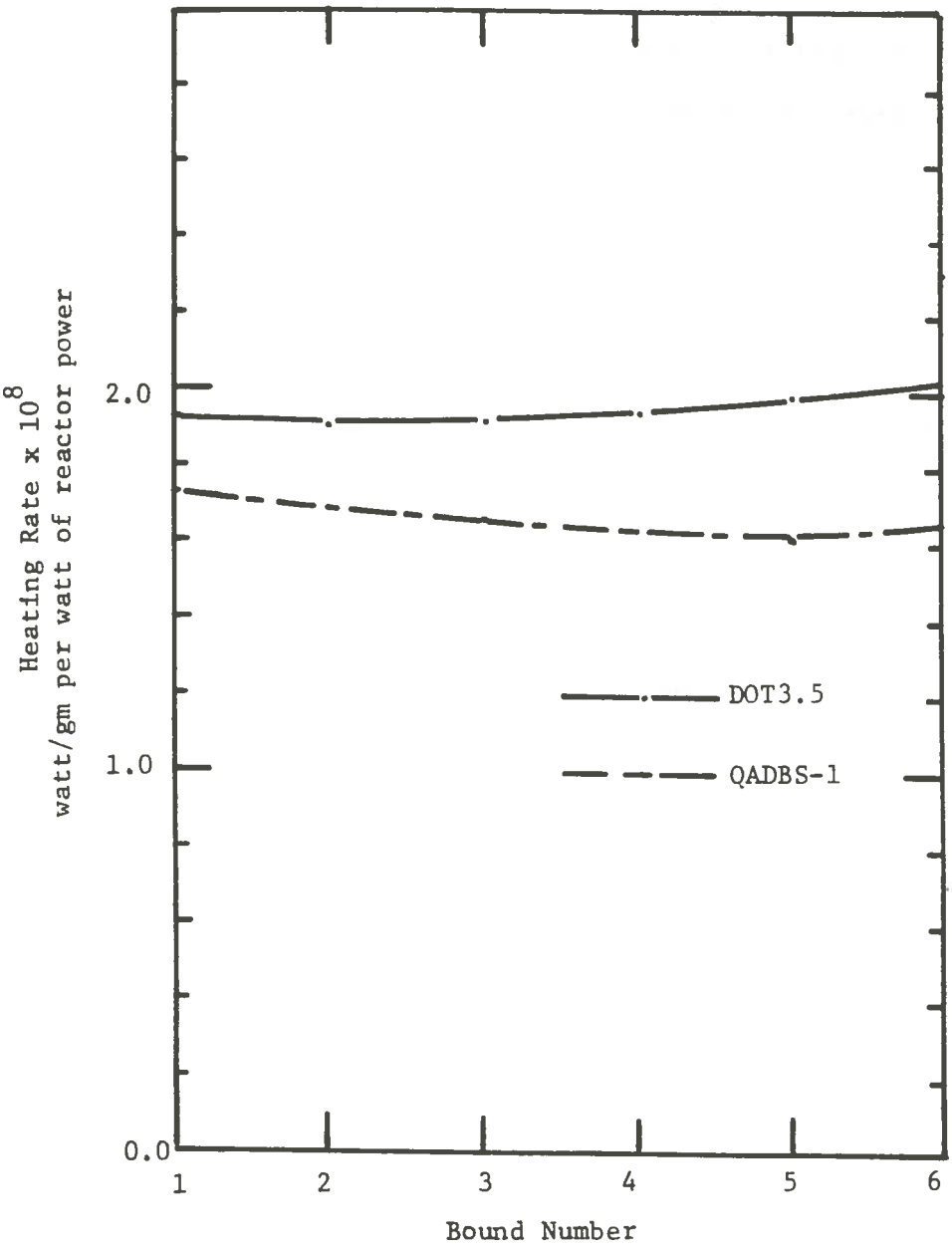

Figure 5.12. Heating Rate at Various Points of Secondary Pressure Boundary of TREAT Upgrade Reactor with Modified QADBS-1 Results to Correct for Fission Product Decay Gammas.

The heating rate distribution in the axial direction is substantially different (Figure 5.13) after adjusting for the inclusion of fission product-decay gammas in the point-kernel method.

In the point-kernel method the axial heating rate distribution were estimated, based on the axial buckling of the neutron flux in the TREAT reactor. While in this study the axial heating rate results were computed explicitly by the DOT3.5 code. Hence, the axial heating rates obtained in this work are more accurate.

The agreement of the gamma heating results of the GRIST-2 pressure boundaries between the coupled neutron-gamma transport method and the point-kernel method are well within the range expected for two widely different approaches using different cross section sets and substantiate the realiability of the results.

5.5. Conclusion

The gamma heat deposition rates at any point in a nuclear reactor is related to several functions: gamma flux density energy spectrum at that point; the energy dependent cross sections for the various interactions possible between radiations and matter, and the concentration of the various constituents at that point.

The gamma heating rate is generated in TREAT upgrade reactor as a result of the primary and secondary gamma energy deposition in the reactor material. Gammas deposit their energy via pair production, photoelectric effect and Compton scattering interactions.

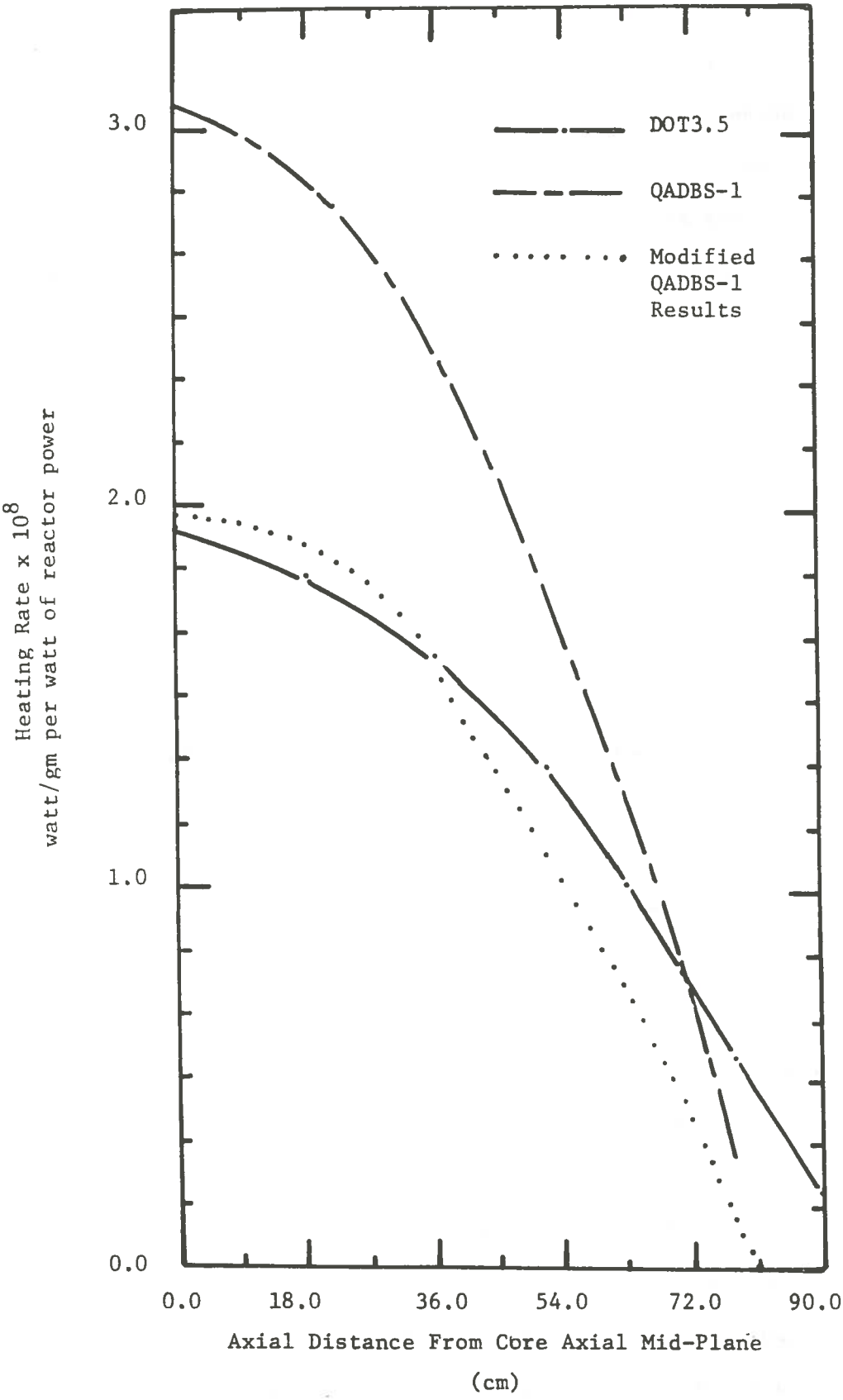

Fifure 5.13. Heating Rate in Primary Pressure Boundary as a Function of Axial Distance from the Axial Mid-Plane at Radial Coordinate of 6.81 cm.

Determination of gamma flux density and its energy spectrum as a function of position are done by the use of ANISN and DOT codes. The accuracy of the results depends on certain extents on the selection of the phase space mesh. Once the space mesh, angle and energy are reasonably fine, the solution of the transport equation by ANISN and DOT codes may reach a high degree of accuracy.

Coupled neutron-gamma cross section libraries are utilized in the calculations. The compatability of such libraries in performing gamma heating calculations has been examined in this work.

The heating rates in the primary and secondary pressure boundaries are obtained by ANISN and DOT codes. ANISN does not provide good gamma heating results, because the one-dimensional model does not accurately represent the gamma-ray attenuation distances. The DOT results are compared with those obtained by QAD code. The maximum heating rate in the primary and secondary pressure boundaries calculated by ANISN are 1.524×10^{-6}, and 1.7544×10^{-6} watt/gm per watt of reactor power respectively. Those calculated by DOT code are 1.96×10^{-8} and 2×10^{-8} watt/gm per watt of reactor power in the primary and secondary pressure boundaries respectively.

The QAD code results which included equilibrium fission product-decay gammas are some what higher than those obtained by DOT. They deviate by a factor of 1.5. But after subtracting the contribution of fission product-decay gammas from QAD results,

there still remains minor discrepancies of $\pm$ 5%. The remaining differences are due to the inherent difference between (S_N) method and point-kernel method in which QAD code is based on. Another reason is the difference in the two cross section sets group structure used in the two cases.

Finally, using the (S_N) method for gamma heating calculation has shown potential advantages over the point-kernel method. Advantages include eliminating multiple buildup factors to account for multiple scattering, relative low computer usage, ease of problem set-up, and ease of output analysis.

REFERENCES

1. Carlson, B. G., "Solution of the Transport Equation by S_N Approximation", LA-1599 (revised version, LA-1891 (1953).

2. Duane, B. H., "Neutron and Photon Transport: Plane, Cylinder, Sphere (Digital Computer Program S)." APEX-394 (1957).

3. Duane, B. H., "Neutron and Photon Transport Plane-Cylinder-Sphere GE-ANPD Program S," XDC-59-9-118 (1959).

4. Lathrop, K. D., "DTF-IV, A Fortran-IV Program for Solving the Multigroup Transport Equation with Anisotropic Scattering," USAEC Report LA-3373, Los Alamos Scientific Laboratory (July 1965).

5. Engle, W. W., Jr., "A User's Manual for ANISN, a One-Dimensional Discrete Ordinate Transport Code with Anisotropic Scattering", K-1693, Union Carbide Corporation, Nuclear Division (1967).

6. "Two-Dimensional Discrete Ordinates Code System Programs", LA-4600, LASL.

7. Rhoades, W. A. and F. R. Mynatt, "DOT3.5, Two-Dimensional Discrete Ordinates Radiation Transport Code", RSIC Computer Code Collection, ORNL, CCC-276 (1976).

8. Mynatt, F. R., "A User's Manual for DOT", K-1694 (January 1967).

9. Mynatt, F. R., "DOT, Two-Dimensional Discrete Ordinate Transport Code", CCC-89, RSIC (May 1969).

10. Bartine, D. E., J. R. Knight, J. V. Pace, III and R. Roussin, "Production and Testing of the DNA Few-Group Coupled Neutron-Gamma Cross-Section Library", ORNL/TM-4840.

11. West, J. T., G. P. DeBeer, B. Nakhai and R. W. Roussin, "BUGLE: Coupled 45 Neutron, 16 Gamma-Ray, P_3 Cross-Sections for Studies by the ANS G.1.2 Shielding Standard Working Group on Multigroup Cross Sections", DLC-47, RSIC, ORNL (September 1977).

12. Roussin, R. W. and J. B. Wright, "CASK: 40 Group Coupled Neutron and Gamma-Ray Cross Section-Data", DLC-23, RSIC, ORNL (September 1973).

13. Engle, W. W., Jr., "DLC-2, Data Retrival Program", RSIC, ORNL.

14. Engle, W. W., Jr., "A Routine to Prepare a 'Group Independant' Cross Section Tape", RSIC, ORNL.

15. Straker, E. A., et al., "The MORSE Code - A Multigroup Neutron and Gamma-Ray Monte Carlo Transport Code", ORNL-4585, ORNL (1970).

16. Clairborne, H. C., "Survey of Methods for Calculating Gamma-Ray Heating", ORNL-RSIC-8 (June 1965).

17. Kalra, M. S. and M. J. Drisolt, "Gamma Heating in LMFBR Media", COO-2250-18 (February 1976).

18. Lamarsh, J. R., "Introduction to Nuclear Reactor Theory", Addison-Wesley Publishing Co., Inc., (1966). pp. 57.

19. Olson, A. P., "Gamma-Ray Heating in Power Reactors", Nuclear Service Corp., PB-250 569, Prepared for EPRI (January 1976).

20. Olson, A. P., Reference 19 , pp. 5.

21. Schaeffer, N. M., "Reactor Shielding for Nuclear Engineers", TID-25951 (1973).

22. Stenstrom, D. G., "Calculation of Gamma Heating in a Fast Reactor Environment", Trans. Am. Nucl. Soc. 15:1-551 (June 1972).

23. Miles, R. E., "Internal Report, TREAT Reactor, ANL(West), Idaho.

24. Disney, R. K. and H. C. Romesburg, "Calculating Transport and Heat Deposition of Gamma-Rays by S_N Transport Program", Trans. Am. Nucl. Soc. 8:190 (1965).

25. Dudley, T. E., M. R. Mendelson, and N. E. Holden, "The Use of Infinite Medium Spectra in Gamma-Ray Heating Calculations", Nucl. Sci. and Engr. 30:328-339 (1967).

26. Wick, G. C., "Uber ebene Diffusion Problem", Physick 121:702 (1943).

27. Chandrasekhar, S., "Radiative Transfer", Clarendon Press, Oxford (1950).

28. Carlson, B. G., "Solution of the Transport Equation by S_N Approximation", LA-189 (1953).

29. Mynatt, F. R., F. R. Muckenthal and P. N. Stevens, "Development of Two-Dimensional Discrete Ordinates Transport Theory for Radiation Shielding", CTC-INF-952.

30. LSU-SNCC, "User's Guide for the IBM 360/65 Computer", (1976).

31. IBM System/370, "OS/US Linkage Editor and Loader", GC26-3813-4, File No. S370-31, Fifth Edition (November 1975).

32. IBM System/370, "Principle of Operation", GA22-7000-5, File No. S/370-01, Fifth Edition (August 1976).

33. Iskenderian, H. P., "Physics Analysis of the TREAT Reactor Design", ANL-6025 (August 1959).

34. MacFarlane, D. R. and G. A. Freund, "Hazards Summary Report On the Transient Reactor Test Facility (TREAT)", ANL-5923 (October 1958).

35. Handwerk, J. H. and R. C. Lied, "The Manufacturer of the Graphite-Urania Fuel Matrix", ANL-5963 (January 1960).

36. Kirn, F., J. Boland, H. Lawroski, and R. Cook, "Reactor Physics Measurements in TREAT", ANL-6173, (October 1960).

37. Okrent, D., C. E. Dickerman, and J. Gasiello, "The Reactor Kinetics of the Transient Reactor Test Facility (TREAT)", ANL-6174 (September 1960).

38. Evans, R. D., "The Atomic Nucleus", McGraw-Hill Book Company, Inc., NY (1955).

39. Chilton, A. B., "Methods for Calculating Radiation-Induced Heat Generation", Nucl. Engr. and Design 18 (1972). pp. 401-413.

40. Abdu, M. A., "Calculational Method for Nuclear Heating", Ph.D Thesis, University Microfilms Inc. 74-8981.

41. Lucius, J. L. and W. E. Ford, III, "SMUG: An AMPX Module for Generating Multigroup Photon Cross Sections", PSR-63, RSIC (1978).

42. Knight, J. R. and F. R. Mynatt, "MUG - A Program for Generating Multigroup Photon Cross Sections", CTC-17, Union Carbide Corporation, Computing Technology Center (1970).

43. Ford, W. E., III and D. H. Walace, "POPOP4, A Code for Converting Gamma-Ray Spectra to Secondary Gamma-Ray Production Cross Sections", CTC-12, Union Carbide Corp., ORNL (1969).

44. Hubbel, J. M. and M. J. Berger, "Photon Attenuation Coefficients, Energy Absorption Coefficients, and Related Quantities", Engineering Compendium on Radiation Shielding, Vol. 1, Shielding Fundamentals and Methods (Springer-Verlag, NY) 1968, Section 4.1.

45. Bell, G. I, and S. Glasstone, "Nuclear Reactor Theory", Van Nostrand Reinhold Company, NY (1970).

APPENDIX A

Job Control Cards for Creating a LOAD MODULE of DOT3.5

```
//LOADMOD JOB (7011,44560,1,5),'AZIZ'
/*SETUP          T2998
//STEP1 EXEC ASMFC,PARM.ASM='LOAD,NODECK,NOLIST',REGION.ASM=260K,
//  TIME.ASM=1
//ASM.SYSGO DD SPACE=(TRK,(400,50),RLSE)
//ASM.SYSIN DD UNIT=TAPE,VOL=(,RETAIN,SER=T2998),DISP=(OLD,PASS),
//  LABEL=16,DSN=GRIND,
//  DCB=(RECFM=FB,LRECL=80,BLKSIZE=3200)
//STEP2 EXEC ASMFC,PARM.ASM='LOAD,NODECK,NOLIST',REGION.ASM=260K,
//  TIME.ASM=1
//ASM.SYSIN DD UNIT=TAPE,VOL=(,RETAIN,SER=T2998),DISP=(OLD,PASS),
//  LABEL=17,DSN=WWESOL,
//  DCB=(RECFM-FB,LRECL=80,BLKSIZE=3200)
//STEP3 EXEC ASMFC,PARM.ASM='LOAD,NODECK,NOLIST',REGION.ASM=260K,
//  TIME.ASM=1
//ASM.SYSIN DD UNIT=TAPE,VOL=(,RETAIN,SER=T2998),DISP=(OLD,PASS),
//  LABEL=18,DSN=ALOCAT,
//  DCB=(RECFM=FB,LRECL=80,BLKSIZE=3200)
//STEP4 EXEC ASMFC,PARM.ASM='LOAD,NODECK,NOLIST',REGION.ASM-260K,
//  TIME.ASM=1
//ASM.SYSIN DD UNIT=TAPE,VOL=(,RETAIN,SER=T2998),DISP=(OLD,PASS),
//  LABEL=19,DSN=CMVBT,
//  DCB=(RECFM=FB,LRECL=80,BLKSIZE=3200)
//STEP5 EXEC ASMFC,PARM.ASM='LOAD,NODECK,NOLIST',REGION.ASM=260K,
//  TIME.ASM=1
//ASM.SYSIN DD UNIT=TAPE,VOL=(,RETAIN,SER=T2998),DISP=(OLD,PASS),
//  LABEL=20,DSN=JOBNUM,
//  DCB=(RECFM=FB,LRECL=80,BLKSIZE=3200)
```

```
//STEP6 EXEC ASMFC,PARM.ASM='LOAD,NODECK,NOLIST',REGION.ASM=260K,
//  TIME.ASM=1
//ASM.SYSIN DD UNIT=TAPE,VOL=(,RETAIN,SER=T2998),DISP=(OLD,PASS),
//  LABEL=21,DSN=ITIME,
//  DCB=(RECFM=FB,LRECL=80,BLKSIZE=3200)

//STEP7 EXEC ASMFC,PARM.ASM='LOAD,NODECK,NOLIST',REGION.ASM=260K,
//  TIME.ASM=1
//ASM.SYSIN DD UNIT=TAPE,VOL=(,RETAIN,SER=T2998),DISP=(OLD,PASS),
//  LABEL=24,DSN=ICLOCK,
//  DCB=(RECFM=FB,LRECL=80,BLKSIZE=3200)

//STEP8 EXEC FORTHC,REGION,FORT=512K,TIME.FORT=5,PARM.FORT='NOSOURCE'
//FORT.SYSIN DD UNIT=TAPE,VOL=(,RETAIN,SER=T2998),DISP=(OLD,PASS),
//  LABEL=25,DSN='MAIN.LOCO.DOT',
//  DCB=(RECFM=FB,LRECL=80,BLKSIZE=3200)

//STEP9 EXEC FORTXC,REGION.FORT=868K,TIME.FORT=5,PARM.FORT='NOSOURCE'
//FORT.SYSIN DD UNIT=TAPE,VOL=(,RETAIN,SER=T2998),DISP=(OLD,PASS),
//  LABEL=26,DSN=INP,
//  DCB=(RECFM=FB,LRECL=80,BLKSIZE=3200)

//STEP10 EXEC FORTHCL,REGION.FORT=1024K,TIME.FORT=5,PARM.FORT='NOSOURCE',
//PARM.LKED='XREF,LET,LIST,OVLY',REGION.LKED=1024K
//FORT.SYSIN DD UNIT=TAPE,VOL=SER=T2998,DISP=(OLD,PASS),
//  LABEL=27,DSN=DOT3-5,
//  DCB=(RECFM=FB,LRECL=80,BLKSIZE-3200)

//LKED.SYSLMOD DD DSN='NSMILE.DOT3-5.LOADS',
//  DISP=NEW,KEEP),SPACE=(TRK,(40,10,6),RLSE),UNIT=DISK,VOL=SER=USER02

//  LKED.SYSIN DD *

 ENTRY MAIN
 OVERLAY ALPHA
 INSERT MESAGE,HEADER,FHLPR,JOBNUM,LETTER
 OVERLAY ALPHA
 INSERT INP,FIDA,FIDAS,FFREAD,IDOT
 INSERT CLEARX,CMASGN
```

```
OVERLAY BETA
INSERT TPCOPY,TPXF
OVERLAY BETA
INSERT DSTEST,S860,SLIBE,S863,S864
INSERT CLUGE,CMVBT,LOCO
OVERLAY BETA
INSERT PCON,S862,MAPR,S865
OVERLAY ALPHA
INSERT INIT
INSERT UNCL,FUNCTO,TRAPO,PCON1,PICTUR
OVERLAY ALPHA
INSERT S8847,FISCAL,S8830,CNNP
OVERLAY ALPHA
INSERT OUTER
OVERLAY DELTA
INSERT INNER,GRIND,WWESOL,ANFOOL
OVERLAY DELTA
INSERT INNER1,INNERI,INNERJ,IFLUXN,INNERX
OVERLAY ALPHA
INSERT S8850,ACTVTY,TPSAVE,PUNSH,DTFPUN,FLTFX
INSERT EDIT,TABLE
NAME DOT(R)
//
```

APPENDIX B

Typical JCL for DOT3.5 Run

```
//STEP1 EXEC PGM=DOT,REGION=2048K,TIME=10
//STEPLIB DD DSN=NSMILE.DOT3-5.LOADS,DISP=SHR
//LKED.SYSIN DD *
//GO.FT05F001 DD DDNAME=SYSIN
//GO.FT06F001 DD SYSOUT=A
//GO.FT01F001 DD DUMMY
//GO.FT02F001 DD UNIT=SYSDA,DISP=(NEW,DELETE),
//  SPACE=(3504,(300,300)),
//  DCB=(RECFM=VBS,LRECL=700,BLKSIZE=3504)
//GO.FT03F001 DD UNIT=SYSDA,DISP=(NEW,DELETE),
//  SPACE=(3504,(300,300)),
//  DCB=(RECFM=VBS,LRECL=700,BLKSIZE=3504)
//GO.FT10F001 DD UNIT=SYSDA,DISP=(NEW,DELETE),
//  SPACE=(3504,(300,300)),
//  DCB=(RECFM=VS,LRECL=3500,BLKSIZE=3504)
//GO.FT11F001 DD UNIT=SYSDA,DISP=(NEW,DELETE),
//  SPACE=(3504,(300,300)),
//  DCB=(RECFM=VS,LRECL=3500,BLKSIZE=3504)
//GO.FT18F001 DD UNIT=SYSDA,DISP=(NEW,DELETE),
//  SPACE=(3504,(300,300)),
//  DCB=(RECFM=VS,LRECL=3500,BLKSIZE=3504)
//GO.FT19F001 DD UNIT=TAPE,VOL=SER=T2140,LABEL=29,DISP=(NEW,KEEP),
//  DSN='SCAL.FLUX.OUTPUT',
//  DCB=(RECFM=VBS,LRECL=2652,BLKSIZE=2656)
//GO.SYSIN DD *
                .  .
                .  .
                .  .
            Input data
                .  .
                .  .
//
```

APPENDIX C

Sample TREAT Problem for DOT3.5

```
61$$  0 3 27 90 30 13 3 4 16 0 110 0 110 1 16 1 1 0 1 0 20 9 20 0 1
      2 4R0 2R1 8R0 1 2 27  5R0  8 100  2 1 4  8R0

62$$  16 17  3R18  19 2 18  20 3 8  120  2R0

63**  1.0 0.0001 0.001 1000.0  11R0.0 1.0 0.001  0.0001   T

 7** -0.94281 -0.88192 -0.33333 M2 -0.47140 -0.33333 M1 Q8 5R-0.33333
     3R-0.88192 5R0.33333 3R0.88192   T

 6**  0.0 4R0.08333 0.0 2R0.08333 Q8  T

14**                .   .   .
                    .   .   .
                    .   .   .
              Cross Section Input
                    .   .   .
                    .   .   .

31$$  F3    T

 3**  F1.0  T

 1**  9.498-1 1.500-1 9.029-5 7.115-8 1.195-10 8R0.0

 2**  29I0.0 90.0

 4**  2I0.0 2I0.5932 2I1.5693 2I2.5888 1I3.608 1I3.8483 1I4.55 1I4.65
        4.9 2I5.875 2I6.005 5I6.18 7.125 4I7.365 1I7.45 4I9.15 10.1 4I10.16
      2I12.507 2I14.853 2I17.198 4I19.49 4I26.366 4I33.244 4I40.123
      4I51.59 4I108.91 177.700

 5**  5R1.0 8R0.0

 8$$  3R1 3R2 3R3 3R4 2R5 1R6 2R7 2R8 1R9 3R10 3R11 6R12 1R13 5R14 2R15
     5R16 1R17 5R18 3R19 3R20 3R21 5R22 5R23 5R24 5R25 5R26 5R27 29Q90
```

```
 9$$ -1 -5 -9 -13 -17 -21 -25 -29 -33 -37 -41 -45 -49 -53 -57 -61 -65
     -69 -73 -77 -81 -85 -89 -93 -97 -101 -105

19$$ -109  -110

20$$ 1  1

29$$ F16

30$$  25I1 27   T T
```

APPENDIX D

Discrete Ordinate Difference Equations for Cylindrical r-z Geometry

The time-independent transport equation for two-dimensional cylindrical r-z geometry may be represented[29] by the following equation:

$$\frac{d\Phi(r,z,\theta,\psi,E)}{ds} + \Sigma^T(r,z,\theta,E)\Phi(r,z,\theta,\eta,\psi,E) = S(r,z,\theta,\eta,\psi,E) + \int_{-1}^{+1}\int_{0}^{2\pi}\int_{0}^{\infty} \Sigma^S(r,z,\theta,E',\vec{\Omega}'\rightarrow E,\vec{\Omega})\,(r,z,\theta,\eta',\psi',E')dE'd\psi'd\eta' \qquad (D\text{-}1)$$

Where the parameters are defined by the total macroscopic cross section, Σ^T, the scattering cross section, Σ^S, the flux, Φ, the radius, r, axial displacement, z, polar direction cosine, η, azimuthal angle, ψ, the source, s, and the energy, E.

The first term of the equation may be expressed by:

$$\frac{d\Phi}{ds} = \frac{d\Phi}{dr}\frac{dr}{ds} + \frac{d\Phi}{dz}\frac{dz}{ds} + \frac{d\Phi}{d\theta}\frac{d\theta}{ds} + \frac{d\Phi}{d\eta}\frac{d\eta}{ds} + \frac{d\Phi}{d\psi}\frac{d\psi}{ds} \qquad (D\text{-}2)$$

One can determine from (Figure D-1) that

$$\frac{dr}{ds} = \mu, \quad \frac{dz}{ds} = \eta, \quad \frac{d\theta}{ds} = \frac{\xi}{r}$$

$$\frac{d\eta}{ds} = 0.0, \quad \frac{d\psi}{d\theta} = -1 \quad \text{and} \quad \frac{d\psi}{ds} = \frac{d\psi}{d\theta}\frac{d\theta}{ds} = -\frac{\xi}{r}$$

We assume P is the phase space cell, defined by (r,z,θ,η,ψ and E) where

$$\Phi(P) = \Phi(r,z,\theta,\eta,\psi,E) \quad \text{and}$$
$$\Phi(P') = (r,z,\theta,\eta',\psi',E'). \tag{D-3}$$

But in the two-dimensional r-z geometry, the material composition and geometry are invariant with respect to θ, so Equation (D-1) becomes

$$\mu \frac{d\Phi(P)}{dr} + \eta \frac{d\Phi(P)}{dz} - \frac{\xi}{r} \frac{d\Phi(P)}{d\psi} + \overset{T}{\Sigma}(r,z,E)\Phi(P) =$$

$$S(P) + \int_{-1}^{+1} \int_{0}^{2\pi} \int_{0}^{\infty} \overset{S}{\Sigma}(r,z;E',\vec{\Omega}'\rightarrow E,\vec{\Omega})\Phi(P')dE'd\psi'd\eta'. \tag{D-4}$$

and the differential phase space cell may be given now by

$$dP = 2\pi r \, dr \, dz \, d\eta \, d\psi \, dE \tag{D-5}$$

by integrating (D-5) over (r,z,η,ψ and E), the finite difference phase space cell, DP, is

$$DP = \int_{r_i}^{r_{i+1}} \int_{z_j}^{z_{j+1}} \int_{\eta_k}^{\eta_{k+1}} \int_{\psi_{n+1}}^{\psi_n} \int_{E_g}^{E_{g+1}} 2\pi r \, dr \, dz \, d\eta \, d\psi \, dE \tag{D-6}$$

Notice ψ_n mesh is constructed in a way, such that n increases as ψ decreases, and which gives

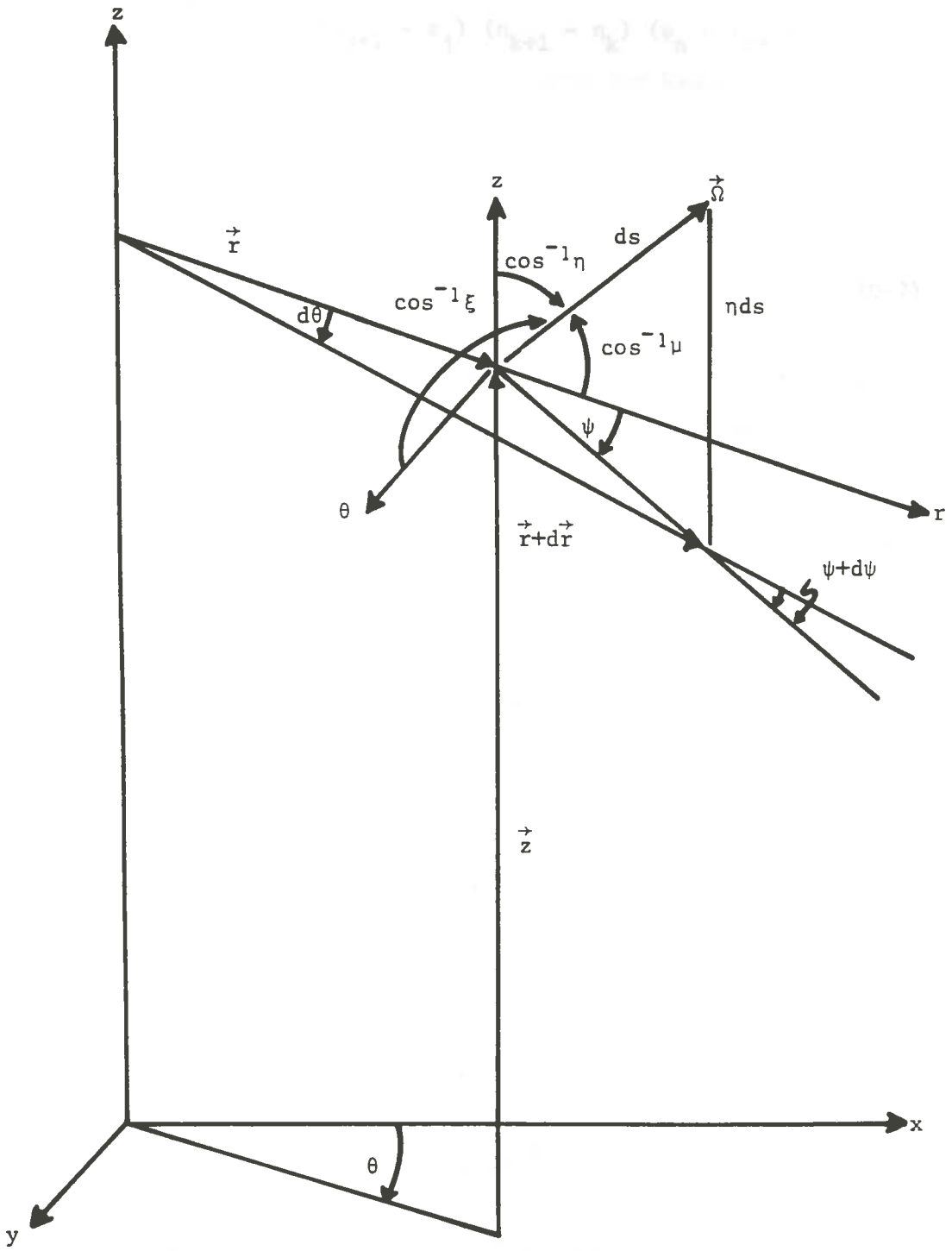

Figure D.1. The Coordinate System for Cylindrical Geometry.

$$DP = (r_{i+1}^2 - r_i^2)\ (z_{j+1} - z_j)\ (\eta_{k+1} - \eta_k)\ (\psi_n - \psi_{n+1})$$

$$(E_{g+1} - E_g)$$

or

$$DP = V_{I,J}\ D\eta_K\ D\psi_N\ DE_G \tag{D-7}$$

where V is the volume of the space cell, and the subscripts i, j, k, n, g, refer to quantities evaluated at the surface of the finite phase space cell, and I, J, K, N, G, refer to quantities defined for the cell as a whole, or having been averaged or integrated over the cell.

Once we integrate Equation (D-4) term by term[29] by applying the integral operator (D-6), the discrete ordinates difference equation for r-z geometry is obtained as:

$$2\pi\ \Delta z_J\ \bar{\mu}_D(r_{i+1}\Phi_{G,i+1,J,D} - r_i\Phi_{G,i,J,D}) +$$

$$2\pi\bar{r}_I\ \Delta r_I\ \bar{\eta}_D(\Phi_{G,I,j+1,D} - \Phi_{G,I,j,D}) +$$

$$\frac{\Delta z}{w_D}\ (\gamma_{n+1}\Phi_{G,I,J,n+1,K} - \gamma_n\Phi_{G,I,J,n,K}) +$$

$$V_{I,J} \sum_{G}^{T} \Phi_{G,I,J,D} = V_{I,J}\ S_{G,I,J,D} +$$

$$V_{I,J} \sum_{\ell=1}^{LMAX} \sum_{m=0}^{\ell} A_D^{\ell,m} \sum_{G'=1}^{G} S_{G,G'}^{\ell,m} \sum_{D'=1}^{NOA} A_{D'}^{\ell,m}\ \Phi_{G',I,J,D'}\ w_{D'} \tag{D-8}$$

where

μ and w are the ordinates and weights for Gaussian quadrature respectively.

NOA = the total number of points

m and ℓ are integers.

$$A_D^{\ell,m} = P_\ell(\bar{\eta}_D), \text{ when } m = 0$$

and

$$A_D^{\ell,m} = \left[2 \frac{(\ell-m)!}{(\ell+m)!}\right]^{1/2} P_\ell^m (\bar{\eta}_D) \text{ Cos } m\bar{\psi}_D, \text{ when } m \neq 0$$

γ_n = the curvature coefficients, defined by

$$\gamma_n = \frac{1}{2} \Delta r_I \Delta \eta_K \xi_n$$

$$= \frac{1}{2} \Delta r_I \Delta \eta_K \left(1 - \eta_K^2\right)^{1/2} \text{ Sin } \psi_n \qquad \text{(D-9)}$$

The last term of Equation (D-8) is the derivation of the scattering integral of Equation (D-4), after the scattering cross section was expanded in Legendre polynomials.

A supplementary difference equations which relate the central flux with each pair of associated cell face fluxes are:

$$\Phi_{G,I,J,D} = a\Phi_{G,i+1,J,D} + (1-a)\, \Phi_{G,i,J,D} \qquad \mu>0.0$$

$$\Phi_{G,I,J,D} = (1-a)\, \Phi_{G,i+1,J,D} + a\Phi_{G,i,J,D} \qquad \mu<0.0$$

$$\Phi_{G,I,J,D} = b\Phi_{G,I,j+1,D} + (1-b)\ \Phi_{G,I,j,D} \qquad \eta>0.0$$

$$\Phi_{G,I,J,D} = (1-b)\ \Phi_{G,I,j+1,D} + b\Phi_{G,I,j,D} \qquad \eta<0.0$$

$$\Phi_{G,I,J,D} = c\Phi_{G,I,J,n+1,K} + (1-c)\Phi_{G,I,J,n,K} \qquad \text{(D-10)}$$

where a, b, and c are constants.

The combination of (D-8) with (D-10) determines the complete flux array for a given source. The degree of accuracy depends on the order of calculation (mesh sweep), which subsequently depends on the sequence of cosines[45], $\bar{\mu}_D$ and $\bar{\eta}_D$.

APPENDIX E

TAPEMAKER SAMPLE INPUT

```
      150000
   68      3      4     61   642      0     57     73      0      1
10$
 2I      58           61 4Q          4Q          4Q           4Q
 4Q         4Q           4Q          4Q          4Q
 2I      62           65 4Q          4Q          4Q           4Q
 4Q         4Q           4Q          4Q          4Q
 2I      66           69 4Q          4Q          4Q           4Q
 4Q         4Q           4Q          4Q          4Q
 2I      70           73 4Q          4Q          4Q           4Q
 4Q         4Q           4Q          4Q          4Q
 2I      74           77 4Q          4Q          4Q           4Q
 4Q         4Q
 2I      78           81 4Q
 2I      82           85 4Q          4Q
 2I      86           89 4Q          4Q          4Q
 2I      90           93 4Q          4Q          4Q           4Q
 4Q         4Q           4Q          4Q          4Q           4Q
 2I      94           97 4Q          4Q          4Q           4Q
 4Q         4Q           4Q          4Q          4Q           4Q
 2I      98          101 4Q          4Q          4Q           4Q
 4Q         4Q           4Q          4Q          4Q           4Q
 2I     102          105 4Q          4Q          4Q           4Q
 4Q         4Q           4Q          4Q          4Q           4Q
 2I     106          109 4Q          4Q          4Q           4Q
 4Q         4Q           4Q          4Q          4Q           4Q
 2I     110          113 4Q          4Q          4Q           4Q
 4Q         4Q           4Q          4Q          4Q           4Q
 2I     114          117 4Q          4Q          4Q           4Q
 4Q         4Q           4Q          4Q          4Q           4Q
 2I     118          121 4Q          4Q          4Q           4Q
 4Q         4Q           4Q          4Q          4Q           4Q
 2I     122          125 4Q          4Q          4Q           4Q
 4Q         4Q           4Q          4Q          4Q           4Q
 2I     126          129 4Q          4Q          4Q           4Q
        130          130
11$
 4Z        6I           10        1726I         30          57
 4Z        6I           10        1726I         30          57
 4Z        6I           10        1726I         30          57
 4Z        6I           10        1726I         30          57
 4Z        2I           10        1318I         30          49
 4Z        2I           14          17
 4Z        2I           14          17 2I         22          25
 4Z        6I            2           9 2I         14          17
 4Z      101I           10        2118I         26          45 6I       50
        57
 4Z      101I           10        2118I         26          45 6I       50
        57
 4Z      101I           10        2118I         26          45 6I       50
```

```
4Z      57
          101      10          2118I       26          45 6I       50
4Z      57
          101      10          2118I       26          45 6I       50
4Z      57
          101      10          2118I       26          45 6I       50
4Z      57
          101      10          2118I       26          45 6I       50
4Z      57
          101      10          2118I       26          45 6I       50
4Z      57
          14I       2          17 2I       22          25
2I      30          33 6I      38          45 6I       50          57
4Z        101       2          13 2I       38          41
            0       1
12*
 4R 0.0       4R 3.1760-5 4R 1.2500-2 4R 1.2460-3 4R 1.1820-4 4R 4.5110-3
 4R 7.7880-4 4R 9.9310-5 4R 5.8170-3 4R 4.3230-4
 4R 0.0       4R 3.1760-5 4R 1.2490-2 4R 1.2460-3 4R 1.1820-4 4R 4.5110-3
 4R 7.7880-4 4R 9.9310-5 4R 5.6280-3 4R 6.1740-4
 4R 0.0       4R 3.1760-5 4R 1.2480-2 4R 1.2460-3 4R 1.1820-4 4R 4.5110-3
 4R 7.7880-4 4R 9.9310-5 4R 5.1282-3 4R 4.5659-3
 4R 0.0       4R 3.1760-5 4R 1.2470-2 4R 1.2460-3 4R 1.1820-4 4R 4.5110-3
 4R 7.7880-4 4R 9.9310-5 4R 5.5659-3 4R 1.6674-3
 4R 0.0       4R 4.0300-4 4R 1.5810-2 4R 1.5000-3 4R 5.7230-2 4R 9.8820-3
 4R 1.2600-3
 4R 0.0       4R 2.500-10
 4R 0.0       4R 3.0676-3 4R 1.6183-3
 4R 0.0       4R 3.1957-3 4R 1.2944-2 4R 1.0000-2
 4R 0.0       4R 6.8584-2 4R 2.2815-4 4R 1.1052-4 4R 1.2448-5 4R 5.1579-4
 4R 1.3566-5 4R 2.0820-3 4R 1.2692-5 4R 1.0666-4 4R 7.4149-6
 4R 0.0       4R 6.8665-2 4R 1.8914-4 4R 1.1052-4 4R 1.2448-5 4R 5.1579-4
 4R 1.3566-5 4R 2.0820-3 4R 1.2692-5 4R 8.8420-5 4R 6.1469-6
 4R 0.0       4R 6.8716-2 4R 1.6394-4 4R 1.1052-4 4R 1.2448-5 4R 1.1579-4
 4R 1.3566-5 4R 2.0820-3 4R 1.2692-5 4R 7.6645-5 4R 5.3283-6
 4R 0.0       4R 7.3022-2 4R 1.4322-4 4R 9.0423-5 4R 1.0184-5 4R 4.2201-4
 4R 1.1100-5 4R 1.7034-3 4R 1.0384-5 4R 6.6958-5 4R 4.6548-6
 4R 0.0       4R 7.3060-2 4R 1.2490-4 4R 9.0423-5 4R 1.0184-5 4R 4.2201-4
 4R 1.1100-5 4R 1.7034-3 4R 1.0384-5 4R 5.8410-5 4R 4.0600-6
 4R 0.0       4R 7.3100-2 4R 1.0290-4 4R 9.0423-5 4R 1.0184-5 4R 4.2201-4
 4R 1.1100-5 4R 1.7034-3 4R 1.0384-5 4R 4.8110-5 4R 3.3450-6
 4R 0.0       4R 7.3150-2 4R 8.1360-5 4R 9.0423-5 4R 1.0184-5 4R 4.2201-4
 4R 1.1100-5 4R 1.7034-3 4R 1.0384-5 4R 3.8040-5 4R 2.6440-6
 4R 0.0       4R 7.3230-2 4R 4.0940-5 4R 9.0423-5 4R 1.0184-5 4R 4.2201-4
 4R 1.1100-5 4R 1.7034-3 4R 1.0384-5 4R 1.9140-5 4R 1.3300-6
 4R 0.0       4R 1.2823-7 4R 5.1939-7 4R 7.6210-2 4R 1.6460-5 4R 9.8600-4
 4R 5.2200-8 4R 1.4450-5 4R 7.7050-9 4R 7.6761-6 4R 5.5653-7
 4R 0.0       4R 3.6828-8 4R 1.4917-7 4R 8.3660-2 4R 1.8010-5
   0.0          1.0
138
          1      22      23      24      25      26
         27      28      29      30      31      32
         33      42      43      44      45      62
         63      64      65      66      67      68
         69      82      83      84      85      86
         87      88      89      90      91      92
         93      94      95      96      97      98
         99     100     101     106     107     108
        109     134     135     136     137     138
        139     140     141
T
```

APPENDIX F

ANISN Sample Input

```
15$$  1 0 3 4 2 1 0 27 90 1 13 3 4 16 0 110 0 110 5R0 60 2R0 2 1 60 2
      3R0 1 1 0
16**  1.37451 0.0 0.0001 1.4209 180.0 2R0.0 1.0 0.0 0.5 0.0001 0.05
      0.001 0.75  T
14**                  .      .      .
                      .      .      .
                Cross Section  Input Data
                      .      .      .
                      .      .      .
          T
 3**  F1.0  T
 1**  9.498-1 1.500-1 9.029-5 7.115-8 1.195-10 8R0.0
 4**  2I0.0 2I0.5932 2I1.5693 2I2.5888 1I3.608 3.8483 1I4.55 1I4.65
      4.9 2I5.875 2I6.005 5I6.18 7.125 4I7.365 1I7.45 4I9.15 10.1
      4I10.16 2I12.507 2I14.853 2I17.198 4I19.49 4I26.366 4I33.244
      4I40.123 4I51.59 4I108.91 177.7
 5**  5R1.0 8R0.0
 6**  0.0 2R0.166667 0.0 4R0.166667
 7**  -0.471405 -0.333333 0.333333 -0.942809 -0.881917 -0.333333
       0.333333 0.88197
 8$$  3R1 3R2 3R3 3R4 2R5 1R6 2R7 2R8 1R9 3R10 3R11 6R12 1R13 5R14
      2R15 5R16 1R17 5R18 3R19 3R20 3R21 5R22 5R23 5R24 5R25 5R26
      5R27
 9$$  1 5 9 13 17 21 25 29 33 37 41 45 49 53 57 61 65 69 73 77 81
      85 89 93 97 101 105
19$$ 27R3
22$$ -109 -110
23$$ 1 1  T  T
```

APPENDIX G

List of Symbols

$\Phi(\vec{r},E)$	Space and energy dependent flux.
$\sigma^{j}_{n,\gamma}(E)$	Microscopic capture cross section of isotope j at energy E.
$N^{j}(\vec{r})$	Atom density of isotope j at radial point $\vec{r}$.
$\gamma^{j}(E)$	Capture gamma energy spectrum for isotope j at energy E.
$E_{n,\gamma}$	Average capture energy emitted per fission.
E_{ℓ}	Kinetic energy of the incident neutron in the laboratory system.
E_{c}	Total energy of neutron and nucleus in the center of mass system.
A	Atomic weight.
E_{t}	Inelastic threshold energy.
ϵ_1	Energy of the first excited state.
ξ	Average logarithmic energy decrement per collision.
Σ_{s}	Macroscopic scattering cross section.
F_1	Coefficient of the P_1 term in the Legendre expansion for the neutron elastic scattering section.
S(I,J,L,G)	The source at radia interval, I, axial interval, J, angular moment, L, group, G.

$\overset{\ell}{\varepsilon}(G' \rightarrow G)$	Legendre coefficient of the scattering cross section from group G' to G.
Φ_u	Uncollided flux in the direction cosine, μ.
$\cos(m\psi)$	The radius vector.
L	A particular pair of indices ℓ and m.
u	Ordinates for Gaussian quadrature.
W	Weights for Gaussian quadrature.
NOA	Total number of points.
γ_n	Curvature coefficients.
EPA	Epsilon.
MAX	Maximum.
k	The reactor multiplication factor.
Σ_f	Macroscopic fission cross section.
ν	Fast fission factor.
$P_{j,k}$	Atom density for the j-th isotope in the k-th formed region.
A_i	Cross sectional area of the i-th converter region.
$\vec{\Omega}$	Solid angle which defines the neutron directions.

$H_\gamma(\vec{r})$	Gamma heating rate at the spatial point $\vec{r}$.
$N_i(\vec{r})$	Number density of isotope, i, at point $\vec{r}$.
$\sigma_{ji}(E)$	Microscopic cross section of element i for reaction j at gamma energy E.
$\varepsilon_{ji}(E)$	Energy deposition per reaction j in element i.
$k_{ji}(E)$	Microscopic kerma factor for reaction j in element i at energy E.
$k_i(E)$	Kerma factor for all materials in the system at energy E.
k_γ^i	Gamma kerma factor for element i.
σ_{pe}^i	Photo electric effect microscopic cross section for element i.
σ_{pp}^i	Pair production microscopic cross section for element i.
σ_{ca}	Comptom microscopic cross section for element i.
q'''	Volumetric thermal source.
$\sigma_s^m(E \rightarrow E')$	Modified zeroth moment gamma scattering cross section.
$\sigma_{so}(E \rightarrow E')$	The zeroth moment gamma scattering cross section.
δ	The krouecker delta.
$\sigma_{gg'}$	Microscopic cross section from group, g, to group, g'.

MCR	Materials from cards.
MTP	Materials from tape.
GIP	Group Independent Tape.
MT	Total number of materials.
W_f	Weighting function.
M	An appropriate transport of diffusion theory operator.
FNORM	Normalization factor.
$(\mu_k)^i$	Energy tranfer coefficient of material i.
(μ_k/p)	Kerma.
P	Reactor Power in watts.
λ	The system eigenvalue.
$\bar{E}_r$	Average recoil energy.
E_n	Incident neutron energy.
$\bar{E}_{n'}$	Average kinetic energy of the secondary neutron emitted in the laboratory system.
$\bar{\epsilon}$	Average excitation of the residual nucleus.
$E^{in}_{\gamma,g\to g'}$	Gamma energy produced per inelastic collision from neutron g to g'.

$\overline{E\sigma}^{in}_{g}$ Inelastic scattering gamma-energy-production cross section for neutron group g.

$\sigma^{in}_{g\to g'}$ Inelastic scattering cross section from group g to group g'.

VITA

Abdelaziz Ezzat Eljabri was born on November 20, 1941, in Iraq El-Manshiyah, Palestine. He attended Hussien Ibn-Ali High School in Alkhalil, and graduated in 1959.

In 1959 he entered Teacher Training College at Al-Arroub and graduated in May 1961, with Diploma (Science Division). He taught in Jordan from 1961-1966 including one year (1964-1965) on a special teaching assignment in Algeria, and from 1966-1970 in Kuwait.

In September 1970, he entered Bethel College, North Newton, Kansas, and received a B.Sc. degree in Physics and Chemistry in May 1973.

In January 1974 he entered Texas A & M University, and received a B.Sc. degree in Nuclear Engineering in December 1975.

In June 1977, he decided to persue graduate study in Nuclear Engineering at LSU. He is a candidate for the degree of Master of Science in Nuclear Engineering.

He is a student member of the American Nuclear Society.

EXAMINATION AND THESIS REPORT

Candidate: Abdelaziz Ezzat Eljabri

Major Field: Nuclear Engineering

Title of Thesis: Gamma Heating of GRIST-2 Test Cluster Pressure Boundaries During Transient Test in the TREAT Upgrade Reactor

Approved:

Robert E. Miles
Major Professor and Chairman

James D. Trayham
Dean of the Graduate School

EXAMINING COMMITTEE:

Frank A. Silady

John C Courtney

Edward N. Lambremont

Robt C. McMurry

Date of Examination:

April 26, 1979